Diss. ETH No. 19053

Acquisition of Quantitative Magnetic Resonance Spectra

A dissertation submitted to the

ETH ZÜRICH

for the degree of **Doctor of Sciences, ETH Zürich**

presented by **Susanne Heinzer**, Dipl. Biol. ETH Zürich

born May 9th, 1981

citizen of Därligen BE and Illgau SZ

Zürich 2010 accepted on the recommendation of

Prof. Dr. Peter Boesiger, examiner

Prof. Dr. Markus Rudin, co-examiner

Prof. Dr. Spyros Kollias, co-examiner

Stefan und meinen Eltern gewidmet

Contents

Zusammenfassung

Die Magnetresonanzspektroskopie (MRS) hat sich während der letzten Jahrzehnte zu einer wertvollen Methode für die Untersuchung physiologischer Prozesse im menschlichen Körper entwickelt. Sie erlaubt den Einblick in den Metabolismus verschiedener Organe und wird oft als komplementäre Diagnosemethode für Stoffwechselveränderungen eingesetzt, die durch bestimmte Krankheiten wie Krebs oder multiple Sklerose entstehen. Die Konzentrationen der Metaboliten reflektieren dabei Aspekte der Physiologie und der Biochemie und sind von fundamentalem Interesse sowohl für die Wissenschaft als auch für eine genauere klinische Diagnose von Krankheiten.

Durch den Einsatz höherer Feldstärken an den Magnetresonanztomografie-Geräten (MRT) konnten das Signal-zu-Rausch-Verhältnis sowie die spektrale Auflösung kontinuierlich erhöht werden. Trotzdem sind noch einige technische Hürden zu überwinden, um das umfassende Potential der Technik für die wissenschaftliche Forschung und die routinemässige klinische Anwendung der MRS voll auszuschöpfen. So behindern oft Blutfluss, Suszeptibilitäts-Unterschiede zwischen den verschiedenen Gewebetypen und der im Vergleich zu den tiefen Metabolitenkonzentrationen hohe Wassergehalt die Akquisition guter Spektren. Zudem sind heutige Methoden zur quantitativen Bestimmung von Metabolitenkonzentrationen aufwändig oder ungenau. Während Konzentrationsverhältnisse zwischen Metaboliten oft zuverlässig bestimmt werden können (sogenannte „relative“ Quantifizierung), ist es schwierig, die millimolaren Konzentrationen der Metaboliten zu bestimmen („absolute“ Quantifizierung). Verschiedene Quantifizierungsmethoden mit separaten Referenzstandards („externe Referenz“) oder unter Annahme einer konstanten Wasser- oder Metabolitenkonzentration innerhalb des Gewebes („interne

Referenz“) wurden entwickelt. Externe Referenzen haben jedoch den Nachteil, dass sie für jede Untersuchung zusätzliche Messungen erfordern, während bei internen Referenzen die Konzentration des Referenz-Metaboliten durch physiologische Vorgänge oder Krankheit verändert sein kann.

Mittels funktioneller MRS können Zeitverläufe von physiologischen Parametern, von Metabolitenkonzentrationen und des pH-Wertes in Ruhe und während Aktivierung gemessen werden. So ist es beispielsweise möglich, die Veränderungen der am Muskel-Stoffwechsel beteiligten Metaboliten während der Muskelkontraktion zu verfolgen. Zusätzlich zur Quantifizierung der Metabolitenkonzentrationen ist bei solch dynamischen Spektroskopie-Messungen jedoch eine zuverlässige Normierung der Belastung des Muskels nötig, um eine Standardisierung unter Probanden oder Patienten zu erreichen. Diese kann durch die Messung der individuellen Maximalkraft und eine darauf angepasste Belastung während der Spektroskopie-Messung erfolgen.

Das Ziel der vorliegenden Dissertation war die Entwicklung von Methoden zur zuverlässigen Quantifizierung von Metabolitenkonzentrationen in Ruhe und unter normierter Belastung. Die Quantifizierung sollte für physiologische und klinische Studien an verschiedenen Kernen einfach anzuwenden und wenig zeitintensiv sein.

Quantifizierung von Metabolitenkonzentrationen. Für die Quantifizierung millimolarer Metabolitenkonzentrationen wurde ein Verfahren aus der NMR-Spektroskopie (ERETIC, **E**lectric **RE**ference **T**o access **I**n vivo **C**oncentrations) auf die Bedingungen in der *in vivo*-Spektroskopie angepasst. Bei dieser Methode kommt ein elektronisches Kalibrationssignal zur Quantifizierung der Spektren zum Einsatz. Durch eine kleine Kalibrationsspule wird dieses zuvor mittels eines Präzisionsphantoms kalibrierte Referenzsignal

eingespeist. Es erscheint im Spektrum anschliessend als zusätzlicher Peak. ERETIC wird während der Akquisition des Spektrums über einen zusätzlichen Breitband-Kanal des Magneten gesendet. Das Referenzsignal simuliert ein relaxierendes Spin-Signal mit vordefinierter Linienbreite, Phase, Amplitude und Frequenz. Um eine genaue Skalierung des Kalibrations- Signals mit den Metaboliten- Signalen zu erreichen, wird der Referenz-Puls induktiv in eine Sende- und Empfangsspule mit homogenem Feld (Volumenspule) gekoppelt. Eine optische Signaltransmission verhindert das Übertragen von Störsignalen, welche durch Sender oder elektrische Komponenten innerhalb des Scanner-Raums auftreten können. Das entwickelte Setup ermöglicht die Quantifizierung von Metaboliten in Spektroskopie- Messungen mit verschiedenen Kernen ohne zusätzlichen Aufwand während der Untersuchung. Ein solches System soll in Zukunft auch für klinische Anwendungen eingesetzt werden und damit eine zuverlässige Quantifizierung ermöglichen.

Quantifizierung von physiologischen Parametern während dynamischer Spektroskopie- Messungen im Muskel. Für die Bestimmung von Metabolitenkonzentrationen unter Belastung wurde ein Ergometer entwickelt, welches mittels Dynamometer die aufgebrachte Kraft des Wadenmuskels während isometrischer Kontraktion messen kann. Der Kraftwert während der Messung wird von einer für die funktionelle MRT entwickelten Software aufgezeichnet und dem Probanden via Projektor als visuelles Feedback angezeigt. Vor einer Messung kann jeweils die maximale Kraft des Probanden gemessen werden. Ein bestimmter Prozentsatz dieser Maximalkraft wird dem Probanden danach während der Muskelkontraktion als Zielwert vorgegeben und zusammen mit dem momentan erreichten Kraftwert auf eine Leinwand projiziert, während die Spektren gemessen werden. Um den Start der

Kraftmessung mit der Spektroskopiemessung zu synchronisieren war es notwendig, die Steuerungs-Software des Scanners zu modifizieren. Die Analyse und Quantifizierung der spektroskopischen Daten erfolgte anschliessend mit Hilfe einer speziell entwickelten Software auf Basis von IDL.

Das entwickelte Ergometer-Setup wurde in zwei metabolischen Studien erfolgreich eingesetzt. In diesen wurde das Verhalten des Muskelmetabolismus unter Belastung und in Ruhe untersucht. In einer ersten Studie wurde der Einfluss von ischämischem Krafttraining auf den untrainierten Muskel bei gesunden Probandinnen erforscht, während sich eine zweite Studie mit den Veränderungen von pH-Werten, Metabolitenkonzentrationen und Erholungskonstanten von phosphorhaltigen Metaboliten an Diabetikerinnen befasste.

Summary

Over the last decades, magnetic resonance spectroscopy (MRS) has become a valuable method for the assessment of physiologic processes in the human body. MRS provides an insight into the metabolism of different organs and is used as a complimentary method for the diagnosis of metabolic alterations that result from various diseases such as cancer and multiple sclerosis. The concentrations of the metabolites reflect aspects of physiology and biochemistry and are of fundamental interest for the assessment of scientific questions and for the diagnosis of diseases in clinics.

The spectral resolution as well as the signal to noise ratio have continually improved due to the availability of higher magnetic field strengths. Still, there are many technical issues to address in order to make use of the extensive potential of the MRS technique for scientific and routine clinical applications.

Blood flow, differences in susceptibility between different tissue types and a high water content compared to the low metabolite concentrations often impair the acquisition of high quality spectra. In addition, many methods that are available today for the determination of quantitative metabolite concentrations are either laborious or inaccurate. While concentration ratios of different metabolites can often be determined quite accurately (so-called „relative" quantification), it remains difficult to determine millimolar concentrations of the metabolites („absolute" quantification). Several quantification methods that involve separate concentration standards („external reference") or assume a certain water or metabolite concentration within a tissue („internal reference") have been developed. A main disadvantage of external references is the need for an additional measurement for each examination. Using the internal

reference method, on the other hand, bears the risk of assuming wrong reference metabolite concentrations in the case of disease or when physiological changes have occurred.

Using functional MRS, time courses of physiological parameters, metabolite concentrations and pH values can be followed at rest and under activation. For instance, it is possible to measure changes of metabolites that are involved in muscle metabolism during muscle contraction. In addition to the reliable quantification of metabolite concentrations in these measurements, it is necessary to achieve a normalization of the load that the muscle experiences, so that standardization among patients and volunteers can be attained. A possible approach is to measure the individual maximal voluntary contraction force and to subsequently adjust the load during the exercise according to this value.

The goal of this thesis was the development of spectroscopic methods for the reliable quantification of metabolite concentrations at rest and under normalized loading conditions. The quantification should be easy to apply and minimally time-consuming so that it could be successfully applied in physiological and clinical settings.

Quantification of metabolite concentrations. For the millimolar quantification of metabolite concentrations, a technique from nuclear magnetic resonance (NMR) spectroscopy (ERETIC, **E**lectric **RE**ference **T**o access **I**n vivo **C**oncentrations) was adapted to the conditions encountered in clinical *in vivo* spectroscopy. The ERETIC method is based on the use of an electric calibration signal for spectral quantification. After pre-calibration with a phantom containing well-known concentrations of metabolites, the artificial reference signal is injected through a small calibration coil, and it then appears as an additional peak in the spectrum. ERETIC is emitted during the acquisition

of the spectra through a broadband channel of the MR system. The reference signal simulates a relaxing spin signal with a pre-defined line width, phase, amplitude and frequency. To achieve an accurate scaling of the reference signal with the metabolite signals, the reference signal was inductively coupled into a transmit/receive coil with a homogenous field (volume coil). An optical signal transmission line was built to inhibit the carriage of interfering signals, which may arise through radio transmitters and electronic devices in the scanner room. The developed ERETIC setup enables the quantification of metabolites in spectroscopic measurements with different nuclei. No additional measurements have been made during the MRS examination. In the future, such a system shall also be used in clinical settings to enable the reliable quantification of metabolite concentrations.

Quantification of physiologic parameters during dynamic spectroscopy measurements in the muscle. For the determination of metabolite concentrations under load, an ergometer has been developed which measures the force that is exerted by the calf during isometric contractions by means of a dynamometer. The force that is exerted during the measurement is recorded by a software package that was developed for functional magnetic resonance imaging (fMRI). It is then displayed to the subject as a visual feedback via a projector. Before the spectroscopy measurement, the maximal voluntary contraction force against the pedal (MVF_P) can be determined for each subject. During the acquisition of the spectroscopy scans, a certain percentage of the MVF_P is then displayed to the subject on a screen as a target force, together with the currently exerted force. To synchronize the start of the spectroscopy measurement with the measurement of the exerted force, it was necessary to modify the controller software of the scanner. The analysis and quantification

of the spectroscopic data was subsequently performed using a custom-made software on the basis of IDL.

The developed ergometer setup was successfully applied in two metabolic studies, where the behavior of the muscle metabolism was assessed at rest and under exercise. In a first study, the influence of ischemic force training on the untrained muscle was investigated in healthy subjects. A second study was focused on changes of pH values, metabolite concentrations and recovery constants of phosphorus containing metabolites in diabetes patients.

Chapter 1:

QUANTIFICATION OF TISSUE METABOLITE LEVELS BY ^{1}H MRS

1.1 Introduction

In vivo magnetic resonance spectroscopy methods have been available for more than three decades. They allow for a non-invasive assessment of tissue metabolite levels over time. Metabolites that contain hydrogen (^{1}H), phosphorus (^{31}P) and carbon (^{13}C) atoms, as well as certain molecules containing other resonating nuclei such as fluorine (^{19}F) can be observed. Depending on their chemical environment, i.e. the molecule in which they reside, these nuclei resonate at specific frequencies. Each metabolite then gives rise to distinct peaks in a magnetic resonance spectrum.

Theoretically, millimolar concentrations of these metabolites can be calculated from the peak area since all atoms of a kind induce exactly the same amount of measurable signal. However, many physical parameters, as well as tissue-specific properties, are not known exactly.

Knowing the metabolite concentrations in tissues and being able to follow their time courses is important for physiological studies as well as in clinical settings. Diseases and physiological processes can be assessed, and treatments can be monitored using such information. However, obtaining quantitative information from MRS is a challenge in that data acquisition times are generally long, the spectral resolution is limited and the signal to noise ratio (SNR) is low.

Nevertheless, different calibration strategies have been developed that allow for the quantification of an *in vivo* metabolite concentrations by comparing its peak area to the area of a reference standard of known concentration.

One possibility is to acquire water spectra in a separate scan and reference them to the measured metabolite signals (Thulborn & Ackerman, 1983; Barker *et al.*, 1993). The water signal is then assigned a tissue-specific millimolar

concentration. This concentration is assumed to be constant for a specific tissue and absolute metabolite concentrations are estimated from the ratio of the water signal to the metabolite signal. Water has a very high SNR, so that only a few averages are needed to acquire a reference spectrum.

Similarly, the concentration of any metabolite in the tissue, such as creatine (Frahm *et al.*, 1989), can be assigned an average literature value that has been determined i.e. from tissue extracts. One has to assume that this literature value is similar in any subject and remains constant. The quantification techniques that rely on a signal that is present in the body are known as **internal referencing methods**.

Another quantification technique involves the measurement of an **external reference standard** with known metabolite concentrations. This reference standard is placed next to the subject or measured in a separate scan (Buchli *et al.*, 1994; Murphy-Boesch *et al.*, 1998). The measured metabolite areas are then compared.

A third quantification method that has been widely applied is based on the reciprocity principle (Hoult & Richards, 1976; Hoult, 2000) and uses the voltage that is needed in order to obtain the maximal signal response for calibration (see (Kreis *et al.*, 2001) and references in (Kreis, 1997)). Using this technique overall load on the coil - a value that depends on patient size and shape and leads to a more or less strong damping of the signal - can be compensated so equal metabolite signals can be obtained from different patients and phantoms. This method can be combined with the use of an external reference standard.

Most of the above quantification methods require additional measurements. In the case where a metabolite that is naturally present in the spectra is used to determine millimolar concentrations of the other metabolites, no additional

scan time is needed. However, one relies on the correct estimation of the reference metabolite concentrations. Many metabolite concentrations change under physiological conditions, e.g. with the age of the volunteer (Tofts, 2003) or with physiological stress, and during the course of a disease (Helms, 2001; Laule *et al.*, 2004). Depending on the tissue under investigation, no metabolite may be present that is qualified to serve as an internal reference.

Recently, a quantification technique has been developed in nuclear magnetic resonance (NMR) that allows for the acquisition of reference signal and metabolite signals in a single scan and does not rely on assumptions about metabolite concentrations (Barantin, 1997). It is based on the injection of an artificial synthetic reference signal (ERETIC, Electric REference To access In vivo Concentrations) that mimics the properties of the spin signal. This synthetic reference is calibrated once and then appears as an additional peak in the spectrum. The ERETIC method has been successfully applied in many studies *ex vivo* for the determination of metabolite concentrations in tissue homogenates and solutions. For an effective *in vivo* application, however, many additional subject specific and hardware parameters have to be considered.

1.2 Objectives

The main objective of the first part of this thesis was the development of in vivo MRS hardware and software that allow for accurate and precise *in vivo* quantification of tissue metabolite concentrations. More specifically, it was the aim to further develop the ERETIC quantification method so that accurate metabolite concentrations can be quantified *in vivo* without the need for an

additional measurement and with no discomfort for the subject. Moreover, the setting should be fully compatible with clinical settings.

The ERETIC technique has been previously used for in vitro quantification of metabolites using a broad band antenna (Barantin, 1997; Akoka *et al.*, 1999). In this publication, the antenna is attached to the front of the scanner bore and the signal is freely travelling through the room.

This calibration method is limited to small animals and to in vitro studies. The amplitude of the received calibration signal, and hence the calibration factor, are strongly affected by objects in the vicinity of the antenna and RF coil, including the sample itself. This means that the received calibration signal may vary with patient size and shape. In addition, an in vivo NMR system imposes several restrictions on calibration measurements. Inhomogeneities of the main magnetic field B_0 and the effective radio field B_1, and magnetic field drifts compromise the measurements. Also, in a clinical setting, patients must be repositioned so that there is a need for flexible cabling of the calibration setup. These problems have been addressed in the first part of this thesis.

1.3 Theoretical Background

Successful quantification depends on many sequence-, subject- or metabolite-specific factors that influence the signal intensity and the resulting spectral peak area. These additional influence factors need to be taken into consideration when estimating tissue concentrations given in mM from signal intensities in the acquired spectrum. The following formula gives an overview of the parameters that have to be considered when quantifying metabolite (M) concentrations from a metabolite signal S_M ((De Graaf, 2007), Equation 9.2.):

$$S_M = NS\ x\ RG\ x\ \omega_0\ x\ [M] x\ V\ x\ f_{sequence}\ x\ f_{coil}$$ **Equation 1**

NS denotes the number of scans, RG is the receiver gain, ω_0 is the Larmor frequency, [M] is the molar concentration, V is the measured volume, and $f_{sequence}$ and f_{coil} denote functions that account for different signal modulations due to the coil and MRS pulse sequence. Sequence- specific parameters include the repetition time TR, the echo time TE, the number of RF pulses and their flip angles, and variables such as nucleus specific relaxation (T_1, T_2). Coil- specific parameters include the B_1 radio-frequency field and coil load. The most important of these influence factors are detailed below. In addition, it is shortly described how different reference standards account for these influence factors.

B_0 inhomogeneity and field drifts

B_o is the conventional symbol for the main magnetic field strength (magnetic flux density or induction) in a MRI system, which is given in units of magnetic induction, Tesla. Current clinical MR systems have a constant magnetic field with field strengths of 1.5 to 3 Tesla. More recently, systems with field strengths of up to 7 Tesla have been developed. They provide a better signal to noise ratio (SNR). The static magnetic field inside the scanner bore is generated using superconductive magnet coils and is very homogeneous in clinical state-of-the-art scanners. However, the introduction of phantoms or a human body leads to inhomogeneities in the static magnetic field. Gross changes in resonance frequency and distortions of the static magnetic field occur at tissue to air and bone borders, where the susceptibility difference between the tissues is large. In these areas, the B_0 field is inhomogeneous. In addition, materials

with magnetic susceptibilities very different from water, such as iron, cause gradient distortions and severe artifacts in the spectra.

Small changes of the main magnetic field can occur during the scans due to varying reasons such as the heating of passive iron shims. Continuous averaging of the spectra in such a drifting field will lead to broadened resonance lines in the final spectrum if not corrected. These in turn can lead to inaccuracies when spectral peak areas have to be quantified. Broad peaks start to overlap and signals cannot be distinguished from one another or may completely disappear in the noise. To avoid this, the center frequency is continually monitored and updated during the scan in modern MR scanners.

Coil loading and the reciprocity theorem

The load on a coil is either a phantom or a subject being imaged. The interaction of the patient with the RF coil causes shifts of the resonance frequency and damping of the coil's resonance such that the magnetic induction and dielectric losses in the patient cause the quality factor of the coil to decrease.

The quality factor (Q) applies to any resonant circuit component; it is inversely related to the fraction of the energy in an oscillating system lost in one oscillation cycle. In a parallel tuned circuit (such as used in a MR coil), the quality factor is defined as:

$$Q = vL/R, \qquad \textbf{Equation 2}$$

where L is the coil inductance, R is the circuit resistance, and v is the angular frequency. An increase in the quality factor produces a sharper frequency response. The Q of a coil depends on the circumstances under which it is measured, e.g. whether it is 'unloaded' (no patient) or 'loaded' (patient).

Each patient induces a different load on the coil, which in turn affects the received signal. Any quantification method for in-vivo NMR needs to take this into account.

When using a "phantom replacement method" (Buchli *et al.*, 1994), where the phantom is measured before or after the subject, the coil loads for both scans are different. In such a case, a special calibration measurement is needed to correct for the differences in coil load. It is based on the reciprocity principle (Hoult & Richards, 1976; Hoult, 2000), which is usually formulated as follows in classical antenna theory (http://www.ebyte.it/library/educards/ nmr/ Nmr_ AntennaTheorem.html): Given two antennas *A* and *B* placed at some distance, each of them can be operated either as a transmitting antenna or as a receiving antenna. Suppose that antenna B is kept intact, while the performance of antenna *A* as a transmitter is modified so that, for a fixed amount of input power, the signal received by antenna *B* changes by a factor F. Then the same modification changes also the performance of antenna *A* as a receiver and does so by the same factor F. Translated to an NMR principle, this may read (http://www.ebyte.it/library/educards/nmr/Nmr_AntennaTheorem.html): The sensitivity of a magnetic resonance assembly, used as a receiver, to nuclides present at a point X is proportional to that assembly's efficiency, when used as a transmitter, to generate at that same location X a radiofrequency field B_1.

From this, it follows that the voltage needed to produce a 90° pulse, V_{90}, is proportional to the observed signal S_{obs}. The calibrated signal, $S_{cal} = S_{obs}V_{90}$ is therefore largely independent of coil loading (Austin *et al.*, 1991; Michaelis *et al.*, 1993).

If V_{90} is determined in a calibration experiment or during power optimization, its multiplication with the actual signal will correct for differences in coil loading between the calibration phantom and the actual in-vivo experiment.

However, B_1 effects (see next section, "B_1 and B_1 inhomogeneities") may only be corrected for using this calibration procedure if it is carried out in the same volume as the subsequent actual spectroscopy scan (Kreis, 1997).

B_1 inhomogeneities and power optimization

B_1 denotes the effective radio frequency field strength. Typical pulse amplitudes for Philips volume coils are 10-20 μT. The current that needs to be applied to reach this desired RF field depends on the quality factor Q of the coil, which in turn depends on the coil load and placement of the load within the coil.

The spatial distribution of the magnetic radiofrequency field varies depending on the coil design. Inhomogeneities of the RF field are essential sources of error for quantification of NMR parameters in MRI and MRS.

For the successful quantification of metabolite concentrations, it is important to know the accurate transmission field distribution within a sample and reception sensitivity of the coil (also termed B_1^-, (Hoult, 2000)). The B_1 transmission field is generally more or less homogenous when transmitting with the body coil or birdcage coils, however large variations occur when using surface coils or when measuring at high field strengths where the wavelength in the tissue is similar to the dimension of body structures. The induced currents further depend on the shape of the object and its electric properties. Several approaches have been developed to measure the transmission and reception patterns. While there are different methods available to measure transmission fields (i.e. (Stollberger & Wach, 1996; Brunner *et al.*, 2007)), reception field mapping remains a challenge (Wang *et al.*, 2005). However, several correction methods using simulation methods have been implemented and the coil sensitivity can

be determined separately using the principle of reciprocity (see "coil loading and the reciprocity theorem").
For single voxel spectroscopy, localized power optimization and load corrections may suffice to obtain a homogenous excitation within a volume of interest. Alternately, adiabatic excitation schemes such as LASER (Garwood & DelaBarre, 2001) can be used.

Power optimization procedures are performed previous to each scan to optimize the flip angle to 90°. To achieve this, the transmission power (RF drive scale) is adjusted according to the resistance that the patient induces into the coil and according to the B_1 distribution until the maximal signal response is reached.
The angle α of a constant RF pulse is defined as

$$\alpha = \gamma B_1 t_P, \qquad \textbf{Equation 3}$$

where B_1 denotes the pulse amplitude and t_P is the pulse length. In order to maximize the bandwidth and avoid T_2 decay during the pulse, the pulse duration needs to be as short as possible.
Several optimization schemes have been proposed (Perman *et al.*, 1989; Danielsen *et al.*, 1995). Most of the power optimization schemes executed on clinical scanners are either based on non-selective hard pulse experiments or slice-selective measurements. Although they do not correct for local B_1 effects, they allow for correct adjustments of the flip angle for different coil loads. To include local B_1 variations in the calibration, localized power optimization schemes have to be implemented. However, all power optimization schemes are only sufficient to achieve a correct flip angle in small volumes or single

voxel spectroscopy. For the normalization and quantification of CSI data, B_1 corrections remain indispensable.

Receiver Gain

The receiver gain (RG) defines the amplification of the signal coming from the sample. The gain of the receiver chain can be set to optimize the spectral signal strength so that the complete range of the receiver is filled without a truncation of the signal. Then, the digitization and demodulator noise become minimal. Setting the gain too high results in a clipped free induction decay (FID) signal. After Fourier transformation, this will result in a distorted spectrum. If the gain is set too low, only part of the voltage range of the system's digitizer is used, and digitization becomes inefficient.

When performing quantification, it is important that the reference scan and the actual *in vivo* scan are acquired at the same receiver gain or that appropriate mathematical corrections are made after the scan.

Repetition Time

When comparing metabolite concentrations between a reference standard and a signal from tissue, the difference in T_1 time needs to be either closely matched or corrected for. At a repetition time TR that is shorter than the longitudinal relaxation time T_1, the magnetization cannot completely recover and partial saturation occurs. The reduction of the steady-state longitudinal magnetization in a simple pulse-acquire measurement is given by:

$$M_z(TR) = M_0 \frac{1-e^{-\frac{TR}{T_1}}}{1-cos\varphi * e^{-\frac{TR}{T_1}}}, \qquad \textbf{Equation 4}$$

where M_z denotes the longitudinal magnetization, M_0 is the equilibrium magnetization, and φ is the nutation angle. This correction has to be applied to every metabolite and reference metabolite when using a repetition time that is shorter than $5T_1$. When using relaxation times equal to or longer than $5T_{1max}$ (T_{1max} being the longest relaxation time in the solution or tissue), the magnetization of all metabolite spins has recovered to more than 99% of M_0 and one can avoid this correction.

Echo Time

Transverse relaxation time T_2 may vary considerably between a sample and a reference standard. The amplitude of the measured signal depends on the echo time TE of the sequence, according to

$$\boldsymbol{M_{xy}(TE) = M_{xy}(0)e^{-TE/T_2}}, \qquad \textbf{Equation 5}$$

where M_{xy} denotes the transverse magnetization.

For long echo time sequences, the T_2 times of all metabolites need to be known and corrected for. Short echo times down to 10s have been achieved in localized spectroscopy and have been used to minimize quantification errors from T_2 decay. However, for metabolites with short T_2 relaxation times, such as myoinositol, even short repetition times lead to considerable signal loss. In addition, short echo time spectra contain many signals form macromolecular compounds which lead to baseline distortions and fitting difficulties.

Localization and Chemical Shift Displacement Artifact

The measured metabolite peak areas are directly proportional to the measured volumes. However, the location of the volume needs to be very accurate in

order to accurately quantify the metabolite concentrations in a specific region of interest.

In spectroscopy, identical nuclei in different molecules can be discriminated from one another because of their different magnetic shielding that leads to differences in resonance frequency. This chemical shift in turn leads to the selection of a different volume for each resonance when gradient localization schemes are used, since the frequency ω of spins with Larmor frequency ω_0 in x direction is given as follows in the presence of a magnetic field gradient G_x:

$$\omega(x) = \omega_0 + \gamma x G_x \qquad \textbf{Equation 6}$$

The location x is therefore

$$x = \frac{\omega(x)-\omega_0}{\gamma G_x} \qquad \textbf{Equation 7}$$

and the chemical shift displacement between two metabolites becomes equal to

$$\Delta x = \frac{\Delta\omega}{\gamma G_x} = \frac{\Delta\delta B_0}{G_x} = \frac{x\Delta\omega}{BW} \qquad \textbf{Equation 8}$$

Therefore, the resonance lines of the different metabolites in a spectrum acquired in a "single voxel" actually stem from different volumes. The so-called "chemical shift displacement artifact" (see Figure 1) leads to signal cancellations of J-coupled metabolites, such as lactate (Edden *et al.*, 2006; Lange *et al.*, 2006; Edden & Barker, 2007) and artifacts (Kreis, 2004). In addition, it limits reliable spectral analysis and quantification to central regions of the investigated FOV when MRSI is used (Henning *et al.*, 2008). Increases in pulse bandwidth diminish the displacement artifact but compete with limits for tissue-specific absorption rates (SAR).

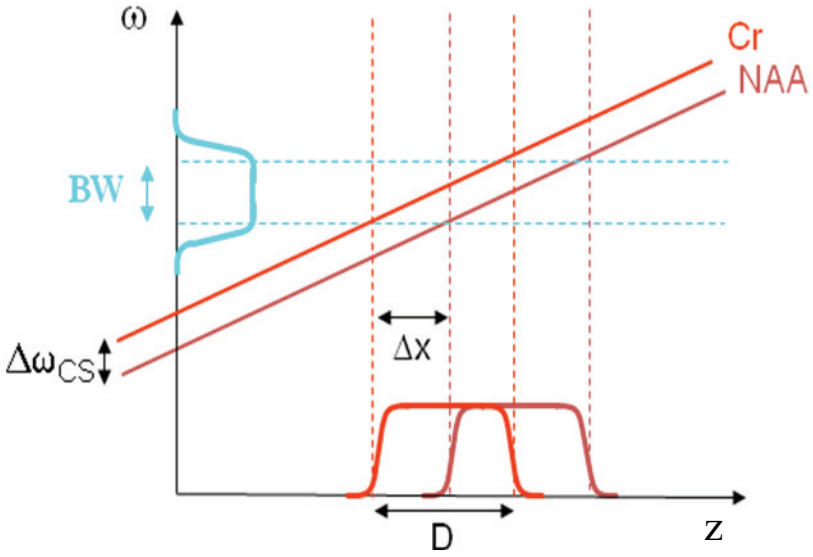

Figure 1 *Chemical shift displacement artifact. A difference in the chemical shift of two metabolites, $\Delta\omega_{CS}$, leads to the selection of a different voxel. The voxel offset Δx gets smaller as the bandwidth of the RF pulse, BW, increases.*

Pulse Shape

Depending on the spatial selection profile of a pulse, not all frequencies may be equally well excited. This will lead to smaller apparent metabolite concentrations.

Also, when water suppression is applied, resonances close to the water resonance may be partly suppressed. However, such effects may be easily corrected for if the pulse profiles are known.

Temperature

The equilibrium magnetization M_0 is proportional to the Boltzmann distribution (Hoult & Richards, 1976), as given by:

$$\boldsymbol{M_0 = \Delta n \mu_z = \frac{n\gamma\hbar B_0}{2k_B T_s}\,\mu_z = \frac{n\gamma^2\hbar}{2k_B T_s} B_0 = \chi_0(T_s) B_0} \quad \textbf{Equation 9}$$

Here, $\boldsymbol{\Delta n}$ denotes the difference in occupation numbers of spins with magnetic quantum number m = ½ and m= -1/2, $\boldsymbol{\mu_z}$ is the magnetic dipole moment $\boldsymbol{\gamma}$, signifies the gyromagnetic ratio, $\boldsymbol{T_s}$ is the sample temperature, ħ the Boltzmann constant and $\boldsymbol{\chi_0}$ the magnetic susceptibility. Thus, when measuring the final MR signal, it is inversely proportional to the absolute temperature of the sample (Kreis, 1997). This must be taken into account when quantifying a metabolite signal from living tissue at 37° with a reference standard at room temperature. A conversion table can be found in ((Tofts, 2003) on page 306).

NMR visibility

Nuclei with very short T_2 times are hardly visible in in-vivo MRS since they lead to very broad resonances. The width at half height, $\Delta\nu_{1/2}$, of the absorption line of a Lorentzian lineshape is inversely proportional to the T_2^* time, according to:

$$\Delta\nu_{1/2} = \frac{1}{\pi * T_2^*} \quad \textbf{Equation 10}$$

T_2* is related to the rotational mobility of the metabolite. If the metabolite's motility is strongly reduced, T_2* may become very short and the measured metabolite concentration does not correspond to the actual concentration, as is i.e. the case for water, where the concentrations measured in MRS severely underestimate the actual concentration ((Menon & Allen, 1991; Mackay *et al.*, 1994; Kreis, 1997). It is generally very difficult to correct for this error.

Estimations of the actual concentrations can only be obtained with invasive methods.

Other sources of quantification errors

Magnetization transfer can occur when water suppression is applied and can lead to significantly lower metabolite areas. Also, movement may cause the spectra to appear completely normal but with decreased signal areas only (Kreis, 2004). A further source of quantification errors are post-processing steps and inaccurate fitting procedures (for further information see (De Graaf, 2007), Chapter 9).

How do different quantification methods account for the confounding factors?

Table 1 displays factors that compromise quantification using the most common quantification schemes and the ERETIC method that has been further developed in this thesis. Several quantification methods are available that account for coil loading. One option is to measure the reference signal under identical loading conditions as the sample. This is done in the “internal water referencing method” (Thulborn & Ackerman, 1983), where the internal water signal is acquired in a separate measurement using the same hardware settings. The measurement is performed on the same volunteer and the same volume of interest so that the coil load remains the same.

	Internal Reference	External Reference	ERETIC
B_1 inhomogeneities	unaffected	affected	affected
Coil loading	unaffected	Partly affected	unaffected
Power optimization	unaffected	affected	affected
Receiver gain	unaffected	affected	unaffected
TR, TE (T_1, T_2)	affected	affected	affected
Temperature	unaffected	affected	affected
Post-Processing	Partly affected	affected	unaffected

Table 1 *A summary of some parameters that influence quantification and how they affect the different quantification methods.*

A second MRS quantification method is available that does not need corrections for loading, the so-called "simultaneous phantom acquisition method" (Murphy-Boesch *et al.*, 1998). A phantom containing a reference solution with known metabolite concentrations is placed near the sample in the field-of-view (FOV) of the coil. Before or after the actual spectroscopy scan, a scan of the solution in the phantom is acquired. This calibration requires additional measurement time and the subject has to remain in the scanner, however, the quality factor of the coil remains the same for both scans. The ERETIC method developed for in-vivo applications (Heinzer-Schweizer *et al.*; Marro *et al.*, 2008) also scales linearly with coil load due to inductive coupling of the calibration signal into the receiver coil. Since this is also the mechanism by which the local B_1 field arising from excited nuclei in the sample couples

with the receiver coil, any subsequent manipulations of the data have an equal effect on both signals. This makes the calibration factor immune to changes in coil loading conditions, receiver gain settings and data processing methods.

All quantification methods are equally affected by corrections that are necessary for T_1 and T_2 relaxation times with differing TRs and TEs. Any method that relies on a reference signal that does not stem from the same volume of interest also depends on an accurate power optimization so that exact flip angles are reached. Also, corrections for temperature differences between the reference standard and the subject have to be made, and post-processing of all spectra needs to be performed equally.

Table 2 lists the most common quantification techniques as well as the ERETIC and their general advantages and disadvantages.

	Internal Reference	External Reference	ERETIC
Advantages	- Easy to apply - Accounts for B_1 inhomogeneities and errors in power optimization	- Easy to apply when established	- Spectrum and reference acquired in a single scan - Applicable for MRS scans with all nuclei
Disadvantages	- Requires assumption about metabolite concentrations - Not all tissues contain a metabolite that can be used as a reference	- Extra scan time needed - Load adjustments needed in some cases	- Only works with volume coils - Requires additional hardware

Table 2 *Advantages and disadvantages of different quantification methods.*

Chapter 2:

IN-VIVO QUANTIFICATION OF METABOLITE CONCENTRATIONS USING THE ELECTRIC REFERENCE TO ACCESS IN VIVO CONCENTRATIONS (ERETIC) METHOD

2.1 Introduction

Magnetic resonance spectroscopy (MRS) is an established technique to assess metabolite distributions in vivo (Kreis, 1997; Kemp *et al.*, 2007). Tissue concentrations of various molecules and compounds can be indicated by either a ratio to a reference metabolite such as total creatine (relative quantification), or in millimoles (also referred to as absolute quantification). While relative quantification is widely used, it has the major disadvantage of ambiguities whenever several metabolite concentrations change simultaneously, as is the case for most diseases. Hence absolute quantification is an indispensable tool to precisely determine metabolite changes for clinical diagnostics and physiological studies.

The goal of this study was the development of a simple and reliable method that enables absolute quantification of water and metabolite concentrations based on in vivo ^{1}H MRS. More specifically, the method should be applicable to clinical diagnostics, where it ought to yield reproducible results with no additional measurement time needed, and no interference with already implemented measurement procedures (including proton decoupling for multi-nucleus acquisitions). Also, it ought to be robust in disorders that lead to structural changes and thus changes in tissue water concentrations.

Absolute quantification based on internal water referencing has been available for a long time (Thulborn & Ackerman, 1983; Barker *et al.*, 1993) and is the current method of choice. It accounts for B_1 variations across the field of view, but imposes problems when assessing diseases that lead to alteration of tissue

water concentration (Helms, 2001; Laule *et al.*, 2004) and relaxation behavior. Simultaneous phantom acquisition methods (Narayana *et al.*, 1989; Hennig *et al.*, 1992; Ernst *et al.*, 1993; Kreis *et al.*, 1993) and phantom replacement methods (Buchli & Boesiger, 1993; Duc *et al.*, 1998) have also been successfully used for many scientific studies, but these methods have never been established for routine clinical diagnostics.

The ERETIC (Electric REference To access In vivo Concentrations, (Barantin, 1997; Akoka *et al.*, 1999; Akoka & Trierweiler, 2002) method was introduced as an innovative approach to in vivo quantification by Barantin *et al*. (Barantin, 1997). It uses a synthetic reference signal that is induced by means of a small loop coil that couples to the RF coil. This low-power reference signal is turned on during the acquisition only and simulates the free induction decay (FID) of spin signals, which will give rise to an additional peak with Lorentzian line shape in the spectrum.

ERETIC offers several advantages in that (1) it is applicable to all nuclei, (2) spectra can be acquired simultaneously with the artificial reference signal in a single scan, (3) scaling of the received signal with the coil load and receiver gain is achieved and (4) the signal intensity is not affected by different medical conditions. Re-calibration is not necessary for every measurement, leading to an easy handling of the calibration method for clinical applications. In addition, ERETIC signal amplitude is independent of TE and TR. The reference signal does not correct for B_1 variations across a volume – for this reason, its successful application depends on the use of a homogeneous volume coil and/or B_1 mapping and correction. In addition, the ERETIC method is susceptible to errors in power optimization; however changes in coil loading, matching, receiver gain, and data processing (Marro *et al.*, 2008) are directly included. Further effects on estimated metabolite concentrations, such as magnetization

transfer, frequency response of the RF pulse, and MR visibility of a molecule, are described in more detail by Marro *et al* (Marro *et al.*, 2008).

While quantification with ERETIC has been proven to be an accurate method for the assessment of concentrations of various dissolved compounds using ultra-high field NMR spectrometers (Barantin, 1997; Akoka *et al.*, 1999; Akoka & Trierweiler, 2002; Michel & Akoka, 2004), only preliminary results from in-vivo spectroscopy measurements have been shown using clinical MR scanners (Barantin, 1997; Marro *et al.*, 2008). In the earliest in-vivo ERETIC (Barantin, 1997) implementation, the ERETIC loop was attached at the front of the scanner bore in a fixed position and the calibration signal was transmitted via radiation, which leads to signal variations whenever the mutual coupling between the loop and the receive coil changes. Marro *et al*. (Marro *et al.*, 2008) have modified the ERETIC approach to an inductive injection of the signal into the receive coil, thus directly considering changes in coil loading and receiver gain settings. Using this approach, cables must be run through the scanner bore. Transmission of the calibration signal via an electrical transmission line may cause parasitic coupling and thus inaccurate quantification results when cables are not carefully repositioned for each measurement. Another source of error are B_1 inhomogeneities.

In order to solve these problems, a new implementation scheme based on fiber optic transmission of the ERETIC signal and induction into a transmit/receive birdcage head coil on a clinical 3T scanner is presented in this work. A low-power transmit channel is used for transmission of the artificial reference peak. Stability, scaling with coil load and a small inter-scan variability of the ERETIC signal are demonstrated. With this optical setup, reliable and reproducible quantification results were obtained for ^{1}H MRS on a clinical 3T system in vivo. The comparison of brain ^{1}H MRS quantification results based

on the ERETIC approach is in accordance with internal water reference calibration in healthy volunteers and meta-analysis literature values (Keevil, 1998).

2.2 Theory

The concentration c_{met} of any given metabolite in an in-vivo spectrum can be determined by comparing its intensity to the ERETIC peak, according to the following formula (Akoka *et al.*, 1999):

$$c_{met} = \frac{k * c_{ERETIC} * A_{met,\,invivo}}{A_{ERETIC,\,invivo}} \qquad \text{Equation 11}$$

Here, k accounts for the number of protons contributing to a resonance line, c_{ERETIC} is the equivalent concentration of the calibrated ERETIC peak and A_{met} and $A_{ERETIC,invivo}$ stand for the areas of the metabolite and ERETIC peaks, respectively. The equivalent concentration of the ERETIC peak must be determined beforehand with the known concentration of a calibration solution. There, the peak area of the ERETIC peak $A_{ERETIC,invitro}$ is compared to the peak area of the calibration peak A_{calib} and multiplied by the concentration of the calibration solution c_{calib} [Equation 12].

$$c_{ERETIC} = \frac{c_{calib} * A_{ERETIC,\,invitro}}{A_{calib}} \qquad \text{Equation 12}$$

For an accurate calibration of a metabolite signal with a phantom, T_1 saturation and T_2 times of phantom metabolites compared to in-vivo relaxation times need

to be taken into account (Mlynarik *et al.*, 2001). Additionally, a temperature correction must be applied to correct for the offset in spin populations between the phantom and the brain (Venkatesan *et al.*, 2000), and volume corrections must be made depending on the voxel size of the acquired spectra compared to that used for the reference spectrum (Kreis *et al.*, 2001).

2.3 Methods

Signal generation

When quantifying the spectra with any software package such as LCModel (Provencher, 1993), jMRUI (Naressi *et al.*, 2001), or TDFDfit (Slotboom *et al.*, 1998), an FID- like signal with line broadening adjusted similarly to that of the real resonance lines is needed. Frequency drifts during the scan due to temperature changes or other variables must be compensated for by means of a communication path between the signal generator and the scanner. In this work these issues are readily addressed by using the spectrometer itself to generate the ERETIC signal. An amplitude modulated RF pulse is sent through a separate channel of the system. The frequency is thus updated whenever the system frequency changes, so that additional line broadening due to averaging is avoided.

Signal transmission

When using a setup based on electrical signal transmission, the ERETIC signal suffers from considerable instabilities when cable positions are changed. This is due to the fact that any electronic device, such as the T/R switch or cabling, may act as a parasitic radiation source of its own. Therefore, several coupling

paths are present simultaneously between the signal source and RF coil, which can lead to signal cancellations. Depending on the strength of confounding signals, the ERETIC reference signal that is coupled to the receive coil can vary by more than 70 percent from the mean value. An example of a scan with three extreme cable positions is shown in Figure 2. To achieve reliable quantification results, cable traps and careful grounding of the wires are required to lessen parasitic coupling, and the ERETIC cable must be positioned in the same way for all scans. To avoid such rigid constraints on cable positioning, we here propose a new implementation of the ERETIC method for in-vivo applications, featuring an optical fiber RF transmission system to provide a flexible scanning setup for clinical applications.

For multi-nuclear signal acquisition, only two transmit channels are available on most commercial systems, i.e., one for proton and one for other nuclei. In order to enable parallel use of all channels for future multi-nucleus applications, we here make use of an auxiliary low-power RF channel to generate the ERETIC signal, leaving the proton and multi-nuclear channels free to function normally. Enhancements of signal-to-noise ratio and spectral resolution using multinuclear techniques are thus unaffected.

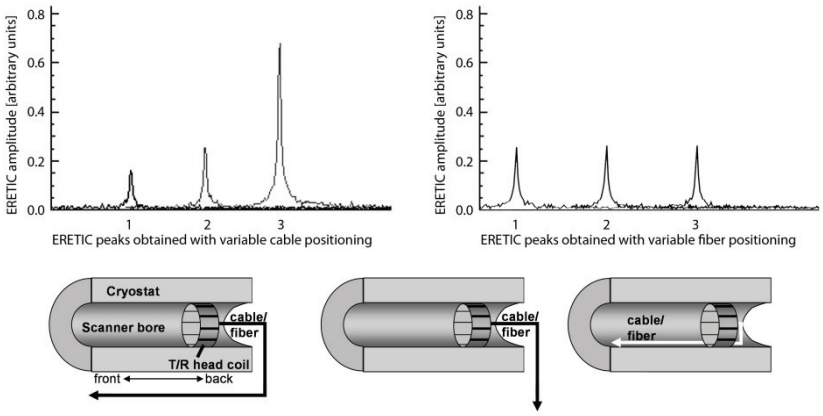

Figure 2 *Example of measuring the ERETIC amplitude at extreme cable/fiber positions. A double shielded coaxial cable was used for the electric transmission. The figure displays ERETIC peaks acquired with the cable (left) and optical fiber (right) positioned in different ways (see schematic, bottom):*

1. cable/fiber running along the scanner bore,

2. cable/fiber running away from the scanner bore, and

3. cable/fiber running through the scanner bore.

The ERETIC amplitude stays stable with the optical setup while showing large variations due to prasitic coupling when it is injected through the cable.

Signal injection

The ERETIC loop must be placed as close as possible to the receiver coil in order to couple the signal inductively and to avoid electric coupling effects. Loop dimensions must be minimal so that the transmitted ERETIC signal remains stable with varying coil loading. In the setup presented here, coupling through electric fields is further reduced by using an end-capped birdcage coil[24]

whose ground plane (RF mirror) separates the load from the ERETIC loop and provides stable grounding.

Hardware implementation

The proposed technique was implemented on a Philips Achieva 3.0 T scanner (Philips Healthcare, Best, The Netherlands) with a modified commercial transmit/receive birdcage proton coil. During acquisition, the ERETIC signal was sent to a loop that was placed behind the rear RF mirror of the transmit/receive head coil.

The broadband tune channel of the system is used to generate the ERETIC signal [Figure 3, top] at any given resonance frequency, such as that of ^{1}H, ^{13}C, ^{19}F or ^{31}P.

A directly modulated RF-over-fiber link was used to transmit the ERETIC signal from the spectrometer to the coupling loop. The link consists of a matching network, a directly-modulated light emitting diode (LED), a polymer optical fiber and a photodiode detector which is connected to the ERETIC loop [Figure 4, left]. This setup guarantees that only the signal that is coupled through the ERETIC loop will be picked up by the receive coil and that all sources of parasitic coupling are eliminated.

A high-frequency LED (L9534, Hamamatsu, Japan) is used as the modulator, while the injector loop contains a non-magnetic PIN photodiode powered by a DC voltage source available at the birdcage head coil and is positioned behind its rear RF mirror. The injector loop couples inductively with one of the birdcage legs near the point where it is connected to the RF mirror [Figure 3, bottom].

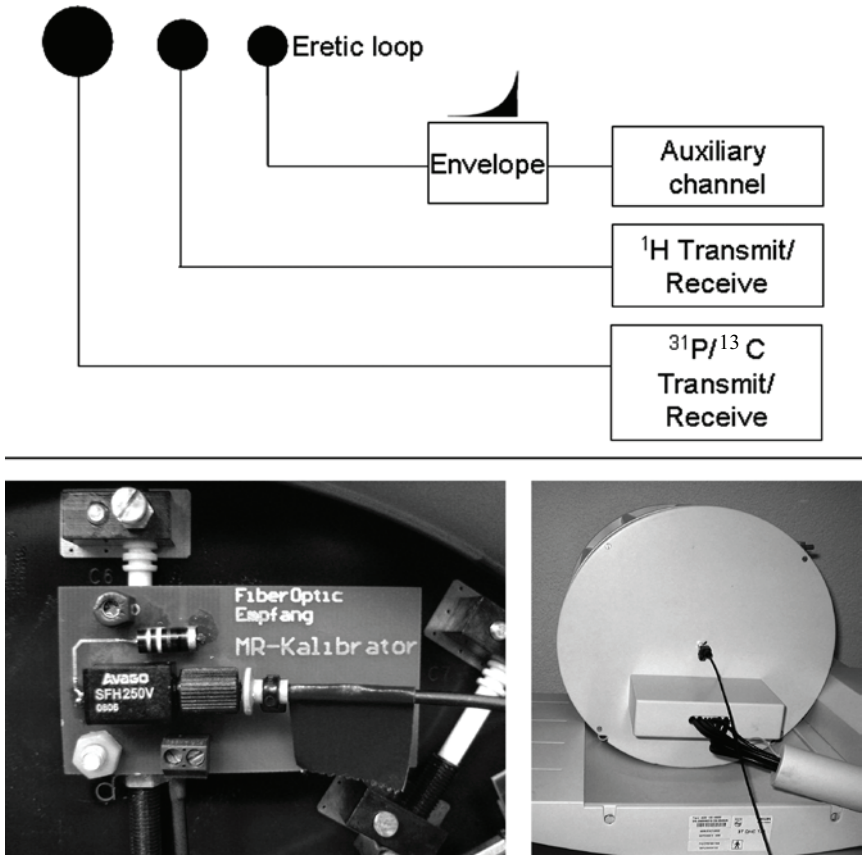

Figure 3 ***Top:*** *Signal paths from the coils to the spectrometer. An auxiliary channel is used for transmission of the ERETIC signal.* ***Bottom:*** *The ERETIC loop as it is placed behind the rear RF mirror of the birdcage coil (left). The setup is patient-friendly and easy to handle (right).*

Software

The ERETIC pulse shape, phase, decay time constant, amplitude, frequency and phase cycling schemes can be adjusted directly at the scanner console. Frequency updates during a scan with multiple averages result in a simultaneous update of the ERETIC signal.

2.4 Validation and test measurements of the ERETIC setup

1) Scaling with variable coil load

According to theory, the ERETIC and metabolite signals scale similarly with changes in coil load. To show concordant scaling behavior the NAA and ERETIC signals with varying coil load, different loading conditions were simulated using resistors. Using this setup, inaccuracies such as B_1 effects, changes in scanner settings and automatic power optimization, that may arise when the load is adjusted through the use of different phantoms, can be excluded. Six 1kΩ resistors in parallel were connected to the coil ports at the back of the T/R coil as shown in Figure 4, right. Switches allowed any combination of resistors to be included or excluded. To ensure equal loading of the birdcage coil's two orthogonal modes, two such boards were used and connected to the corresponding ports. These boards included a T/R switch, which ensured that the resistors were loading the ports during acquisition only, while in transmit the resistors were disconnected to ensure that transmit B_1 and power settings of the scanner remained unchanged.

Measurements were carried out using a spherical MRS phantom (MRS "Braino" phantom, GE Healthcare). Scans were acquired using a single voxel PRESS sequence (TR=2000ms, TE=144ms, voxel size: 2x2x2cm) with 64 signal averages per loading condition. Receiver optimization and other scan preparation settings were kept constant throughout the entire experiment. Load scaling as a function of parallel resistance was compared for the NAA and the ERETIC signal.

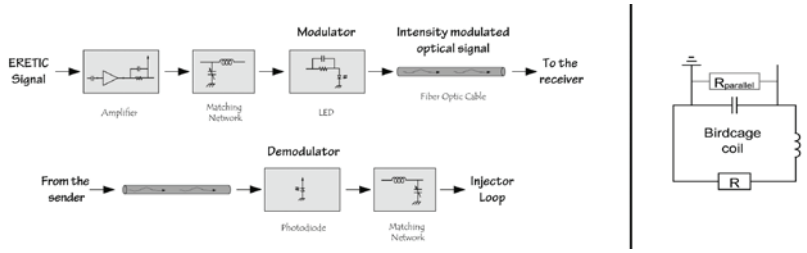

Figure 4 ***Left:*** *Schematic of the optical setup. The signal is amplified before it is sent to the scanner room and finally reaches the injector loop.* ***Right:*** *Simplified schematic of the resonance circuit with 6 parallel resistors ($R_{parallel}$) added to the birdcage coil. The resistors have a value of 1 kV each. A set of resistors was added to each quadrature port of the coil in order to load both orthogonal modes in a similar fashion.*

2) Concentration series

To demonstrate calibration capabilities of the ERETIC method, phantoms containing variable glycine (Gly) concentrations [10-50mM] were prepared and quantified. Phantoms were prepared using a precision balance (precision: ±0.0001g) to reach an error estimate below 1%. Settings for each scan were as follows: TR=2000ms, TE=29ms, voxel size=1x1x1cm, 128 averages. A preparation phase including automatic power and receiver gain optimization

was performed prior to each measurement. The phantom with the highest concentration and SNR was used for calibration.

3) Sensitivity to movements (Inter-scan variability)

The ERETIC signal must remain stable when changing patient positions and after moving the coil out and back into of the scanner bore. To test signal stability, PRESS scans (TR= 2000, TE= 144ms, voxel size = 2x2x2cm) were made using the "Braino" phantom. After 60 signal averages the coil was moved out of the scanner bore, cables were repositioned and the coil was placed back to the iso-centre of the bore. The scanning was then continued without adjustments of the scan settings. This procedure was repeated 10 times.

4) Short-term and long-term stability of the ERETIC signal

Short-term stability of the calibration signal was assessed in a time series scan with 1024 individual acquisitions using the "Braino" phantom. A PRESS sequence (TR=5000 ms, 2 signal averages/dynamic, TE = 29 ms) accounting to a total measurement duration of 2 hours was scanned. The ERETIC signal was plugged in at the beginning of the measurement. Long-term stability was assessed using a long-time PRESS protocol (TR=10'000 ms, TE=29 ms, 10 signal averages/dynamic) of 11 hours and 48 minutes. The ERETIC signal had been plugged in beforehand to avoid warm-up effects (see Results). A longer repetition time was chosen to limit the amount of data acquired while having no influence on signal amplitude. The spectra were analyzed for the stability of the ERETIC signal by measuring its amplitude in the magnitude spectrum.

5) In-vitro Reproducibility

The intrinsic reproducibility of a quantification method cannot be conclusively determined in-vivo due to confounding factors such as inter-and intra-subject variability of metabolite concentrations. The random error of the ERETIC quantification was therefore compared to that of the internal water reference by repeating a single-voxel PRESS scan including all preparation steps, such as automatic power and receiver gain optimization 20 times in a phantom containing natural metabolite concentrations. Parameters were as follows: TR= 2000ms, TE=29ms, 64 signal averages, voxel size = 2x2x2cm.

6) In-vivo acquisition of single voxel spectra and concentration determination

To determine the robustness and reproducibility of the ERETIC reference standard for in vivo metabolite quantification, the ERETIC quantification method was cross-validated with the internal water reference method in healthy volunteers and quantification results were compared with literature values. In addition, the proposed optical signal transmission was compared to ERETIC signal transmission through an electrical cable with quasi fixed cable position.

Experiment 1. To assess the reproducibility of quantifying tissue concentrations of metabolites in vivo with ERETIC, the ERETIC-signal to metabolite ratio was measured in three independent scans each for six subjects (age = 28 ± 8.8 years). The subjects were repositioned between the scans and all preparation steps were repeated. Voxels were placed in the centrum semiovale (CSO) of the brain and single voxel PRESS scans (TR=2500ms, TE= 47ms) were performed. Each scan was performed twice, once using an electrical transmission of the ERETIC signal and the second time using the proposed optical ERETIC signal transmission. For the electrical transmission, the ERETIC cable was carefully

repositioned for each measurement inside the scanner bore to avoid parasitic coupling. The position of the coaxial cable was entirely fixed between the signal generator and the entrance of the scanner bore and the cable position inside the scanner was reestablished with an accuracy in the mm range.

Experiment 2. In-vivo brain metabolite concentrations were assessed in five healthy subjects (age = 28±3.9 years) for cross-validation of the ERETIC reference method using the proposed optical signal transmission setup with the internal water reference method. In an independent measurement series, water concentrations were determined in six subjects (age = 28±5.8 years). All single voxel PRESS (TR=2500ms, TE= 47ms) spectra were acquired in the CSO.

The above experiments were then followed by metabolite signal fitting and internal water referencing using LCModel. While ERETIC peak fitting is possible using LCModel fitting the ERETIC peak using *TDFDfit* was found to be more reliable (see Discussion) and was therefore used to obtain the amplitude of the reference peak.

The obtained concentration values were subsequently corrected for temperature, voxel volume, and T_1 and T_2 using literature values (Mlynarik *et al.*, 2001). A water reference scan was acquired for all metabolite spectra to allow quantification of the metabolite concentrations with the internal water reference method.

2.5 Results

1) Scaling with variable load

The scaling of ERETIC signal amplitude under variable loading conditions [Figure 5] is in good agreement with that of NAA and demonstrates the robustness of accurate quantification with the ERETIC method under variable loading conditions. The coefficient of variation of the NAA to ERETIC signal ratio is 2.8%.

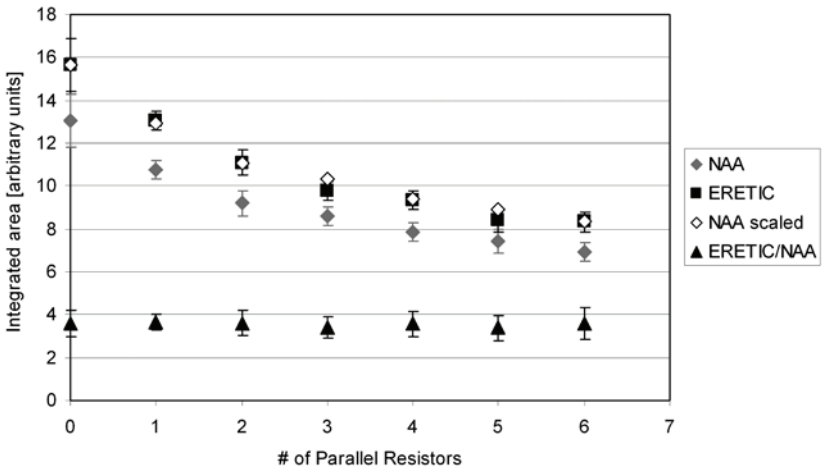

Figure 5 *Scaling of the NAA (grey diamond) and ERETIC (square) signals with varying load. 64 spectra were acquired for each data point. The error bars denote the intra-scan standard deviation of the integrated peak areas and of the ratios. The NAA signal was scaled (white diamond) to visualize the similar scaling behavior of both signals with variable load. The ERETIC/NAA ratio (scaled up 3 times for better visibility) is shown as triangles.*

2) Concentration series

In-vitro quantification with a series of five phantoms with increasing Gly concentration show accurate results (R^2=0.99) even when all preparation steps, such as automatic power and receiver gain optimization, are performed individually for each scan [Figure 6].

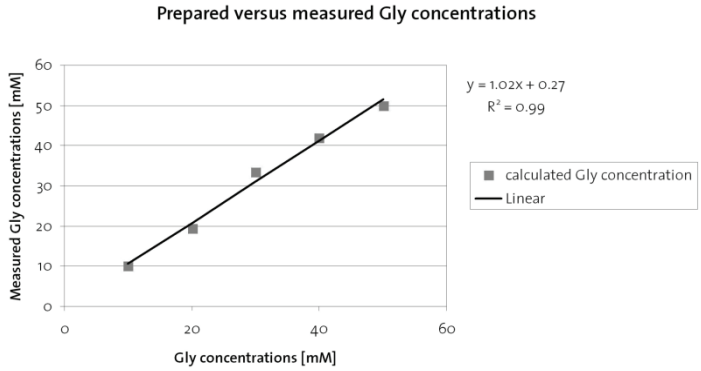

Figure 6 *Calibration curve for Gly concentrations varying from 10 to 50 mM. The R^2 of the measured versus prepared Gly concentrations is 0.99, showing the accuracy of quantification with the ERETIC method.*

3) Sensitivity to movements (Inter-scan variability)

When the phantom is moved out of the scanner and back in between measurements and the receiver gain is not changed, the ERETIC signal exhibits a coefficient of variation of 2.83%.

4) Short-term and long-term stability of the ERETIC signal

After an initial warm-up phase, the ERETIC signal remains stable over a measurement time of several hours. The initial drift is attributed to a

temperature transient when the circuit is switched on. This effect can be avoided by switching the circuit on half an hour before starting the scan.
When omitting the warm-up time from the analysis, the coefficient of variation is 0.67%, while the minimal and maximal value differ by 1.41% and 0.95% from the mean [Figure 7, top].
In the 12 hours scan, the coefficient of variation was 2.16%, with minimum and maximum values differing by 3.79% and 3.40% from the mean value [Figure 7, bottom].

5) In-vitro Reproducibility

When repeating a single-voxel scan 20 times in a calibration phantom and quantifying all metabolite concentrations with LCModel, the accuracy of the internal water scaling method exhibits a mean error of 1.58% for the quantification of NAA, Cho, and Cre, while the ERETIC method performs slightly worse with a mean error of 2.83%.

6) In-vivo acquisition of single voxel spectra and concentration determination

Experiment 1.

The coefficients of variation between scans for the optical setup were 9.1% for the ratio NAA/ERETIC (range across subjects: 2.5%-14.8%), 7.3% (3.2-12.8%) for Cho/ERETIC, and 6.2% (3.3-9.2%) for Cho/ERETIC. Similar values were obtained when transmitting the ERETIC signal through an electrical cable in the case of carefully repositioned cable postions; coefficients of variations were 7.9% (3.9-16.1%) for NAA/ERETIC, 9.3% (4.8-15.0%) for Cho/ERETIC, and 9.5% (6.4-13.4%) for Cre/ERETIC.

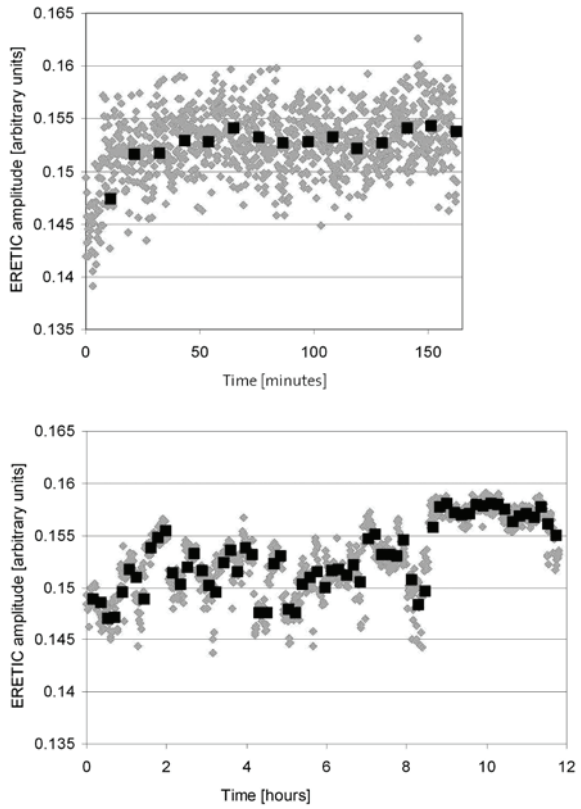

Figure 7 ***Top:*** *Results of the short-term measurement of the ERETIC amplitude on an expanded scale: A warm-up phase of approximately 30 minutes is required. Thereafter, the ERETIC signal remains stable within a low coefficient of variation of 0.66% when acquiring spectra with a signal averaging factor of 130 (squares). The diamonds denote the ERETIC amplitude of the actually acquired spectra.* ***Bottom:*** *Long-term measurement after the warm-up phase: The coefficient of variation for this series is 2.16% when considering 130 signal averages (squares).*

Experiment 2.

In-vivo ERETIC quantification results [Figure 8, Table 3] from the centrum semiovale of five subjects are in agreement with values obtained in the literature (Michaelis *et al.*, 1993; Pouwels & Frahm, 1998; Kaiser *et al.*, 2005; Baker *et al.*, 2008), as well as those obtained using the internal water reference standard. The product-moment correlations of the concentration values determined with internal water referencing and ERETIC are 0.98 for NAA, 0.93 for Cho and 0.91 for Cre and indicate that the two methods correspond well to each other in healthy tissue. The determined NMR-visible water concentration (mM) is defined as 55555* βMR (where βMR equals the water content of brain tissue (Ernst *et al.*, 1993)). The measured values of 35582 ± 2239mM are in good agreement with previously published literature values of 35888 ± 833mM (βMR of 0.65+0.02 (Ernst *et al.*, 1993)) and 37277 ± 1722mM (βMR of 0.67+0.03 (Warntjes *et al.*, 2007)).

2.6 Discussion

The goal of this study was to develop a quantification method which is suited for clinical applications. Major challenges were the achievement of a stable ERETIC signal, maintaining the availability of all transmit channels for future multi-nucleus measurements, and the construction of a hardware and software setup which can be readily used for clinical measurements.

Similar reproducibility was achieved for the in-vivo scans with the optical and electrical setup when the coaxial cable utilized for the latter setup is carefully repositioned (methods, section 6). However, maintaining stable cable positions is not practical under clinical conditions, where patients and coils are moved in

and out of the scanner bore. With the optical setup presented above, quantification can be performed irrespective of fiber positioning and enables flexible scanning. The received coefficients of variation of both the electrical and optical transmission are in agreement with literature values (Marshall *et al.*, 1996) that were measured using the same localization technique. The measured variability between the scans is due to a combination of errors in repositioning the VOI, subject motion, and the limited signal to noise ratio (Marshall *et al.*, 1996).

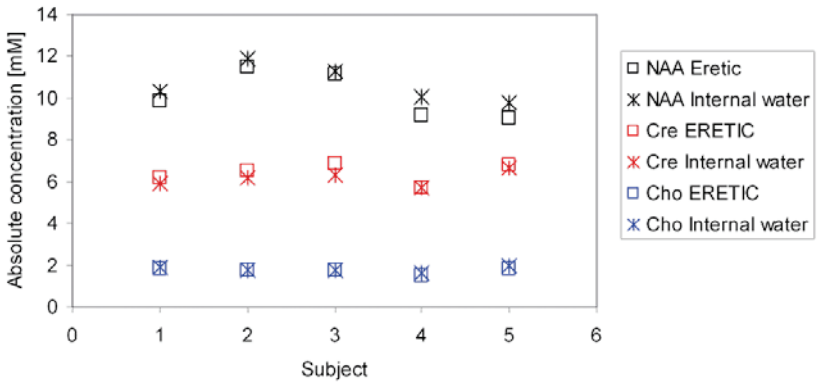

Figure 8 *Results of the in-vivo quantification with the absolute concentration values obtained with ERETIC calibration and the internal water reference method. A PRESS sequence was used to acquire spectra from five subjects.*

	NAA concentration/mM		Cho concentration/mM		Cre concentration/mM	
	ERETIC	Internal Water	ERETIC	Internal Water	ERETIC	Internal Water
S1	9.9	10.4	1.9	1.9	6.2	5.9
S2	11.5	11.9	1.8	1.8	6.5	6.2
S3	11.2	11.3	1.8	1.7	6.9	6.3
S4	9.1	10.1	1.5	1.6	5.7	5.7
S5	9.1	9.8	1.9	2.0	6.8	6.7
Average (± 1 SD)	10.1±1.0	10.7±0.8	1.8±0.1	1.8±0.1	6.4±0.4	6.2±0.3
Literature values[1]	12.1±0.8		1.7±0.3		6.7±0.4	
Literature values[2]	9.5±0.4		1.8±0.1		6.6±0.3	
Literature values[3]	11.2±1.2		1.8±0.3		6.1±0.8	
Literature values[4]	10.6±0.8		1.7±0.3		5.7±0.6	

Table 3 *Metabolite concentration values measured using internal water reference for subjects one through five (S1–S5) and averages over all subjects. Literature values: (1) Baker et al.,2008: 3T single-voxel PRESS study, corrections for T1, T_2 and cerebrospinal fluid content, internal water referencing; (2) Kaiser et al.,2005.: 4T single voxel STEAM study, no corrections applied, internal water referencing; (3) Michaelis et al, 1993.: 2T SV STEAM study, constant T2 correction for all measured locations, phantom calibration; (4) Pouwels et al, 1998.: 2T SV STEAM study, coil load correction, LCModel quantification*

In addition to a high in-vitro reproducibility (see methods, section 5), quantified water and metabolite concentrations recorded in-vivo are in the ranges

commonly reported in literature. The values in healthy volunteers compare well to the concentrations determined with the internal water reference method.
The ERETIC pulse has been completely integrated into the scanner software, which enables the user to turn on the quantification at the scanner console and to modify the ERETIC phase, shape, and amplitude for the spectroscopy measurement.

With this setup, the obtained quantification results exhibit similar measurement uncertainty as phantom replacement methods, yet allowing for calibration in a single scan and without manual adjustments of receiver gain settings and load.
Accurate quantification still requires compensation for B_1 field inhomogeneities.
The use of a birdcage coil significantly reduces B_1 field variations compared to other coil designs such as surface coils. In addition, the transmit B_1 inhomogeneity can be mitigated with adiabatic excitation schemes such as LASER (Garwood & DelaBarre, 2001) or precise power optimization based on iterative approaches as used in this work. Also, the transmit B_1 may be measured to correct for variations in a post-processing step. On the other hand, the receive B_1 field can change by more than 10 per cent over the entire brain when measuring proton spectra with such a transmit/receive volume coil (Wang *et al.*, 2005). For the experimental conditions considered in this work and at higher field strengths, transmission and reception patterns differ significantly and one may not be deduced from the other (Hoult, 2000). Coil receive sensitivity calibration would further improve the quantification results (Kreis, 1997). Its inclusion in the quantification with ERETIC based on the approach by Wang *et al.* (Wang *et al.*, 2005) or simulations (Moyher *et al.*, 1995) is a topic of ongoing research.

The minor differences between metabolite concentrations determined with the internal water calibration and the ERETIC reference methods (see methods, section 5) may be due to errors in the estimation of parameters. These include the assumed water content for white matter in case of internal water referencing, the estimation of the temperature correction factor when quantifying with the ERETIC method, or flaws in the determined T_1 and T_2 times. The slightly worse accuracy of the ERETIC method in comparison to internal water referencing may be the result of errors in automatic power optimization, which result in excitation angles slightly different from the nominal pulse angle and therefore altered metabolite signal amplitudes. However, this effect is not specific to the ERETIC method, but applies also to all phantom calibration methods.

Metabolite fitting and automatic internal water referencing were performed using LCModel, while the ERETIC peak was fitted using *TDFDfit.* This tool is better suited to fit the ERETIC peak since it allows for adjustment of individual lineshapes. The simple exponential decay used for the ERETIC pulse leads to a Lorentzian curve in the spectrum, while LCModel expects the Voigt shape exhibited by all metabolites. Future implementations will include an additional Gaussian windowing of the ERETIC pulse shape in order to enable a more streamlined spectral quantification with widely available fitting and quantification software such as LCModel or jMRUI.

2.7 Conclusion

In this paper, we have demonstrated the applicability of ERETIC in a clinical environment. The proposed setup, which employs an optical transmission line,

enables accurate quantification of metabolite concentrations in a single scan. In vivo quantification yields reliable results that are in good agreement with literature values and with internal water referencing.

For proton spectroscopy, quantification using the ERETIC method leads to accurate metabolite concentrations even in cases where the tissue water concentration or water relaxation behavior (T_1, T_2) are altered. Such changes may occur in various lesions, whose investigation is currently one of the main applications for clinical ^{1}H MRS. ERETIC is therefore ideally suited for the acquisition of reliable quantitative ^{1}H spectra in a clinical environment.

Chapter 3:

QUANTIFICATION OF METABOLIC PARAMETERS BY ^{31}P MRS

3.1 Introduction

Phosphorus spectroscopy. ^{31}P spectroscopy has become a popular means to assess dynamic metabolic processes in muscles *in vivo*. Its relatively high sensitivity (approximately 7% of ^{1}H), together with a 100% natural abundance and the lack of a baseline allows for the acquisition of high quality spectra within a few minutes. Furthermore, the chemical shift dispersion is large (20-30ppm), so that an excellent spectral resolution can be reached. In addition to the determination of all fundamental metabolites that are involved in energy metabolism, functional metabolic parameters such as pH (Petroff *et al.*, 1988), Mg^{2+} concentrations (Gupta & Moore, 1980), equilibrium constants of a certain fraction of creatine kinases (Wallimann, 1996), and ADP concentrations (Veech *et al.*, 1979) can be indirectly deduced.

Internal reference standard. Accurate quantification of millimolar metabolite concentrations presents a lot of challenges (see Chapter 1: QUANTIFICATION). In contrary, relative quantification is comparatively straightforward if a few rules are followed. The metabolite that is chosen as a standard inside the measurement voxel will experience the same local B_1 and B_0 fields, and receiver gains, coil loads and temperatures that are equal to the quantified metabolite.

Internal water referencing has previously been used for quantification of metabolites in ^{31}P spectra. To achieve this, dual-tuned coils are needed (Thulborn & Ackerman, 1983; Buchli & Boesiger, 1993). However, an exact calibration for the sensitivity difference between the water and ^{31}P channel is required for an accurate quantification, which requires a lot of diligence since that calibration factor also depends on the coil load (for further reference, see (De Graaf, 2007) and (Buchli & Boesiger, 1993)). .

Adenosine tri-phosphate (ATP) has been used as an internal reference in many muscle physiology studies (i.e. in (Taylor *et al.*, 1986; Blei *et al.*, 1993; Conley *et al.*, 2000), among many others). It is the universal form of immediately available energy in the cell. The ATP concentration in skeletal muscle is kept at approximately 8.2mM and only varies little if the system is only mildly challenged (De Graaf, 2007). In previous studies, no differences in ATP concentration could be found between trained and untrained subjects (Nevill *et al.*, 1989) and relative resting PCr/ATP ratios did not differ between trained and untrained groups (McCully *et al.*, 1989; Johansen & Quistorff, 2003).

Calibration with an internal reference of the same nucleus, such as ATP in the case of ^{31}P spectroscopy, is especially convenient if surface coils are used for the acquisition of un-localized spectra. Although their field homogeneity is low, surface coils have a high sensitivity in proximity to the surface. The localization area corresponds approximately to a hemisphere of one coil radius in which the sensitivity decreases with increasing distance from the coil. Surface coils may be used in combination with localization schemes such as ISIS. However, unlocalized spectroscopy scans are often performed for a better SNR. If they are performed using adiabatic pulses at a TR > 5*T_1, the B_1 and T_1 sensitivity can be eliminated altogether (De Graaf, 2007).

3.2 ^{31}P metabolites in muscle

Adenosine tri-phosphate (ATP)

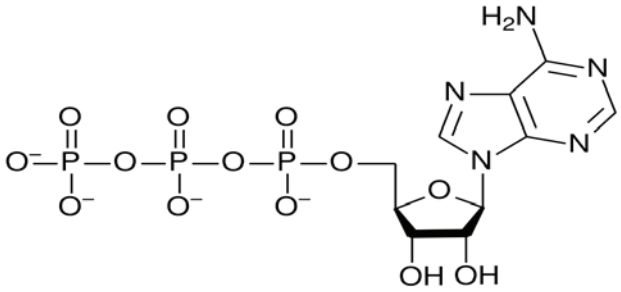

Figure 9 *Adenosine tri-phosphate (ATP) molecule with ribose ring, adenine moiety and tri-phosphate group. The terminal phosphate is split off in the process of energy release. Image source: http://en.wikipedia.org/wiki/Adenosine_triphosphate.*

ATP consists of a sugar ring, an adenine moiety and a terminal tri-phosphate group (Figure 9). Its phosphate groups can be split off by enzymes to release energy for muscle contractions (Figure 10, Figure 11), for the synthesis of biological membranes or organic molecules. In the splitting process, adenosine di-phosphate (ADP) and adenosine mono-phosphate (AMP) are formed and inorganic phosphate is released. Approximately 32.2kJ/mol energy are obtained for each splitting process. If ATP exceeds the equilibrium concentration in a healthy subject, the phosphocreatine stores are replenished, and if it is below equilibrium concentration, energy generating processes are activated. These

involve oxidative phosphorylation, glycolysis and transfer of a phosphate group from phosphocreatine to ADP.

In ^{31}P spectroscopy, ATP gives rise to three distinct peaks (see Figure 12) at -7.52ppm (α-ATP), -16.26ppm (β-ATP), and -2.48ppm (γ-ATP). The muscle ATP concentration remains constant throughout exercise and at rest (see Introduction). In the muscle, ATP is hydrolyzed during muscle contraction. Myosin, a motor protein, moves along actin fibers in the contractile parts of the myofibrils, the so-called sarcomeres (Figure 10). This then leads to a shortening of the muscle.

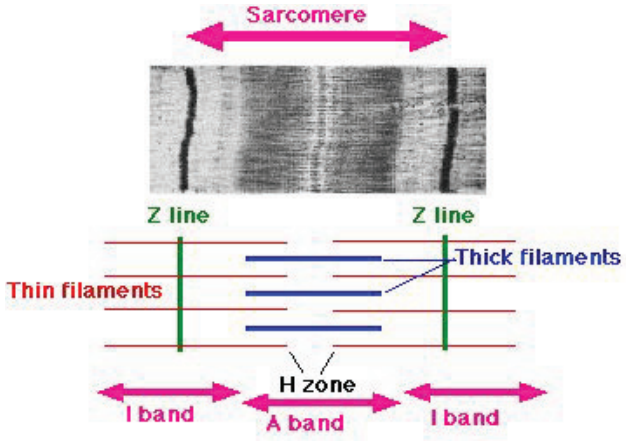

Figure 10 *Cross-section through a sarcomere. Movements of myosin (thick filaments) along the actin fibers (thin filaments) lead to a shortening of the muscle. Image source: http://de.wikipedia.org/wiki/Sarkomer.*

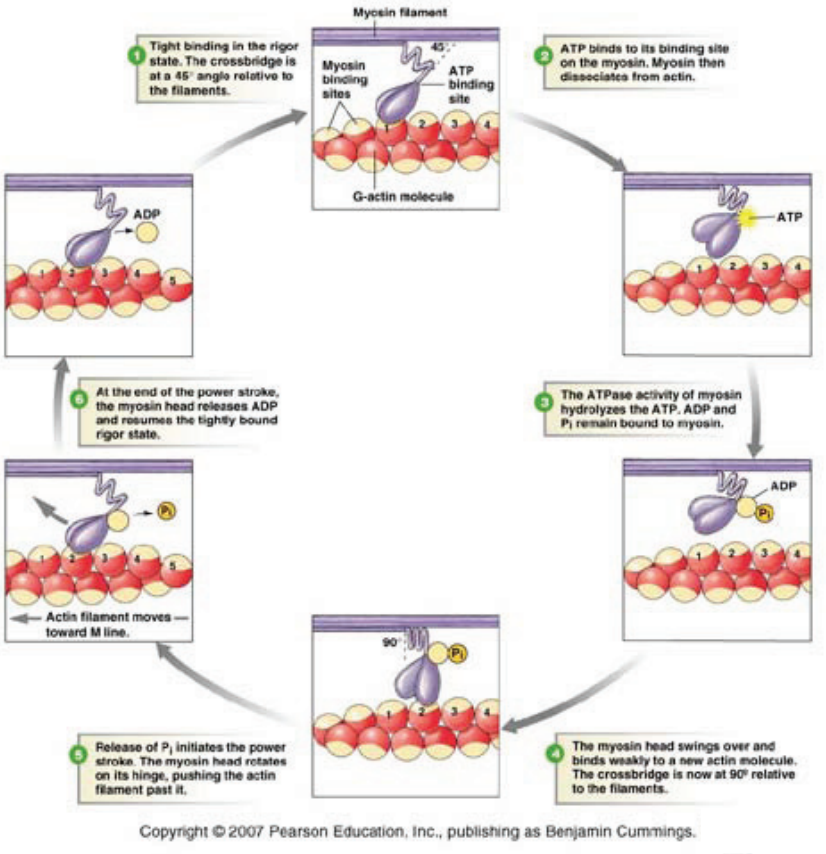

Figure 11 *Myosin, a motor protein, moves along actin fibers in the muscle and enables muscle motion through the use of ATP. Drawing according to the findings of (Rayment et al., 1993).*

Adenosine di-phosphate (ADP)

Adenosine di-phosphate (ADP) is the breakdown-product of ATP and plays an important role in the body as a signaling molecule. It is involved in regulating processes such as glycolysis, gluconeogenesis, and ion transport (Koretsky *et al.*, 1990). In MR spectra, the resonances of ADP appear at -7.05ppm (α-ADP), and -3.09ppm (β-ADP). However, they remain invisible due to the low NMR-visible concentration of ADP, which is at about 6μM in muscle tissue (Roth & Weiner, 1991). Cellular reactions near equilibrium can be used for the calculation of free metabolites at low concentrations. The free ADP concentration can be calculated from

$$K_{eq} = \frac{[Cr][\sum ATP]}{[PCr][\sum ADP][H^+]} \qquad \textbf{Equation 13}$$

The pH can be determined using the chemical shift difference between P_i and PCr. However, one has to be aware that this requires assumptions on the equilibrium constant K_{eq} of the creatine-kinase reaction and creatine (Cr) concentration values (i.e. 15% of the total creatine pool). The equation does not account for variable Mg^{2+} binding and the effect of pH on the equilibrium concentration, which imposes problems for the calculation of ADP concentrations under exercise (Roth & Weiner, 1991).

Phosphocreatine (PCr)

Phosphocreatine (PCr), also known as creatine phosphate, acts as high-energy reserve. The energy given off from donating the phosphate group is used to regenerate ATP. Phosphocreatine plays a particularly important role in tissues

that have high, fluctuating energy demands such as brain and muscle. Its stores can be rapidly depleted in the first few seconds of muscle contraction before the onset of glycolysis and oxidative phosphorylation. In addition, phosphocreatine is an energy shuttle that can diffuse from the energy-producing sites such as mitochondria, to the energy-utilizing sites. In MRS, the resonance of PCr is assigned a chemical shift of 0ppm (Figure 12).

Inorganic Phosphate (P_i)

Inorganic phosphate is a prerequisite for oxidative phosphorylation in muscle mitochondria (for further reference see Chapter 5: Introduction) and reaction product of ATP hydrolysis (Equation 14):

$$ATP + H_2O \leftrightarrow ADP + P_i \qquad \textbf{Equation 14}$$

In addition, it is a buffering agent that is involved in the regulation of metabolic pathways in muscle cells (Walsh *et al.*, 2002), such as glycolysis (Khoja, 1986; Rush & Spriet, 2001).

In skeletal muscle, the P_i concentrations are generally low (around 3-5mM) and the resonance is sometimes completely missing in muscle spectra at rest. If present, the P_i resonance is found at 5.02ppm (Figure 12).

Phospho-Monoesters (PME) and Phospho-Diesters (PDE)

The phosphomonoester and phosphodiester peaks are not always well visible in muscle spectra whereas they are easily recognized in brain spectra. The main constituents of the PME resonance are phosphorylethalonamine (PE) and phosphorylcholine (PC), whereas PDEs are mainly composed of glycero-phosphorylcholine (GPC) and glycerol-phosphorylethanolamine (GPE). PMEs and PDEs are involved in membrane synthesis and degradation. Their

resonances can be found at 5.88 ppm (PC), 6.78 ppm (PE), 2.76ppm (GPC), and 3.20 ppm (GPE).

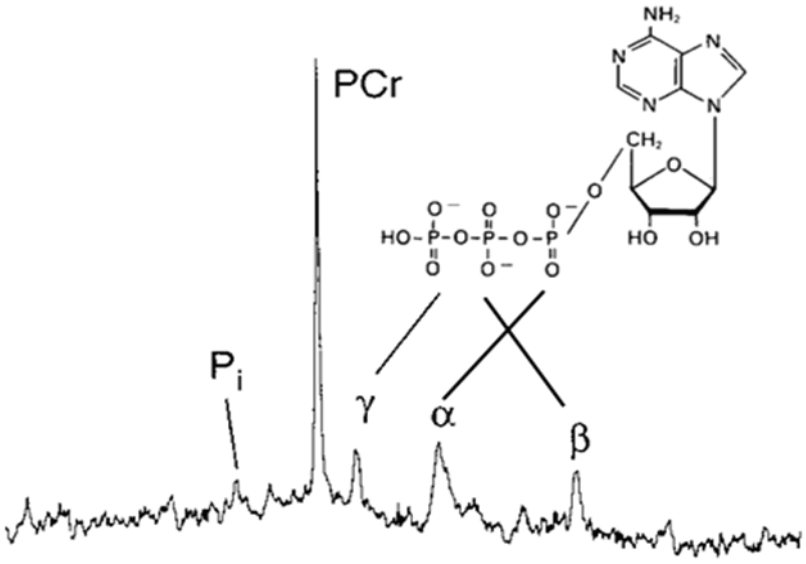

Figure 12 *Typical ^{31}P MRS spectrum of a human muscle. Image source: (De Graaf, 2007), Figure 2.29.*

3.3 Parameters that can be accessed using ^{31}P MRS

Measurement of the pH

The chemical shift of certain metabolites that are visible by using ^{31}P MRS is strongly influenced by the pH and the concentration of Mg^{2+}. A protonated or complexated form of a metabolite will have a different resonance than its non-

protonated/complexated equivalent. However, if the exchange between these two forms is fast, only one peak with an average resonance frequency can be seen in the spectrum. The frequency of that peak then indicates the ratio of the two forms of the metabolite. Inorganic phosphate is a good indicator for pH changes (pK = 6.77), while the PCr resonance frequency stays approximately constant in the physiological pH range (pK = 4.3).

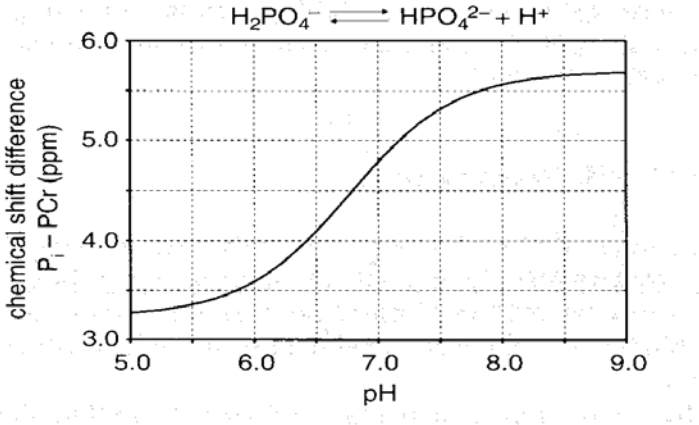

Figure 13 *pH calibration curve for the P_i-PCr system as used for the determination of intracellular pH with in vivo ^{31}P MRS. The curve is described by Equation 15 with pK 6.77, δ_{HA} = 3.23 ppm and δ_A=5.70 ppm. Image source: (De Graaf, 2007), Figure 2.30.*

The expected chemical shift differences between P_i and PCr at different pH values are shown in Figure 13. The pH can be calculated using a modified Henderson-Hasselbalch equation (Petroff *et al.*, 1988):

$$pH = pKa + \log\frac{\delta - \delta_{HA}}{\delta_A - \delta} \qquad \textbf{Equation 15}$$

In the above equation, δ is the observed chemical shift of P_i, δ_A and δ_{HA} are the chemical shifts of the protonated and unprotonated forms of P_i (at 5.7 and 3.23ppm, respectively), and pKA is the logarithm of the equilibrium constant for the acid-base equilibrium between the protonated and unprotonated form of P_i.

PCr recovery constant and oxidative muscle function

Phosphocreatine is depleted during exercise and recovers subsequently. It has been shown that the rate of phosphocreatine (PCr) resynthesis after muscle exercise depends entirely on mitochondrial respiration (Taylor *et al.*, 1983; Arnold *et al.*, 1984). It is therefore a valuable index for the *in vivo* assessment of mitochondrial respiratory function by ^{31}P MRS. It has to be taken into account that mitochondrial respiration, in turn, is influenced by several factors, such as pH and inorganic phosphate concentrations, as well as enzyme concentrations (Walsh *et al.*, 2002).

3.4 Objectives

The goal of the second part of this thesis was to develop an ergometer setup (Chapter 4) and quantification method for reliable and reproducible determination of metabolic parameters and phosphorus metabolite concentrations *in vivo*. Consequently, this setup should be applied to physiological studies (Chapters 5 & 6).

^{31}P spectroscopy has a 100 times lower sensitivity than ^{1}H spectroscopy and the investigation of dynamic metabolic changes require a sufficiently high temporal resolution. Hence, the acquisition of average spectra form large volumes is

necessary to achieve a good SNR in a short amount of time. The use of a surface coil contributes to optimal SNR performance and is compatible with the ergometer setup. In the performed studies, no additional volume selection was performed and an adiabatic excitation pulse was used to further increase the SNR. Although attempts have been made to apply the ERETIC method (see Chapter 2) in combination with surface coils (Lee, 2007), a reliable quantification using this method depends on a homogeneous B_1 field and a well-defined localization volume. Therefore, another quantification technique was applied, which was based on the use of ATP as an internal reference standard.

In a first study, the developed ergometer setup (see Chapter 4) and quantification approach was tested for its test - retest reproducibility. It was subsequently used to assess the effect of physiological training (Chapter 5) and Diabetes Type 1 on muscle metabolism (Chapter 6)

Chapter 4:

DESIGN OF AN ERGOMETER SETUP FOR IN-VIVO MRS STUDIES OF SKELETAL MUSCLE METABOLISM

4.1 Introduction

Magnetic resonance spectroscopy (MRS) has become a popular means to assess dynamic metabolic changes in skeletal muscle during exercise. ^{31}P MRS allows for the measurement of cytosolic pH and the concentrations of ATP, phosphocreatine, and inorganic phosphate during exercise and recovery.

In order to study metabolism during muscle contractions in an MR scanner, ergometers have to be designed that are compatible with the unique field and material constraints which are imposed by the scanner and provide comfortable positioning and good fixation of the subjects. Several measurement setups have been constructed for the measurement of dynamic spectroscopic data during isometric contractions (Miller *et al.*, 1988; Bangsbo *et al.*, 1993; Raymer *et al.*, 2006). However, these ergometers are either limited in their ability to quantify forces, or visual feedback on the momentary contraction is not available. We have designed and constructed an MRS dynamometer for the measurement of muscular force during isometric contractions of the plantarflexor muscles against the pedal. Key features of the setup are a pedal with an integrated strain gauge, adjustment of ankle joint angle over the physiological range, leveling of dynamometer height, and real-time visual feedback for subjects on maximal voluntary contraction (MVC) during contractions. To account for the specific design and material constraints imposed by the magnetic field, non-magnetic materials were used and force values were transmitted optically. Using this setup, we have been able to follow inorganic phosphate an phosphocreatine

time courses as well as pH changes during isometric contractions at targeted MVC levels.

4.2 Materials and Methods

The ergometer is designed to fit into a standard 3T Philips Achieva whole-body MR scanner (Philips Healthcare, Best, the Netherlands).

The ergometer setup has to fulfill several requirements: (1) A good fixation of the subject's leg and foot is needed in order to minimize movements and compensatory force production upon exhaustion, (2) the shoulders must be fixed with a device that can be adjusted to the subject's height, (3) accurate force measurement and (4) a visual feedback for the volunteer is required so that a specific target force over time can be maintained, (5) a scanning software needs to be available which allows for triggering of the measurement, (6) and the foot angle needs to be freely adjustable within the physiological range to optimally address a specific target muscle group. (7) In addition, the measurement setup has to be MR compatible.

MR compatibility

The frame of the pedal is made from polyvinyl chloride (PVC), and Plexiglas® and Ertalite® were used for the foot holder. A support was built on which the pedal is held in a central position to enable measurements in the iso-center of the scanner, while still leaving enough space for comfortable positioning of the second leg. The support is made from aluminum for better stability- it was assured that the distance from the measurement coil was far enough so that the

occurrence of artifacts could be excluded. The entire support is screwed onto the scanner bed.

Ertalite® screws are mounted to the side of the pedal holder to allow an easy adjustment of the foot angle. The angulation of the ankle can be adjusted from 70-120 degrees in steps of 5 degrees. A custom built, MR-safe strain gauge (ETH Zurich, Sensory-Motor Systems Lab, Zurich, Switzerland) is positioned behind the foot plate and measures the force produced by the plantarflexor muscles. It contains an optical link to transmit the signal to a fMRI software (Presentation®, Neurobehavioral Systems, USA). The optical link guarantees a reliable force signal transmission throughout the scan.

The dynamometer is freely adjustable in height to account for the foot size. The ergometer is placed in the iso-center of the bore so that either the left or the right leg can be measured. The non-exercising leg can be comfortably placed beside the ergometer.

Fixation

A photograph of the fixation and placement of the volunteer with the MR-compatible ergometer is shown in Figure 14. Velcro® straps are used to fasten the foot onto the footplate. The foot angle can be adjusted for any measurement and the straps guarantee identical joint angles during the measurement. A Plexiglas® plate with a wide leg strap is placed under the upper leg to tighten it to the measurement table. It provides a good fixation of the leg during muscle contraction and prohibits leg movements during the scan. The position of the Plexiglas® plate on the scanner bed can be freely adjusted using Ertalite® screws and bars inserted into the narrow channels present at the edge of the scanner bed.

A Plexiglas® shoulder and head support was built to prevent movements of the volunteer in the longitudinal direction of the scanner. Cushions above the shoulders and beneath the head provide comfortable positioning for the subject. A mirror is placed above the head and shoulder support so that the subject can see the exerted force value and general instructions which are displayed on a screen inside the scanner room.

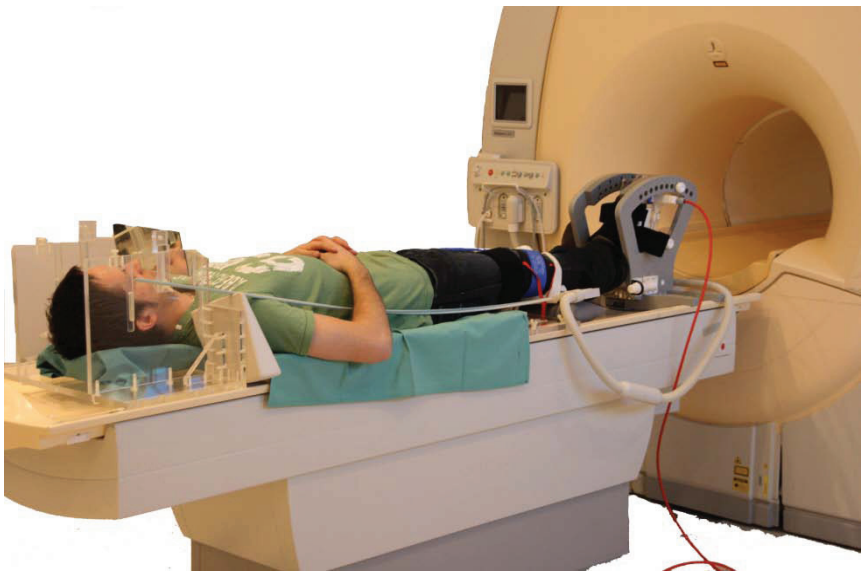

Figure 14 *Photograph of the MR-compatible ergometer with the leg and foot straps, head and shoulder support, and the optical cable (red) leading to the console room.*

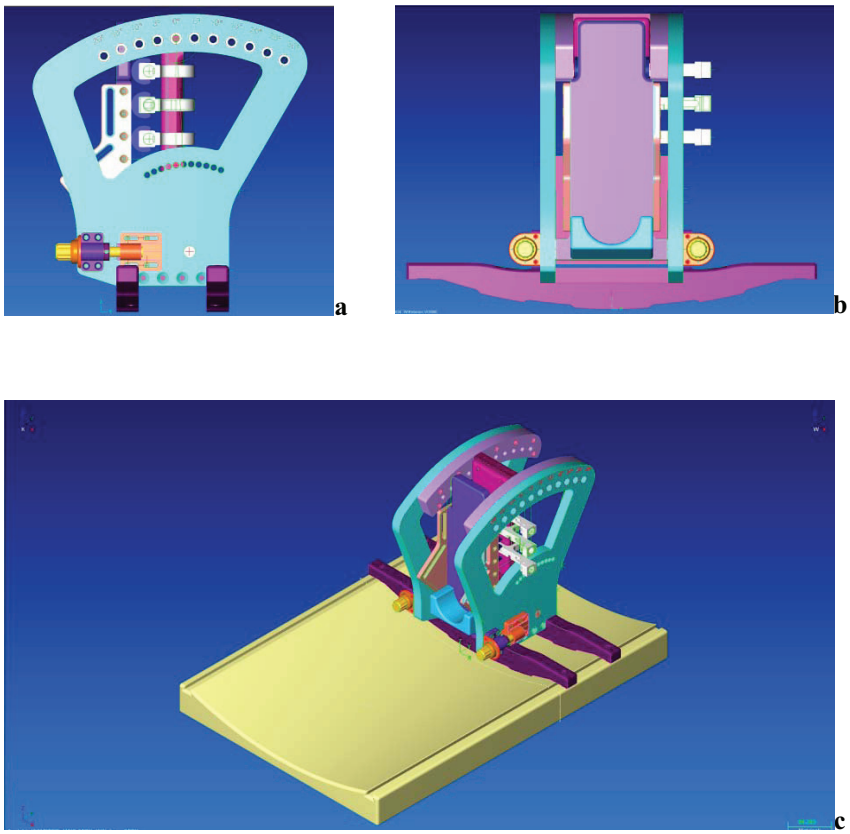

Figure 15 *Computer assisted design (CAD) drawings of the ergometer setup. (a) View from the side, where the holes for the adjustment of the angulation can be seen. (b) View from the front. The holder for the ankle is shown in green, and two straps are then used to secure the foot. (c) Placement of the pedal on the scanner board. Aluminum bars (purple) are used for a rigid fixation of the pedal.*

Software

The measured force value is transmitted to an fMRI software (Presentation®, Presentation, Neurobehavioral Systems, USA), which converts the absolute force values to relative MVC levels. The exerted force level and a target level are then displayed to the subject. Through the visual feedback on MVC, it is guaranteed that all subjects will apply the same percentage of their MVC for a given measurement. Importantly, this enables a standardization of the exercise protocol.

The Presentation® software is triggered by the scanner so that a specific number of spectra can be acquired before the dynamic scan and the display start. If the target force level cannot be maintained for a continuous period of 5 seconds, the display of the target force level is turned off and the exercise is stopped.

Measurements

Positioning of the subject begins by securing the heel in the foot holder and fastening the foot using two Velcro® straps. The ^{31}P spectroscopy surface coil is then placed under the lower leg of the subject before the upper leg is fastened onto the Plexiglas® plate. Subsequently, the head and shoulders are fixated. The subject then exerts a single contraction against the pedal to determine the maximal voluntary contraction force. A certain percentage of this value (70-85%) of this value is then used as target force for the actual spectroscopic measurement. For the acquisition of the spectra, a non-localized excitation is performed using an adiabatic excitation in a pulse-acquire scheme (TR = 1.5s). Twenty spectra are acquired in resting state before the start of the Presentation® software is triggered. The target force level is displayed to the subject and has to be rapidly reached. If the subject is unable to maintain the target force level

and does not reach it again within 5 seconds, the display is turned off and the subject is told to stop the contraction so that the recovery of the metabolite concentrations and pH values can be followed. The reliability of the setup was tested in a study using nine female volunteers. Subjects were measured in two dynamic scans, one with a target force of 85% MVC for 30s and one with a target force of 70% MVC for 120s. Re-test measurements were performed for each subject on different days.

Spectral postprocessing. All free-induction decays (FIDs) were zero-filled to 4096 points, line-broadened with 6 Hz and Fourier-transformed into spectra. We used *tdfdfit* software (Slotboom *et al.*, 1998) for fitting the line-shapes and integrating the metabolite peak areas and calculated inorganic phosphate (P_i) and phosphocreatine (PCr) concentrations using the PCr/ATP and the P_i/ATP ratios. A concentration of 8.2 mM was assumed for ATP (Arnold *et al.*, 1984; Kemp & Radda, 1994).

4.3 Results

All subjects reported that they were comfortable within the scanner at rest. One subject reported a minor discomfort in the shoulder region during heavy exercise, which was ameliorated using thicker cushions. There was adequate room for the non-exercising leg.

The acquired spectroscopy scans showed a nice decrease in PCr and recovery of P_i and PCr concentrations could be easily followed (Figure 16). The exerted force as well as dynamic changes of metabolic parameters can be accurately determined for both lower legs.

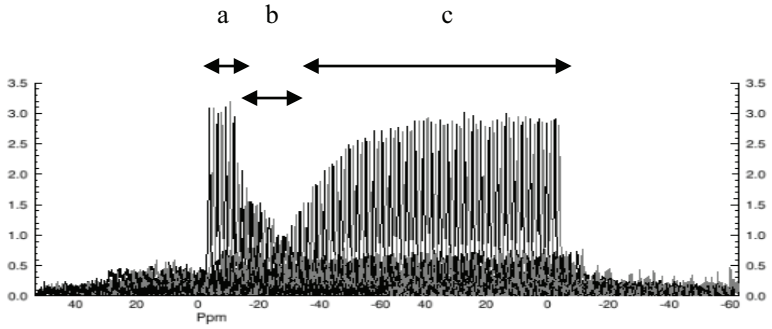

Figure 16 *Phosphorus spectrum acquired with the above setup. The volunteer had to press at 85% of his maximal voluntary contraction for 30s (b) after the acquisition of 20 baseline scans (a). Phosphocreatine [PCr] recovery (c) was subsequently measured.*

A good standardization of the measurements could be reached, as can be seen by a similar phosphocreatine, inorganic phosphate and pH curves in the test and re-test measurements (Figure 17) that were performed on different days.

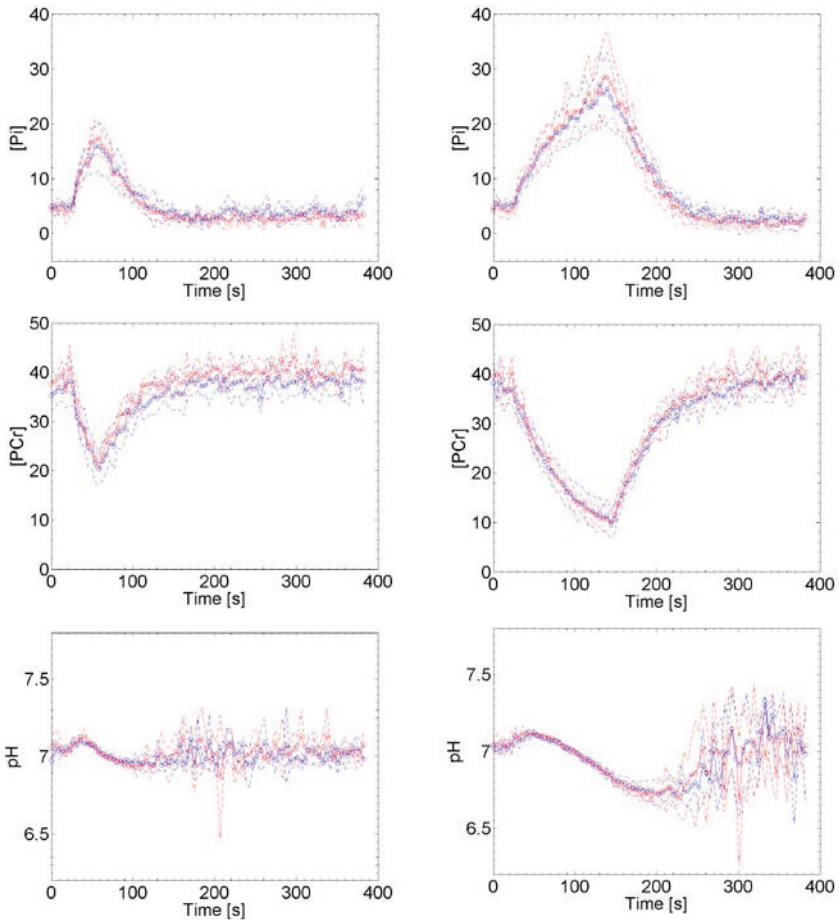

Figure 17 *Time curves for the inorganic phosphate (top), pH (middle) and phosphocreatine (bottom) in the 30s (left) and 120s exercise (right) for the test (blue) and re-test (red) measurements.*

4.4 Discussion

We have described a MR-compatible exercise ergometer setup with a visual force feedback that is well suited for the measurement of metabolic parameters during isometric contractions. The ergometer setup provides the basis for the acquisition of well-standardized spectroscopy scans during exercise. Standardization is an important issue for the acquisition of dynamic spectroscopy scans since the changes in metabolite concentrations scale with the exercise intensity.

Chapter 5:

EFFECTS OF TRAINING UNDER ISCHEMIA ON MUSCLE METABOLISM

5.1 Introduction

Phosphorus spectroscopy is a valuable tool for studying muscle metabolism non-invasively. Resting metabolite concentrations as well as dynamic changes of important metabolites that are involved in energy metabolism can be observed. To assess functional and metabolic changes that occur after a newly developed ischemic exercise training paradigm, in this study, ^{31}P MRS data was analyzed. 12 healthy females (INT) were trained for five weeks on a vibration plate under ischemic conditions. Before and after the training period, metabolic parameters were assessed using phosphorus magnetic resonance spectroscopy (^{31}P MRS). Post-exercise phosphocreatine (PCr) recovery from isometric contractions at fixed force levels normalized to maximal force against a foot-pedal was measured. In addition, time series data of pH, PCr and inorganic phosphate (P_i) during isometric contraction were obtained, and resting metabolite levels, pH, muscle fiber composition as well as body functions were derived. Nine healthy female controls (CON) matched for age, activity level and BMI performed test and retest measurements without training.

Elevated resting [P_i] (brackets denote concentration) levels were measured after five weeks of ischemic training. Also, significant increases of P_i were observed during isometric contractions at long contraction times. Increases in capillarisation as measured with muscle biopsies, stronger maximal forces, and increases in muscle volume show further adaptations to ischemic training. The increase in inorganic phosphate concentration at rest likely indicates a shift in muscle fiber type composition towards more oxidative fibers, whereas the increase in P_i during exercise may serve as a modulator of oxidative metabolism inside the muscle cells.

Inorganic phosphate is a prerequisite for oxidative phosphorylation in the mitochondria, where it is used to form adenosine triphosphate (ATP). In addition, P_i plays an important role as a buffering agent and in the regulation of metabolic pathways in muscle cells (Walsh *et al.*, 2002), such as glycolysis (Khoja, 1986; Rush & Spriet, 2001).

In previous ^{31}P studies, increases in [P_i] have been observed in mitochondrial cytopathies (Chance *et al.*, 2006), with cast immobilization (Pathare *et al.*, 2005), in ischemic conditions in the myocard (Allen & Orchard, 1987), and in muscle of chicken following ischemia (Klabunde & Mayer, 1979). However, the mechanisms that lead to changes in [P_i] and its regulatory functions in vivo are still not completely understood. Regulatory effects of increased [P_i] include the enhancement of NADH generation (Bose *et al.*, 2003), swelling of mitochondria in the presence of substrate (Anagnosti & Tedeschi, 1970; Izzard & Tedeschi, 1973; Halestrap, 1994), decreases in the mitochondrial Mg^{2+} concentrations (Garlid, 1980; Gunter *et al.*, 1988; Jung *et al.*, 1990), and activation of glycolytic enzymes (Khoja, 1986; Rush & Spriet, 2001).

In addition, mitochondrial respiration is influenced by changes in inorganic phosphate concentrations. Mitochondrial respiration is an important metabolic process where the driving power (proton motive force) for ATP production is generated. Electrons are transported through an electron transport chain onto molecular oxygen. A modulatory effect of P_i on mitochondrial creatine kinase (CK), a key enzyme involved in mitochondrial respiration, has been reported as early as 1979 (Vial *et al.*, 1979). Further work on isolated heart mitochondria (Mukherjee *et al.*, 1980; Hall & Deluca, 1984), skinned cardiac fibers (Veksler & Ventura-Clapier, 1994) and soleus muscle fibers (Walsh *et al.*, 2002) have demonstrated that *in vitro*, concentrations in P_i up to 5 mM increase the maximal rate mitochondrial respiration, but when [P_i] exceeds 5 mM, CK starts

to dissociate from the inner mitochondrial membrane and the rate of respiration in presence of creatine decreases. This decrease is likely caused by longer diffusion paths of ATP before it reaches the CK (Hall & Deluca, 1984).

Following the above *in vitro* experiments, it has been hypothesized that increases in $[P_i]$ at low concentrations may be the primary feedback signal for stimulation of oxidative phosphorylation in the heart muscle *in vivo* at different workloads (Wu *et al.*, 2008), while the primary role for stimulation of oxidative phosphorylation has been assigned to adenosine di-phosphate (ADP) in skeletal muscle (Balaban, 1990; Brown, 1992).

Resting P_i concentrations in skeletal muscle remain at levels around 3-6 mM (Chance *et al.*, 2006) depending on the fiber type composition of the muscle (Kushmerick *et al.*, 1992; Takahashi *et al.*, 1996). During high-intensity exercise, $[P_i]$ can increase to concentrations well above 20 mM (Sahlin *et al.*, 1997). At such elevated concentrations, P_i induces concentration-dependent reductions in mitochondrial respiration in isolated soleus muscle fibers (Walsh *et al.*, 2002), as was determined by polargraphic measurements.

Measuring a number of key energy metabolites *in vivo* is possible using ^{31}P magnetic resonance spectroscopy (MRS), in which signals from phosphocreatine, adenosine tri-phosphate (ATP) and inorganic phosphate, as well as intracellular pH are quantifiable from measured spectral intensities. While saturation transfer experiments for the measurement of CK flux only access a small proportion of the total CK (van Deursen *et al.*, 1994; Wallimann, 1996), stimulation-recovery experiments allow for the assessment of full mitochondrial CK functionality through the recovery curve of the PCr that is resynthesized by the enzyme. Phosphocreatine resynthesis after exercise depends on oxidative ATP synthesis (Sahlin, 1978; Taylor *et al.*, 1983) and therefore provides information about the mitochondrial function. However,

many factors can influence the phosphocreatine resynthesis rate. A strong correlation of τ_{PCr} with the intracellular pH after exercise has been shown in many studies ((van den Broek *et al.*, 2007) and references cited therein), while the direct effects of low pH on mitochondrial respiratory rates remain unknown. Reports range from inhibition (Harkema & Meyer, 1997; Walsh *et al.*, 2002) to increased respiratory rates (Connett, 1988; Funk *et al.*, 1990). In addition to a correlation of τ_{PCr} with pH, several reports have shown a correlation of the end-exercise P_i concentrations with τ_{PCr} (i.e. (Kemp *et al.*, 1993)).

In this study, we correlate the PCr recovery constants with pH and $[P_i]$ at the end of isometric contractions before and after five weeks of ischemic training. ^{31}P MRS, magnetic resonance imaging (MRI), dual X-ray absorptiometry (DXA) and muscle cell assays are used to assess muscle metabolism at rest.

5.2 Research Design and Methods

Subjects

We recruited 21 sedentary young women and randomly assigned them to two groups. Twelve healthy (asymptomatic) females were assigned to an intervention group (INT). Nine healthy subjects matched for age, BMI, and activity level were recruited in a control (CON) group. A higher number of subjects was assigned to the INT group because of a higher risk for study dropouts. All subjects were untrained with physical activity of less than half an hour twice a week. Nine and seven women in INT and CON, respectively, were taking oral contraceptives. Physiological parameters are listed in Table 4. After completing a routine health questionnaire, the participants were informed about

the procedures applied and about the associated risks. The participants then signed an informed consent. All experiments were approved by the ethics committee of the canton of Zurich. The study was performed in accordance with the ethical standards laid down in the Declaration of Helsinki for human experimentation.

	INT	CON
Age (Y)	23.5 ± 3.0	24.5 ± 3.8
Body Height (m)	1.68 ± 0.06	1.68 ± 0.07
Body Weight (kg)	61.0 ± 8.2	60.7 ± 5.4

Table 4 Characteristics of subjects in the intervention and control groups

Study design and exercise protocol

The study consisted of 1) baseline measurements (subsequently labelled PRE); 2) five weeks of progressive exercise for INT or a similar period without exercise for CON; and 3) post-intervention measurements (labelled POST). The exercise regimen was designed according to the recommendations of (Toigo & Boutellier, 2006). During the study, macronutrient intake was not monitored, and participants were not given any food or dietary supplements.

Baseline measurements. We performed baseline measurements to assess resting metabolite levels, PCr, P_i and pH time curves during isometric contractions, task-specific strength, calf lean mass and capillary to fiber ratio. Participants

were familiarized with the training and/or strength testing procedures on two separate occasions before the actual measurements.

Training protocol. A detailed description of the training protocol is given elsewhere (Toigo *et al.*, 2010). In brief, participants of the INT group performed three supervised progressive training sessions per week on alternate days for five weeks (16 training sessions), followed by three training sessions with the same load as during the last progressive training session.

A warm-up phase was followed by six sets of resistance exercise with both, superimposed vibration exercise and vascular occlusion: Three sets of loaded (Multipower®, Technogym, Gambettola, Italy) squats were performed while standing on a Galileo® side-alternating vibration platform (Novotec, Pforzheim, Germany) (Rittweger *et al.*, 2001) oscillating at 30 Hz. These were followed by three sets of loaded heel rises on the vibration platform which alternated between sessions as follows: 2 sets of heel rises while standing and 1 set of seated heel rises or vice versa. For both, squat and heel rise exercise a set of 4 min on and 1 min off was employed, whereas between squats and heel rises, participants rested for 5 min. Vascular occlusion during the exercise was induced by inflating tourniquet cuffs (VBM, Sulz a.N., Germany) to suprasystolic pressure, i.e. 197 (3) mmHg [SI: 26.26 (0.40)10^3 Pa]. The cuffs were affixed to the inguinal fold region of the thigh, or to the proximal portion of the lower leg, centered in the space between the superior aspect of the gastrocnemius muscle and the inferior edge of the patella. For both, squat and heel rise exercise, tourniquet cuffs were inflated right before the first set and remained inflated until the 4 min of vascular occlusion were complete. The cuffs were then deflated to a pressure of 100 mmHg (SI: 13.33·103 Pa), and the

participants rested for 1 min before the cuffs were quickly reinflated for the subsequent set.

Post-intervention measurements

The post-intervention measurements were identical in all respects to the baseline measurements.

Magnetic Resonance Spectroscopy

Dynamic ^{31}P magnetic resonance spectroscopy (^{31}P-MRS) scans were acquired during isometric muscle contraction using a 3 Tesla whole body Philips Achieva Scanner (Philips Healthcare, Best, The Netherlands). For this purpose, we designed an MRS-compatible ergometer setup (Heinzer-Schweizer *et al.*, 2009), which was comprised of a dynamometer with an integrated strain gauge (Sensory-Motor Lab, ETH Zurich, Switzerland) for force measurements (see **Figure 14**), a real-time visual feedback system providing the participants with information on the level of exerted force relative to maximal voluntary force, and an appropriate fixation of the leg and body. Presentation® software (www.neurobs.com) was used for the implementation of a visual feedback system and the display was triggered using the scanner software. During the measurements, the participants lay supine on the scanner bed with their non-dominant leg in the centre of the scanner bore. We fastened the foot of the leg to be measured onto the foot holder at an angle of 100° plantarflexion using Velcro® straps. The exercising leg was held in place with a 0.06 m wide strap above the knee to minimize any quadriceps muscle force contribution. The knee of the exercising leg was almost fully extended (170°) to allow near-physiological conditions for calf muscle exercise (Quistorff *et al.*, 1990).

A transmit/receive surface coil (diameter: 14 cm) tuned to 51.8 MHz was placed under the participant's calf and fastened with a Velcro® strap. This way, the field of view (FOV) of the coil included signal from the triceps surae muscles with the main contribution stemming from the gastrocnemius muscle. Prior to the isometric contraction experiment in the magnet, each participant was familiarized with the setup. After the practice session, images of the lower leg were acquired at rest, covering an area from the knee to the ankle. 60 slices of these localizer images were collected using the body coil of the scanner in a turbo-spin echo (TSE) sequence (echo time TE = 6.95 ms, repetition time TR = 399 ms, slice thickness = 6 mm, field of view FOV = 162x162 mm) in 3 stacks to ensure magnetic field homogeneity over the entire volume.

Following the imaging session, the participants performed a single maximal voluntary plantarflexion attempt against the fixed dynamometer pedal, and we measured the maximal force acting on the pedal (MVF_P). ^{31}P-MRS spectra of the triceps surae muscles were acquired using a pulse-acquire technique and an adiabatic hyperbolic secant excitation pulse. A 2nd order FASTERMAP (Gruetter, 1993; Shen *et al.*, 1997) volume shim was applied, and the shim volume was optimized so that bones and fat were excluded from the shim procedure. After acquisition of a fully relaxed spectrum at rest (20 averages, TR = 16s, 5 dummy scans, 2048 sample points), the participants performed 1 isometric plantarflexion at 85% MVF_P – subsequently labeled bout 1 - for 30 s (five dummy scans, 20 spectra before the exercise for saturation correction, TR = 1.5 s and three signal averages per time point, leading to a temporal resolution of 4.5 s). After that, participants were allowed to recover in the fixed position for 20 min before performing an isometric plantarflexion at 70% MVF_P until exhaustion or at maximum for 120 s, denoted as bout 2 in the following text (five dummy scans, TR = 1.5 s and three signal averages per

time point). If the volunteer was not able to reach the required force level for a continuous time of more than five seconds, the display of the visual feedback was stopped and the subject was told to discontinue the contraction so that the recovery period could be followed. Recovery spectra were measured after exercise cessation for 324 (plantarflexion at 85% MVF_P) and 264 seconds (plantarflexion at 70% MVF_P). After both plantarflexion efforts, perceived exertion was rated according to a modified Borg scale from 0 to 10 (Wilson & Jones, 1991a). Two different dynamic spectroscopy measurements were chosen to monitor the changes at various time-scales and close to the maximal performance (85% and 70% MVF_P) of the subjects at different pH levels.

Image processing. The TSE images were segmented using GTVolume Software (Gyrotools Ltd., Winterthur, Switzerland) before the volume of muscle and fat content was evaluated in the same region as for the DXA scans (see below).

Spectral processing. All free-induction decays (FIDs) were zero-filled to 4096 points, line-broadened with 6 Hz and Fourier-transformed into spectra. We used *tdfdfit* software (Slotboom *et al.*, 1998) for fitting the line-shapes and integrating the metabolite peak areas. 12 lines were included in the fit model, one line each for P_i, monoester, diester, PCr, and a baseline component, and two lines for γATP and αATP and three lines for βATP. The spectrum was then fitted as a sum of basic mathematical model functions (Voigt lines).
Inorganic phosphate (P_i) and phosphocreatine (PCr) concentrations were calculating using the PCr/ATP and the P_i/ATP ratios, respectively. To this end, a concentration of 8.2 mM was assumed for ATP (Arnold *et al.*, 1984; Kemp & Radda, 1994). The saturation factor in the dynamic spectra was determined by

the ratio of the relaxed spectra to the partially saturated spectra acquired prior to the plantarflexion exercise.

Calculations. We calculated the PCr recovery rate using a mono-exponential fitting procedure (Iotti *et al.*, 1993). Intracellular pH-values were calculated from the chemical shift of P_i according to the modified Henderson-Hasselbalch equation (Petroff *et al.*, 1988).

Exclusion criteria. Rigorous quality criteria were applied to the spectra. We excluded all spectra of a volunteer acquired under exercise conditions from the analysis if the PCr decrease after bout 1 was below 25%. In these cases, it was improbable that the initial calibration of MVF_P was correct. PRE and POST spectra of those volunteers were excluded. This led to the exlusion of 4 volunteers, all of which were part of the INT group.
For the image segmentation, all but one dataset could be used. In the excluded dataset, there were movement artifacts so that the image segmentation was imperfect. Two data values of the perceived exertion and one data point of MVF_P were lost.

Muscle Biopsy analyses

Biopsies were conducted according to the protocol described in detail in (Toigo *et al.*, 2010). In brief, a percutaneous biopsy was obtained after local anaesthesia from the nondominant soleus muscle several days before the start of the first training session and after the last training session. The muscle tissue was immediately mounted in an embedding medium (Tissue-Tek®, Sakura, Zoeterwoude, The Netherlands) after its removal and was then snap frozen in isopentane cooled to −160 °C with liquid nitrogen. Consecutive 12 μm sections

were cut on a microtome at -25 °C and mounted on glass cover slides for further histochemical and immunohistochemical analyses.
For all fiber analyses, only fibers fully encircled by adjacent fibers were evaluated, and measurements were made for at least 50 of each of the main fiber types (i.e. myosin heavy chain [MyHC] isoform type I and II).

Serial cryocut cross-sections were stained using the myofibrillar adenosine triphosphatase (mATPase) method (Guth & Samaha, 1970), with minor modifications (Muntener, 1979). Fiber cross-sectional areas were estimated from the lesser fiber diameter method (Dubowitz & M., 1985). For the determination of muscle capillarisation, consecutive cryocut sections were fixed with acetone for 10 min at 4 °C and exposed to the monoclonal mouse anti-human CD31 endothelial cell antibody (DAKO, Carpinteria, Canada, 1:600 dilution), which acts as a marker for muscle capillaries. As a control, samples without the addition of an antibody were prepared. There, the antibody was replaced with Tris-buffered saline (TBS) buffer. The overall capillary-to-fiber ratio was calculated by dividing the number of CD31-positive cells by the number of muscle fibers. The sample quality of 8 INT and 5 CON volunteers was sufficient for analysis, i.e. contained more than 50 fibers. 50 fibers are necessary for a reliable, valid representation of an individual's average fiber area and capillary-to-fiber ratio (McCall *et al.*, 1998; Porter *et al.*, 2002).

Dual-energy X-ray absorptiometry

To determine the muscle mass of both calfs, a dual X-ray absorptiometry (DXA) machine (Lunar iDXA™, GE Healthcare, Madison, WI, USA) was used according to the manufacturer's specifications. All total body scans were

conducted in the standard (0.13–0.25 m) mode. Segmental scan analysis were performed using the GE encore software version 11.40.004, using the total body bone and tissue scan images to delineate the regions of interest (ROI) as follows: ROI upper boundary: line through the femoral neck parallel to the inguinal ligament; lower boundary: horizontal line between femur and tibia; lateral boundaries: outer leg cuts.

Statistical analyses

Data are presented as mean ± standard deviation (SD). According to guidelines provided by the statistics helpdesk at University Zurich, group differences between INT and CON were tested for statistical significance by repeated measures ANOVAS with posthoc paired t-tests. The training status (CON, INT) was defined as *between-subject* covariate for the ANOVA analysis. The level of significance was set to $P < 0.05$. For all statistical analyses SPSS 16.0 statistical software (SPSS, Chicago, USA) was used.

5.3 Results

The effects of ischemic training on resting metabolite levels, functional and metabolic changes induced in muscle in the resting state are listed in Table **5**. [P_i] increased by slightly more than 1 mM from 4.7±0.8 mM to 5.9±1.1 mM (+27%, F = 19.732, p < 0.001). The resting pH was significantly increased in a paired t-test in the INT group after training (p< 0.05), however, it did not reach significance in a repeated measures ANOVA (F = 3.161, p= 0.09). Resting [PCr] did not change.

The fat mass of the muscle determined by DXA did not change, however a significant increase in the muscle volume (calf lean mass, +6%, F = 16.957, p <

0.001) was observed. Similar results were observed when muscle volume was assessed using magnetic resonance imaging, MRI (+6%, $F = 6.616$, $p < 0.05$). In addition to muscle volume growth, the perfusion was ameliorated, which was evident from an increased capillary-to-fiber ratio (+14%, $F = 15.731$, $p < 0.01$). No differences were found between test and re-test measurements for the muscle fiber diameter and cross-section (CS).

The maximal force measured with the dynamometer at the scanner (MVF_P) was significantly increased in the INT group based on a paired t-test, but it did not reach significance in a repeated measures ANOVA ($F = 3.866$, $p=0.069$). The perceived strain (Borg rating) remained unchanged. No changes were found in the VO_{2max} determined in a cycling ergometer test (Toigo *et al.*, 2010). Figure 18 displays clustered box plots of the observed changes.

Table 6 lists the dynamic changes that were observed during isometric exercise inside the MR scanner. $[P_i]$ after bout 2 is significantly increased in the INT group (+32%, $F = 7.708$, $p= 0.05$) in the INT group after training.

End-exercise pH values differed for bout 1 in a paired ttest ($p < 0.005$), however no changes were found in a repeated measures ANOVA and this change did not show up when the lowest pH was reached in bout 1 nor did it persist for the longer lasting isometric muscle contraction in bout 2. repeated measures ANOVA test.

Test- retest time courses of the $[P_i]$, pH and [PCr] of the CON group are displayed in Figure 19, indicating a high reproducibility of the measurements. Correlation curves for pH and P_i versus τ_{PCr} are plotted in Figure 20. The large majority of points lies inside the confidence interval.

	INT		CON	
	PRE	**POST**	**PRE**	**POST**
Calf fat mass (g)	868 ± 212 (12)	856 ± 210(12)	788 ± 89(9)	779 ± 83(9)
Calf lean mass (g)	**1700 ± 264(12)**	**1803 ± 275**(12)**	1690 ± 225(9)	1691 ± 206(9)
MRI fat volume (mm^3)	2808 ± 676(11)	2825 ± 657(11)	2885 ± 371(9)	2843 ± 361(9)
MRI Muscle Volume (mm^3)	**7249 ± 858(11)**	**7653 ± 774**(11)**	7221 ± 731(9)	7262 ± 625(9)
Capillary-to-fiber ratio	**1.8 ± 0.4(9)**	**2.1 ± 0.5**(9)**	1.8 ± 0.3(6)	1.8 ± 0.2(6)
Muscle fiber diameter (μm)	58.4 ± 8.4(8)	58.0 ± 7.5(8)	52.3 ± 3.7(5)	56.9 ± 5.8(5)
Muscle fiber CS (μm^2)	2726 ± 761(8)	2677 ± 675(8)	2157 ± 298(5)	2559 ± 531(5)
Resting pH	7.03 ± 0.01(12)	7.05 ± 0.02(12)	7.02 ± 0.02(9)	7.03 ± 0.02(9)
Resting [P_i] (mM)	**4.6 ± 0.8(12)**	**5.9 ± 1.1**(12)**	4.9 ± 0.5(9)	4.4 ± 0.6(9)
Resting [PCr] (mM)	37.5 ± 3.6(12)	39.5 ± 4.4(12)	36.8 ± 3.6(9)	37.8 ± 5.0(9)

Table 5. *Metabolic and systemic parameters that were measured at rest in the INT and CON groups before and after five weeks of ischemic training. The number of valid samples is given in brackets. Parameters whose p-value was statistically significant in a paired t- test are marked in bold and denoted with * ($p<0.05$) or ** ($p<0.005$).Related F-values are given in the text.*

	INT		CON	
	PRE	**POST**	**PRE**	**POST**
τ_{PCr} exercise bout 1(s)	30.4 ± 2.9(8)	36.9 ± 8.9(12)	37.1 ± 10.4(9)	40.2 ± 11.6(9)
τ_{PCr} exercise bout 2 (s)	44.2 ± 5.9(8)	47.9 ± 12.4(8)	48.9 ± 9.2(9)	47.1 ± 6.2(9)
End-exercise pH bout 1	7.00 ± 0.04(8)	7.01 ± 0.04(8)	7.00 ± 0.05(9)	7.00 ± 0.04(9)
Lowest pH bout 1	**6.94 ± 0.06(8)**	**6.90 ± 0.05**(8)**	6.88 ± 0.05(9)	6.87 ± 0.07(9)
End-exercise pH bout 2	6.78 ± 0.14(8)	6.79 ± 0.13(8)	6.82 ± 0.09(9)	6.82 ± 0.14(9)
Lowest pH bout 2	6.64 ± 0.20(8)	6.63 ± 0.14(8)	6.63 ± 0.17(9)	6.64 ± 0.15(9)
End-exercise [P_i] bout 1(mM)	16.2 ± 5.1(8)	18.2 ± 3.6(8)	17.5 ± 5.3(9)	19.4 ± 5.1(9)
End-exercise [P_i] bout 2 (mM)	**25.0 ± 5.7(8)**	**33.0 ± 3.0*(8)**	26.9 ± 5.6(9)	26.5 ± 5.4(9)
End-exercise [PCr] bout 1 (mM)	21.6 ± 5.4(8)	20.5 ± 4.6(8)	17.8 ± 3.9 (9)	18.1 ± 4.6 (9)
End-exercise [PCr] bout 2 (mM)	9.1 ± 5.2(8)	7.6 ± 3.5(8)	7.9 ± 3.5 (9)	7.9 ± 3.5 (9)
Borg Rating bout 1	7.79 ± 1.78(7)	8.21 ± 1.91(7)	8.25 ± 0.96(8)	8.19 ± 0.92(8)
Borg Rating bout 2	9.36 ± 0.94(7)	9.29 ± 1.11(7)	9.38 ± 0.74(8)	9.75 ± 0.46(8)
MVF_P (W)	**517 ± 92(7)**	**595 ± 78*(7)**	588 ± 112(9)	606 ± 99(9)

Table 6. *PCr recovery k-values, changes in metabolite levels and pH during exercise and Borg ratings for the 30s and 120s exercise paradigms. Values that were significant in a paired t-test are denoted with * ($p<0.05$) or ** ($p<0.005$). The number of valid samples is given in brackets. F-values are given in the text.*

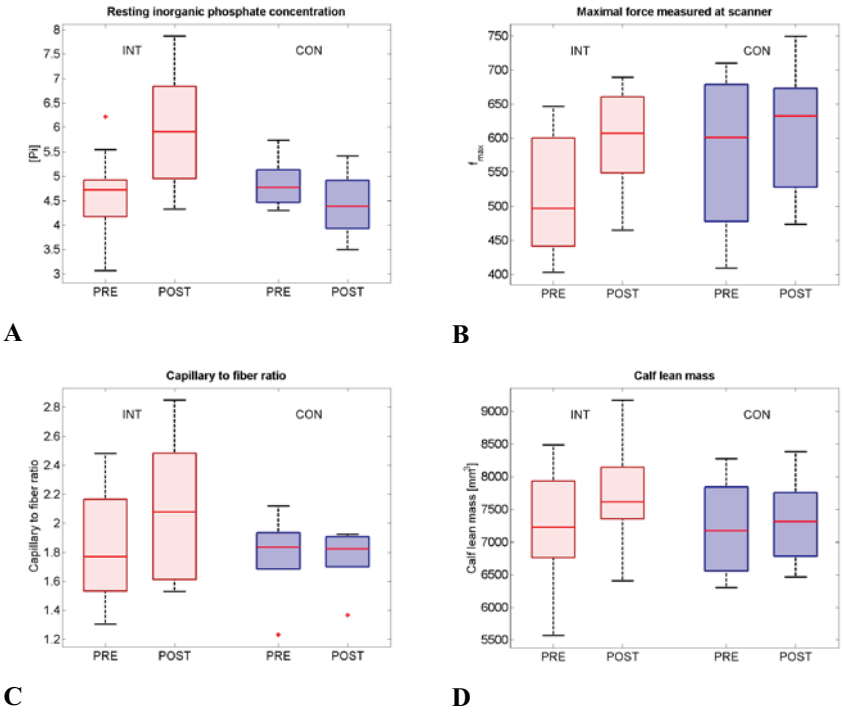

Figure 18 *Systemic and metabolic adaptations to training: PRE and POST measurements are shown for the INT (red) and CON (blue) groups for inorganic phosphate (a), MVF_P (b), capillary-to-fiber ratio (c) and calf lean mass (1d).*

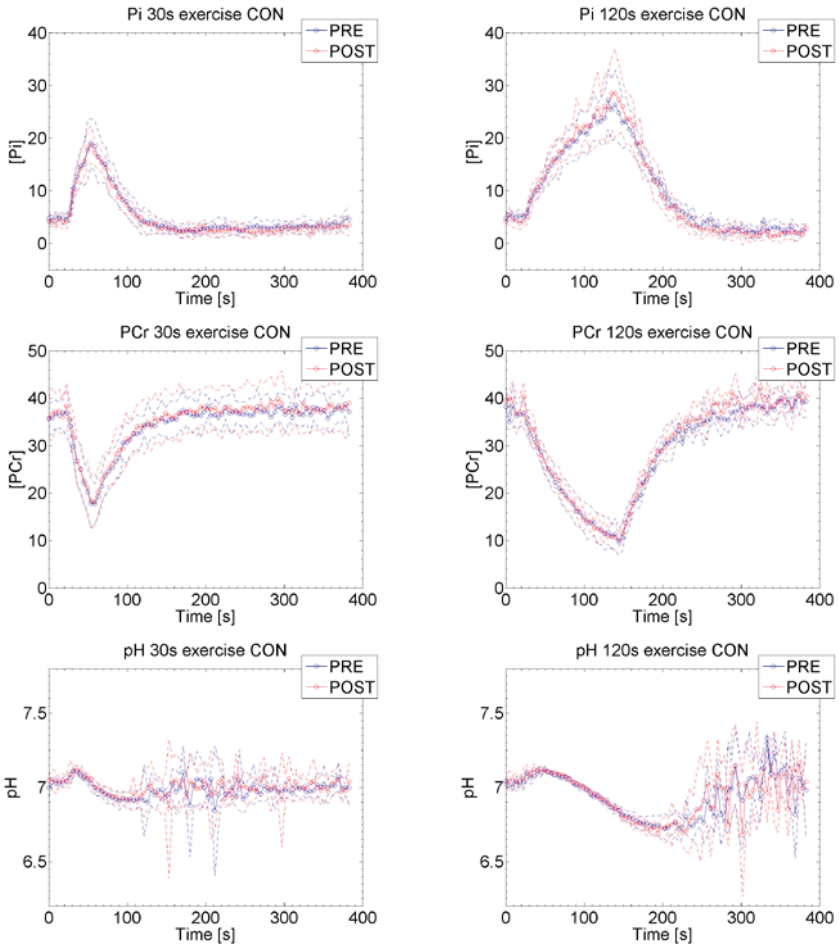

Figure 19 *Time courses of the PRE (blue) and POST (red) measurements are shown for the CON group. Row 1 displays the [P_i],and row 2 the [PCr] time course, while row c displays the pH time course of bout 1 (left) and bout2 (right). PRE- and POST measurements of all volunteers who were able to maintain the contraction force for the entire exercise duration (6 volunteers for bout 2) are shown, indicating a high reproducibility of the measurements*.

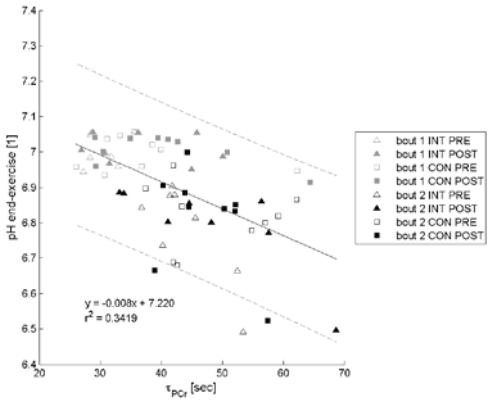

A

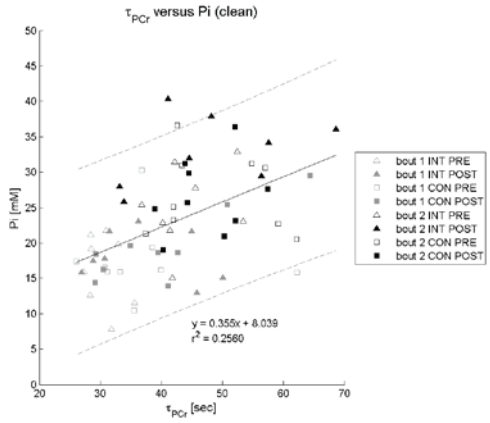

B

Figure 20 *Results of the linear regression analysis of τ_{PCr} versus end-exercise pH (a) and end-exercise [P_i] (b) for all experimental data. A correlation can be seen for all parameters. A better correlation is reached for the lowest pH that is reached after the end of the exercise bouts than for the end-exercise pH.*

5.4 Discussion and Conclusion

Study results. The results indicate that repetitive ischemic strength training increases the resting concentrations of P_i as well as the $[P_i]$ during exercise. A higher resting $[P_i]$ has been observed in muscle with a higher fiber type 1 content (Kushmerick *et al.*, 1992; Takahashi *et al.*, 1996). In addition, in muscle biopsies that have been obtained from the same INT subjects in the vastus lateralis muscle, a shift towards more oxidative type 1 fibers was observed (Toigo *et al.*, 2010). Vastus lateralis muscle has a similar fiber type composition as the gastrocnemius muscle (Spurway & Wackerhage, 2006) and similar training effects may be expected. For the lower leg, muscle fiber types were not determined. No changes were expected to be seen in the soleus muscle, which contains approximately 80% type 1 fibers.

The muscle fiber type dependence of resting [Pi] might be assigned to different buffer capacities, as P_i is one of the key pH buffers, or to its function as an activator of glycolytic enzymes (Khoja, 1986; Rush & Spriet, 2001). However, increasing concentrations of P_i also seem to induce a gradual dissociation of CK from the inner mitochondrial membrane (Vial *et al.*, 1979; Veksler & Ventura-Clapier, 1994; Walsh *et al.*, 2002; Wu *et al.*, 2008) and result in a decrease in post-ADP state 4 respiration in the presence of creatine in isolated mitochondria (Hall & Deluca, 1984). These results suggest that the concentration of inorganic phosphate in vivo serves to regulate the rate of PCr repletion. In the PRE measurements, a higher MVF_P was measured in the CON

group, while the INT group only reached this value in the POST measurement (Figure 18c). Thus the higher end-exercise [P_i] in the INT group in bout 2 (Table 6) may be due to a higher workload. However, the PCr depletion remained similar so that the increase in [P_i] is likely to be a consequence of the increased baseline [Pi] and thus a metabolic adaptation.

Linear regression analysis (Figure 20) shows a linear correlation of the τ_{PCr} with end-exercise [P_i] and end-exercise pH. Linear correlations of τ_{PCr} have been shown in other studies before with end-exercise P_i (i.e. (Kemp *et al.*, 1993)) and with end-exercise pH (i.e. (Iotti *et al.*, 1993; van den Broek *et al.*, 2007) and references cited therein). The points of the INT group in Figure 20 stay within the bounds of the confidence interval, so that no direct change of the oxidative metabolism is directly visible in these analyses. The influence of pH on τ_{PCr} varies greatly among subjects from around 33 s/pH unit to more than 75s/pH unit (van den Broek *et al.*, 2007), so that a correction of k for pH is not appropriate. The differences in the linear correlation may be due to unequal efflux rates in the individual subjects. In addition, the role of pH in the recovery of [PCr] remains unclear (van den Broek *et al.*, 2007). Regulation of PCr resynthesis has been attributed to ADP (Kemp *et al.*, 1993), and argumentation against a regulatory effect of [P_i] was given in the low Michaelis constant of approximately 1mM, which is below the measured resting concentration of P_i and therefore makes the control of respiration through P_i unlikely (Chance *et al.*, 1985). However, in this argumentation, the hypothesis of CK dissociation at high P_i concentrations (Vial *et al.*, 1979; Hall & Deluca, 1984; Walsh *et al.*, 2002) is not considered.

The lower minimal pH that has been observed in bout 1 in the INT group after training is probably the consequence of a higher exerted force and therefore a higher workload. The change is small, and it remains difficult to resolve its physiological impact.

Other changes that have been observed in this study include increases in measured force and muscle diameter. They represent common adaptations to strength training. The measured increase in capillary/fiber ratio most likely occurs as an adaptation to ischemic exercise training. It might be a compensation reaction that increases the oxygen storage capacities inside the muscle for the case of transient ischemia. Increased capillarization has been similarly observed in peripheral vascular disease (Hammarsten *et al.*, 1980; McGuigan *et al.*, 2001).

Possible limitations of the study. When interpreting data from training paradigms, the muscle and/or fat volume may change, as was the case in this study. Such a change leads to different measurement volumes in repeated measurements. In this study, the muscle volume in the INT group increased, while the fat volume remained the same. This indicates that the measured proportion of fat vs. muscle volume did not change. However, different proportions of the different triceps surae muscles may have contributed their signal to the spectrum.

Since the calculation of the resting concentrations of P_i is based on the P_i/ATP ratio with the assumption of a constant ATP concentration of 8.2 mM (Arnold *et al.*, 1984; Kemp & Radda, 1994), one could infer a lower resting ATP concentration instead of a higher P_i concentration. However, resting ATP and PCr concentrations are generally well buffered and thus show little variance

across the populations (Kemp *et al.*, 2007). They have been shown to remain unchanged after 8 weeks of sprint training (Nevill *et al.*, 1989). Also, relative resting PCr/ATP ratios did not differ between trained and untrained groups in this study.

Therefore, an increase in resting P_i concentration after five weeks of ischemic training is plausible. It is unlikely that the rise in resting [Pi] is caused by other processes than a change in muscle fiber type composition, such as inflammation, since none of the subjects reported any muscle ache and the performance of the participants was ameliorated.

In conclusion, changes in [P_i] at rest, which are likely to represent a shift in muscle fiber type composition, have been found. The increased P_i concentrations persist during exercise. They are paralleled by an increase in muscle volume and capillary to fiber ratio. Together, these changes lead to an increase in peak power (Toigo *et al.*, 2010).

Chapter 6:

SKELETAL MUSCLE MITOCHONDRIAL OXIDATIVE FUNCTION AND CARDIO-RESPIRATORY CAPACITY ARE NOT IMPAIRED IN PATIENTS WITH TYPE 1 DIABETES

6.1 Introduction

Currently, there is a debate about the validity of the still widely accepted concept that muscle mitochondrial deficiency and/or dysfunction causes muscle insulin resistance which leads to diabetes (Lowell & Shulman, 2005; Holloszy, 2009). In support of this concept, it has been reported, that genes involved in oxidative phosphorylation are downregulated (Mootha *et al.*, 2003a), and that mitochondrial oxidative enzyme activity, mitochondrial size and content are reduced in patients with type 2 diabetes or in insulin-resistant offspring of patients with type 2 diabetes (He *et al.*, 2001; Kelley, 2002). Accordingly, it has been hypothesized that mitochondrial deficiency/dysfunction impairs the ability of muscle to oxidize fatty acids, and leads to intramuscular lipid accumulation and insulin resistance (Kelley, 2002; Lowell & Shulman, 2005; Morino *et al.*, 2006). In keeping with the concept that muscle mitochondrial dysfunction causes insulin resistance it has also been reported that men with type 1 diabetes have a reduced skeletal muscle oxidative capacity, as assessed by ^{31}P magnetic resonance spectroscopy (^{31}P-MRS) (Crowther *et al.*, 2003b). However, there is also compelling evidence that mitochondrial function is not affected in patients with diabetes. A recently published *ex vivo* study has shown that when oxygen flux is normalized for mitochondrial content, oxidative phosphorylation and electron transport capacity in muscle extracts obtained from patients with type 2 diabetes are not different from a healthy control group (Boushel *et al.*, 2007). These findings are supported by a study on Asian Indians with type 2 diabetes, for whom the capacity for oxidative phosphorylation is similar to healthy controls (Nair 2008). Furthermore, *in vivo* skeletal muscle oxidative function, assessed by ^{31}P-MRS, has been shown to be similar between long-standing, insulin-treated type 2 diabetes patients, persons

with early stage type 2 diabetes, and healthy controls (De Feyter *et al.*, 2008). Taken together, at present, it is unclear whether skeletal muscle mitochondrial deficiency/dysfunction are a consequence of insulin resistance or are instrumental in its development, or whether these factors manifest themselves at all in the insulin resistant state. In fact, Hollozsy (Holloszy, 2009) recently highlighted the latter point when he commented that even if mitochondrial content was reduced, skeletal muscle still would contain sufficient mitochondria to make possible a ~150-fold increase in oxygen consumption per kilogram of muscle under exercise conditions (Andersen & Saltin, 1985), and that it is therefore unlikely that an increase in intramyocellular lipid content and the resulting insulin resistance in patients with diabetes are the result of defects in the mitochondria at their basal state.

In order to further shed light upon the relationship between oxidative metabolism and diabetes, we tested the hypothesis that there is no difference in myocellular and systemic markers of oxidative capacity between young women with type 1 diabetes−a population for which no respective data is available yet−and healthy women of similar age and physical activity level. To this end, we compared the ^{31}P-MRS-derived calf muscle end-exercise rates of oxidative ATP synthesis (i.e. mitochondrial capacity), muscle fiber metabolic phenotype and capillarization, peak and submaximal values for oxygen consumption and cardiac output, as well as endurance capacity between the 2 groups.

6.2 Research Design and Methods

Participants

We recruited 9 sedentary young women with type 1 diabetes (DIA) and 29 healthy women of similar age and activity level (CON). Mean age was 26.9 (SD 5.2) years for DIA, and 24.1 (4.2) years for CON. The participants' anthropometric data are presented in Table 7. Patients with type 1 diabetes had no diabetic complications or coexisting cardiovascular diseases. The duration of diabetes was 13.1 (6.6) years, and mean total daily insulin doses were 41 (13) units. The glycosylated haemoglobin A1c (HbA1c) was 7.6 (0.4) % (DIA) and 5.3 (0.2) % (CON) ($P < 0.001$). Participants in both groups displayed no metabolic risk factors according to Adult Treatment Panel III criteria (Wyszynski *et al.*, 2005) (). Participants in the CON group were healthy (asymptomatic). They showed no sign of either impaired glucose tolerance, i.e. fasting glucose concentration: 4.49 (0.26) $mmol \cdot l^{-1}$, blood glucose concentration 2 h post glucose load: 4.92 (1.19) $mmol \cdot l^{-1}$ (Unwin *et al.*, 2002) or calculated insulin resistance [homeostasis model assessment (HOMA,(Matthews *et al.*, 1985)): 1.4 (0.4)]. All participants were untrained and physically active less than 1 hour per week. After completing a routine health questionnaire, the participants were informed about the applied procedures and the associated risks. Written consent was obtained from all participants. The experimental protocol was approved by the ethics committee of the canton of Zurich and the study was performed in accordance with the ethical standards laid down in the Declaration of Helsinki for human experimentation.

	DIA	CON
Body mass (kg)	69.4 (8.6)	61.4 (6.5) **
Body height (m)	1.68 (0.06)	1.68 (0.06)
Body mass index (kg·m^{-2})	24.6 (3.0)	21.8 (2.1) **
Body fat (%)	35.0 (4.8)	31.6 (5.4)
Body fat mass (kg)	23.9 (5.6)	19.0 (4.5) *
Lean mass (kg)	43.7 (4.1)	40.6 (4.1)
Skeletal muscle mass (kg)	22.5 (2.7)	20.6 (2.4)
Abdominal fat mass (kg)	1.78 (0.71)	1.35 (0.54)
Abdominal lean mass (kg)	2.70 (0.26)	2.46 (0.29) *
Gluteofemoral fat mass (kg)	5.83 (1.30)	4.68 (0.98) **
Gluteofemoral lean mass (kg)	5.92 (0.78)	5.53 (0.58)
Leg fat mass (kg)	10.32 (2.47)	7.97 (1.68) **
Leg lean mass (kg)	15.44 (1.83)	14.10 (1.60) *
Lower leg fat mass (kg)	1.07 (0.26)	0.83 (0.17) **
Lower leg lean mass (kg)	1.87 (0.27)	1.70 (0.24)
Muscle cross-sectional area $_{66\% \text{ tibia length}}$ (cm^2)	7.70 (1.18)	7.30 (0.81)
Fat cross-sectional area $_{66\% \text{ tibia length}}$ (cm^2)	3.85 (1.15)	2.84 (0.55) **

Table 7 *Anthropometric characteristics of study participants. 9 patients with type 1 diabetes (DIA) and 29 healthy controls (CON) participated in this study. Data are expressed as means and standard deviations (SD). * $P < 0.05$, ** $P < 0.01$. The body mass index is the weight in kilograms divided by the square of the height in meters.*

	DIA	CON
Waist-to-hip ratio	0.75 (0.07)	0.71 (0.04)
Systolic blood pressure (mmHg)	130 (22)	120 (10)
Diastolic blood pressure (mmHg)	80 (12)	77 (8)
Triglycerides ($mmol \cdot l^{-1}$)	0.98 (0.29)	0.86 (0.36)
HDL-C ($mmol \cdot l^{-1}$)	1.89 (0.19)	1.70 (0.30)
Total-C ($mmol \cdot l^{-1}$)	5.2 (1.2)	4.6 (0.9)
Total-C/HDL-C	2.8 (0.8)	2.8 (0.6)
hsCRP ($mg \cdot l^{-1}$)	2.5 (1.4)	1.9 (2.4)

Table 8 *Cardiometabolic risk factors of study participants. Blood samples of 4 patients with type 1 diabetes (DIA) and of 21 healthy controls (CON) were available for analysis. Data are expressed as means and standard deviations (SD). None of the denoted cardiometabolic risk factors were statistically significant different between DIA and CON. HDL, high-density lipoprotein; Total-C, total cholesterol; hsCRP, high-sensitivity C-reactive protein.*

Magnetic Resonance Spectroscopy

A detailed description of the magnetic resonance experiments is given in Chapter 5. In brief, dynamic ^{31}P magnetic resonance spectroscopy (^{31}P-MRS) scans were acquired during isometric muscle contraction using a 3 Tesla whole body Philips Achieva Scanner (Philips Healthcare, Best, The Netherlands). For this purpose, an MRS-compatible ergometer setup was used (Chapter 3). A visual force feedback was given to the volunteers using Presentation® software (www.neurobs.com). During the measurements, the participants lay supine on the scanner bed with their non-dominant leg in the centre of the scanner bore.

We fastened the foot of the leg to be measured onto the foot holder at an angle of 100° plantarflexion using Velcro® straps.

A transmit/receive surface coil (diameter: 14 cm) tuned to 51.8 MHz was placed under the participant's calf and fastened with a Velcro® strap. Prior to the isometric contraction experiment in the magnet, each participant was familiarized with the setup in a training session. After the practice session, localizer images of the lower leg were acquired at rest, covering an area from the knee to the ankle.

Following the imaging session, the participants performed a single maximal voluntary plantarflexion attempt against the fixed dynamometer pedal, and we measured the maximal force acting on the pedal (MVF_P). ^{31}P-MRS spectra of the triceps surae muscles were subsequently acquired using a pulse-acquire technique and an adiabatic hyperbolic secant excitation pulse. After acquisition of a fully relaxed spectrum at rest (20 averages, TR = 16s, 5 dummy scans, 2048 sample points), the participants performed 1 isometric plantarflexion at 85% MVF_P for 30 s (five dummy scans, 20 spectra before the exercise for saturation correction, TR = 1.5 s and three signal averages per time point, leading to a temporal resolution of 4.5 s). After that, participants were allowed to recover in the fixed position for 20 min before performing an isometric plantarflexion at 70% MVF_P for 120 s or until exhaustion (five dummy scans, TR = 1.5 s and three signal averages per time point). If the volunteer was not able to reach the required force level for a continuous time of more than five seconds, the display of the visual feedback was stopped and the subject was told to discontinue the contraction so that the recovery period could be followed. Recovery spectra were measured after exercise cessation for 324 (plantarflexion at 85% MVF_P) and 264 seconds (plantarflexion at 70% MVF_P). After both plantarflexion efforts, perceived exertion was rated according to a

modified Borg scale from 0 to 10 (Wilson & Jones, 1991a). Two different dynamic spectroscopy measurements were chosen to monitor the changes at various time-scales and close to the maximal performance (85% and 70% MVF_P) of the subjects at different pH levels.

Spectral processing. All free-induction decays (FIDs) were zero-filled to 4096 points, line-broadened with 6 Hz and Fourier-transformed into spectra. We used *tdfdfit* software (Slotboom *et al.*, 1998) for fitting the line-shapes and integrating the metabolite peak areas. 12 lines were included in the fit model, one line each for P_i, monoester, diester, PCr, and a baseline component, and two lines for γATP and αATP and three lines for βATP. The spectrum was then fitted as a sum of basic mathematical model functions (Voigt lines).
Inorganic phosphate (P_i) and phosphocreatine (PCr) concentrations were calculating using the PCr/ATP and the P_i/ATP ratios, respectively. To this end, a concentration of 8.2 mM was assumed for ATP (Arnold *et al.*, 1984; Kemp & Radda, 1994). The saturation factor in the dynamic spectra was determined by the ratio of the relaxed spectra to the partially saturated spectra acquired prior to the plantarflexion exercise.

Calculations. Oxidative phosphorylation was quantified based on the PCr recovery following the 30 s plantarflexion at 85% MVF_P. During the 30 s plantarflexion at 85% MVF_P muscle pH remained close to 7.0 (Crowther *et al.*, 2002; Crowther *et al.*, 2003b). We calculated the PCr recovery rate using a monoexponential fitting procedure (Iotti 1993), and oxidative capacity ($M_{ox\ cap}$) as the product of the PCr recovery rate constant (k_{PCr}) and the resting PCr concentration ($[PCr]_{rest}$): $M_{ox\ cap} = k_{PCr} \cdot [PCr]_{rest}$ (Conley *et al.*, 2000). Intracellular pH-values were calculated from the chemical shift of P_i according

to the modified Henderson-Hasselbalch equation by Petroff et al. (Petroff *et al.*, 1988).

Exclusion criteria. Rigorous quality criteria were applied to the spectra. We excluded the spectra acquired under exercise conditions from the analysis if the participants' rating of perceived exertion (Wilson & Jones, 1991b) was below 7, and the PCr decrease was below 10%. In addition, we excluded spectra if the deviation of the exerted force from the target force (85 and 70% MVF_P) was > 5% for > 5s within the duration of the measurement, i.e. when the participant was exhausted before the end of the exercise. Altogether the experimental data of 5 subjects (1 DIA and 4 CON) were excluded for the 30 s exercise and the data of 20 subjects (5 DIA and 15 CON) were omitted for the 120 s exercise.

Skeletal muscle biopsy analyses

Sample preparation. After local anesthesia with 1% lidocaine, we obtained percutaneous biopsies from the middle region of the nondominant soleus and vastus lateralis muscles, using a ProMag Ultra device and 14 gauge needles (Angiotech Pharmaceuticals, Gainesville, FL, USA) as previously described (Wälti 2006). After removal, the muscle tissue was immediately mounted in an embedding medium (Tissue-Tek®, Sakura, Zoeterwoude, The Netherlands), snap frozen in isopentane cooled −160 °C with liquid nitrogen, and subsequently stored at −80 °C until use. Consecutive 12 µm sections were cut on a microtome at −25 °C and mounted on glass cover slides for further histochemical and immunohistochemical analyses.

Fiber size and mitochondrial enzyme activity. We stained the serial cryocut cross-sections using the myofibrillar adenosinetriphosphatase (mATPase)

method after acid (pH 4.3 and 4.6) and alkali (pH 10.5) preincubation according to Guth and Samaha (Guth & Samaha, 1970), with minor modifications (Müntener 1979). Subsequently, we classified the muscle fibers according to their myosin heavy chain (MYH) isoform into MYH-1 and MYH-2, and measured the muscle fibers' diameter by the lesser fiber diameter-method (Dubowitz & M., 1985). We estimated the fiber cross-sectional area (CSA) from the lesser diameter. For this purpose, muscle fibers were assumed to be circular. For the analysis of oxidative enzyme activity, we incubated consecutive sections in media containing cytochrome c oxidase.

Muscle capillarization. We fixed consecutive cryocut sections with acetone for 10 min at 4°C and exposed them to the monoclonal mouse anti-human CD31 endothelial cell antibody (DAKO, Carpinteria, Canada, 1:600 dilution), which acts as a marker for muscle capillarization. We performed this staining procedure using the Vectastain® ABC Kit (Vector laboratories, Burlingame, Canada) according to the manufacturer's instructions. For the control samples, we replaced the antibody with Tris-buffered saline (TBS) buffer. The capillary-to-fiber ratio was calculated by dividing the number of CD31-positive cells by the number of muscle fibers.

Quality control. For all fiber analyses, only fibers fully encircled by adjacent fibers were evaluated, and measurements were made for at least 50 of each of the main fiber types (i.e. MYH-1 and MYH-2). Previous studies investigating the skeletal muscle fiber sample size required for a reliable, valid representation of an individual's average fiber area and capillary-to-fiber ratio showed that 50 fiber measurements per individual for type 1 and 2 fibers and capillary contacts

are sufficient to characterize type 1 and 2 fiber areas and capillary-to-fiber ratio of an individual (McCall *et al.*, 1998; Porter *et al.*, 2002).

Image analysis. Images were captured by an optical widefield microscope (Polyvar, Reichert-Jung, Vienna, Austria) with a connected digital camera (Leica DFC 420 C, Wetzlar, Germany) under the same microscope objective (10×). For all histochemical and immunohistochemical analyses, we used the NIH Image J (1.41o, National Institutes of Health, Bethesda, MD, USA) software. Arbitrary cytochrome c enzyme activity levels were derived from the measured mean optical density pixel values of the muscle fibers normalized to the background pixel values on the same section.

Cardiac output and oxygen consumption measurements

We used Innocor™ (Innovision, Odense, Denmark) to determine peak cardiac output by inert gas rebreathing and oxygen consumption by breath-by-breath ergospirometry during a graded cycling exercise test, as previsously described (Fontana *et al.*, 2009). To this end, the participants were equipped with a heart rate monitor (S610i, Polar Electro, Kempele, Finland), a facemask (Hans Rudolph, Shawnee, KS, USA), an anti-bacterial filter (PALL PF30-S, Pall, East Hills, NY, USA), and an arterial oxygen saturation sensor (Innocor™, Innovision, Odense, Denmark). Participants rested in the seated position on the cycle ergometer for 2 min, after which they started cycling at 50 W. Power was increased by 25 W every 2 min until volitional exhaustion, which was defined as the point in time at which the participants stopped cycling. On the 50 W stage of the baseline test, we determined the individually preferred cycling cadence ($\geq$ 70 min $^{-1}$), which the participants then consistently ($\pm$ 5 revolutions·min^{-1}) applied throughout the test. We determined cardiac output at

rest, 50 W, 75 W, and at peak exercise, i.e. immediately before volitional exhaustion. Arterio-venous oxygen difference was calculated by dividing oxygen consumption by cardiac output. .

Endurance capacity

On a separate day, we used constant-load cycling exercise tests to assess time to exhaustion as an indicator of endurance capacity. After 2 min of rest, the participants started pedaling at their individually preferred cycling cadence, as determined during the first graded exercise test. Power of the initial warm-up stage was 40% maximal power of the first graded exercise test. After 1 min, we increased power to 60% peak power (for 2 min) and then to 85% maximal power. Power at 85% maximal power was sustained until volitional exhaustion, which we defined as the point in time, at which the participants stopped pedaling or were no longer able to maintain cycling cadence within the required limits (70 ± 5 revolutions·min^{-1}).

Dual-energy X-ray absorptiometry

Prior to the dual-energy X-ray absorptiometry (DXA) measurement, we assessed body mass and body height. Subsequently, we determined waist and hip circumference, and calculated the waist-to-hip ratio. These physical measurements were performed according Knöpfli et al. 2010. Total body DXA measurements were performed with a Lunar iDXA™ (GE Healthcare, Madison, WI, USA) according to the manufacturer's specifications. All scans were conducted in standard mode (0.13 m), and scan analysis was performed using GE encore software version 11.40.004. Total body fat and lean mass, % body fat (from tissue), as well as abdominal ("android) and gluteofemoral ("gynoid") fat and lean masses were used for subsequent

analyses. Android and gynoid regions of interest (ROI) were defined as previously described (Knoepfli-Lenzin *et al.*). Total skeletal muscle mass was calculated from appendicular lean masses according to Kim *et al*.(Kim et al., 2002).

Blood analyses

Venous blood samples were collected in EDTA, separated, and stored at -20 °C before being assayed. Plasma glucose concentrations were determined by an automated hexokinase method (HK Unit-Kit III, Roche, Basel, Switzerland), and serum insulin concentrations were determined by radioimmunoassay (Insulin ct-kit, Cisbio Bioassays, Bagnols-sur-Cèze, France). HbA1c was immunochemically measured with the DXC 2000® device (Bayer, Leverkusen, Germany). High-sensitivity C-reactive protein (hsCRP) was assessed with the Immulite 2500 kit (Siemens, Los Angeles, CA, USA), triglyceride, high-density lipoprotein (HDL), and cholesterol were analyzed using commercial tests from Roche (Basel, Switzerland). For CON, a standard oral glucose tolerance test (OGTT) was performed in the morning after an overnight (12 h) fast. The participants ingested 75 g of glucose in 0.3 l water. Venous blood samples were drawn 2 times just before, and at 30, 60, 90, and 120 min after ingestion of glucose for determining plasma glucose and serum insulin concentrations. Insulin sensitivity was estimated by the homeostasis model assessment (HOMA) and calculated as HOMA = [fasting insulin ($\mu U \cdot ml^{-1}$] x [fasting glucose ($mmol \cdot l^{-1}$)] / 22.5 (Matthews *et al.*, 1985).

Statistical analyses

Data are presented as mean and standard deviation (SD). Group differences between DIA and CON were tested for statistical significance by *t*-tests for independent samples, and equality of variances was checked using Levene's test. The level of significance was set to $P < 0.05$. For all statistical analyses, SPSS 16.0 statistical software (SPSS, Chicago, IL, USA) was used.

6.3 Results

Skeletal muscle energetics and oxidative capacity

Resting muscle. [PCr] and at rest were not different between DIA (N=9) and CON (N=29) (38.2 [3.7] vs. 37.6 [3.4]) and [P_i] remained equally unchanged (4.67 [0.75] vs. 4.87 [0.75]). Also, the mean pH value at rest was the same for both, DIA and CON (7.03[0.01] vs. 7.03 [0.01]) shows a representative fit of a spectrum acquired under full relaxation (Figure 21).

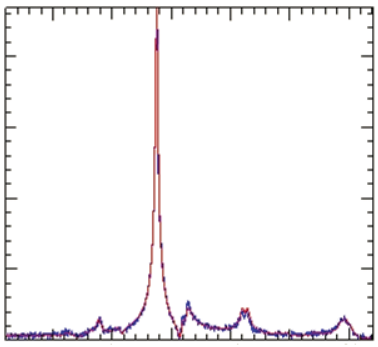

Figure 21 *Representative fit of a spectrum fully relaxed spectrum. The magnitude spectrum is shown in blue, and the fit is displayed in red.*

30 s isometric plantarflexion. The pH curves for DIA and CON displayed concordant behavior with similar standard deviations (Figure 23a). No difference was found between DIA (N=8) and CON (N=25) for neither k_{PCr} (0.032 [0.005] vs. 0.0333 [0.005] s^{-1}) nor $M_{ox\ cap}$ (1.23 [0.30] vs. 1.14 [0.21] $mM \cdot s^{-1}$). Consequently, PCr recovery was similar between the 2 groups (Figure 22a).

120 s isometric plantarflexion. Only 4 DIA and 14 CON subjects were able to maintain the desired force for the entire course of the exercise (see Research Design and Methods) and were subsequently considered for the analysis. While the spectra of the pH time courses (Figure 23b) for DIA were in very good agreement with those of CON (pH at the end of exercise: 6.79 [0.09] vs. 6.78 [0.12]), [PCr] at the end of exercise appeared to be lower in DIA than CON, but the apparent difference was not statistically significant (9.5 [2.1] vs. 12.15 [5.07] mM, Figure 22b). Also, the recovery constants k_{PCr} did not show any difference (0.026 [0.004] vs. 0.024 [0.006] s^{-1}).

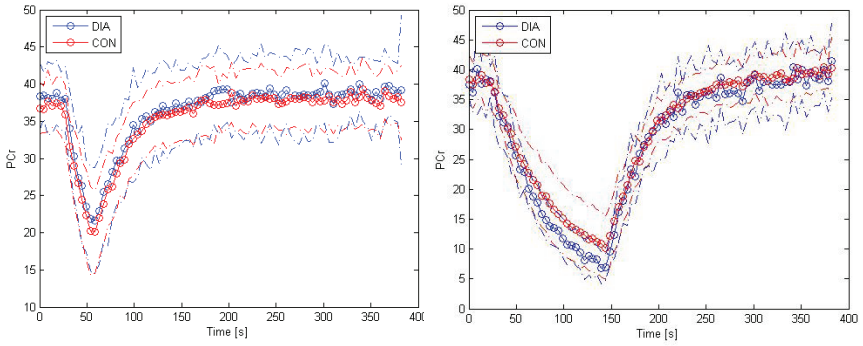

a b

Figure 22 *[PCR] timelines for DIA (blue) and CON (red) subjects. The 30s exercise is displayed on the left. On the right, the 120s exercise is shown.*

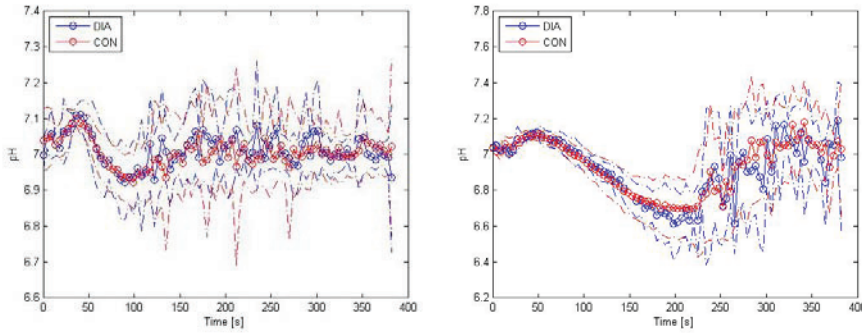

A B

Figure 23 *pH curves for the 30s (left) and 120s (right) spectra for the DIA (blue) and CON (red) groups.*

Skeletal muscle capillarization, phenotype, and oxidative enzyme activity

No differences were found in capillary-to-fiber ratio between DIA and CON in soleus (N=5 for DIA and N=15 for CON) (1.59 [0.29] vs. 1.80 [0.35]) and vastus lateralis (1.50 [0.08] vs. 1.52 [0.20]) muscles. Furthermore, the muscle phenotypes of soleus (MYC I: 82.3 [9.0] vs. 81.5 [9.2] %) and vastus lateralis (MYC I: 61.8 [5.5] vs. 61.4 [9.1] %) muscles, as well as cytochrome c oxidase activity (N=6 for DIA and N=11 for CON) (Figure 24) were similar between DIA and CON.

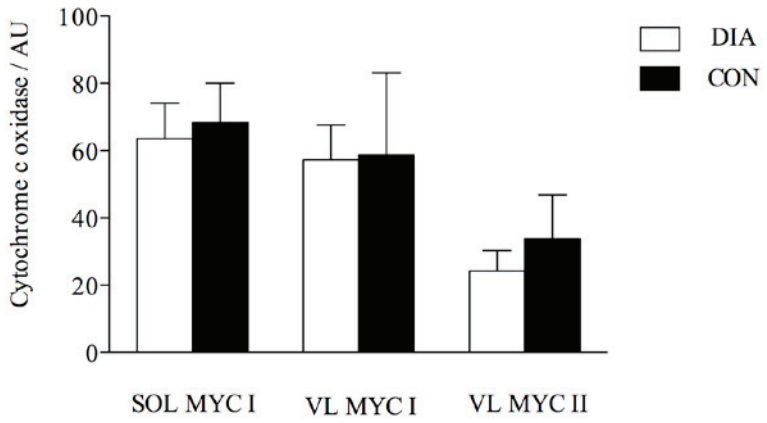

Figure 24 *Cytochrome c oxidase activity of soleus (SOL) and vastus lateralis (VL) muscles are shown of 6 patients with type 1 diabetes (DIA, white bars) and 11 women from the control group (CON, black bars) (P > 0.05). Bars and error bars represent mean value and standard deviations, respectively. AU, arbitrary units; MYC I, myosin heavy chain I; MYC II, myosin heavy chain II.*

Skeletal muscle fiber size

The mean fiber diameter of the soleus muscle was not different between DIA (N=6) and CON (N=14) (MYC I: 60.8 [12.4] vs. 55.9 [7.2] μm). In contrary, the mean fiber diameter of vastus lateralis was higher in DIA (N=6 for MHC I and MHCII) compared to CON (N=16 for MHC I and N=14 for MHCII) (MYC I: 59.1 [8.0] vs. 53.6 [7.7] μm, $P < 0.05$; MYC II: 63.1 [5.7] vs. 54.3 [5.8] μm, $P < 0.01$).

Oxygen consumption, cardiac output, and arterio-venous oxygen difference

Submaximal and maximal values of oxygen consumption, cardiac output, and arterio-venous oxygen difference during the incremental exercise test did not differ between DIA (N=9) and CON (N=29) (Figure 25). Additionally, dividing delta cardiac output (peak minus rest values) by delta oxygen consumption reveals, that dynamic changes during the incremental exercise test were similar between the 2 groups (4.08 [0.62] vs. 4.12 [0.94]). Moreover, maximal oxygen consumption (32 [7] vs. 35 [5] $ml \cdot min^{-1} \cdot kg^{-1}$) and peak cardiac output (180 [40] vs. 198 [26] $ml \cdot min^{-1} \cdot kg^{-1}$) were both not statistically significant different between DIA and CON.

Exercise performance and endurance capacity

In agreement with a lack of metabolic disparity, no differences in maximal power output (incremental exercise test: 171 [25] vs. 163 [26] W) as well as in endurance capacity (time to exhaustion: 471 [119] vs. 532 [212] s) were found between DIA (N=9) and CON (N=29).

Body composition

Lean mass, % body fat, and waist to hip ratio were not different between DIA (N=9) and CON (N=29), while body mass, body fat mass, and body mass index were higher in DIA than in CON (Table 7 and Table 8). The calculated skeletal muscle mass was higher in DIA than in CON and reached almost statistical significance.

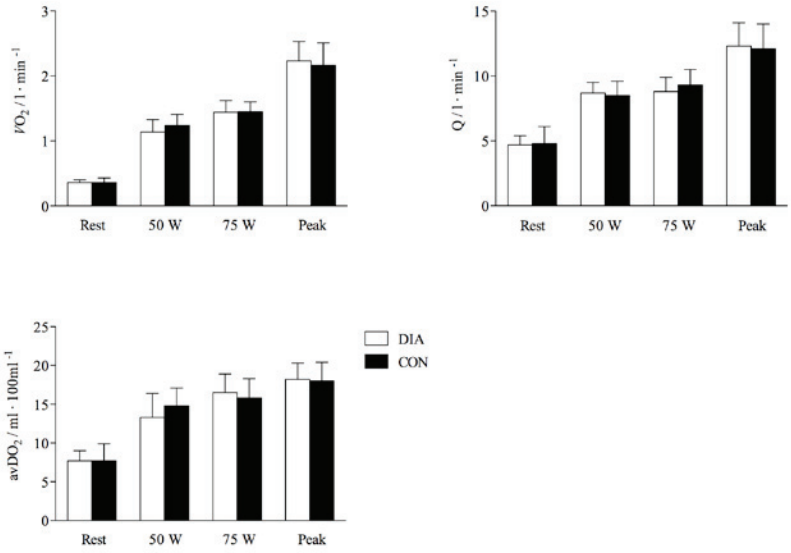

Figure 25 *Haemodynamic kinetics during the incremental exercise test. Oxygen consumption (VO_{2max}), cardiac output (Q), and arterio-venous oxygen difference ($avDO_2$) in patients with type 1 diabetes (DIA, white bars) and healthy controls (CON, black bars) are shown (P > 0.05). Bars and error bars represent mean values and standard deviations, respectively.*

6.4 Discussion

In the present study, we have demonstrated that skeletal muscle mitochondrial oxidative function, muscle capillarization, muscle fiber metabolic phenotype, oxygen consumption, cardiac output, arterio-venous oxygen difference, and

endurance capacity do not differ between women with well-controlled type 1 diabetes and healthy controls. These findings lend further credence to the emerging notion that diabetes might not be associated with impaired mitochondrial and cardiorespiratory function, as well as endurance capacity.

The mitochondrial respiratory function was investigated with an *in vivo* assessment by means of ^{31}P-MRS. The rate of PCr resynthesis after exercise (Figure 22), which depends on mitochondrial respiration (Arnold *et al.*, 1984; Chance *et al.*, 1986; Iotti *et al.*, 1993), is not statistically significant different between patients with type 1 diabetes and control subjects. Furthermore, the pH was similar at rest and after an exercise bout performed until exhaustion (Figure 23). Contrary to our findings, Crowther *et al.* (Crowther *et al.*, 2003a) presented significant differences in the $M_{ox\ cap}$ and in the pH course of men with type 1 diabetes and healthy controls. However, the subjects in this study were obese and suffering from different side effects. Moreover, the discrepancy in the pH course may be due to the fact that in our study, the subjects were all pushing at the same % of their MVF_P, while the course of force values during the exercise in the study conducted by Crowther *et al.* (Crowther *et al.*, 2003a) differs between patients with type 1 diabetes and healthy controls. Hence, there may have been a stronger drop in pH due to a stronger exhibited force rather than a change in metabolism between patients with diabetes and healthy controls. The PCr decline is similar between patients with type 1 diabetes and healthy controls in (Crowther *et al.*, 2003a), however, after about 30 s the ATP supply trough glycolysis reaches a maximum and the hydrolysis of ATP generated this way contributes to a further acidification of muscle tissue. A stronger exerted force therefore could lead to a stronger decrease in pH. Our observation of a normal mitochondrial respiratory function in patients with type

1 diabetes assessed by ^{31}P-MRS is confirmed by skeletal muscle single-fiber analysis of cytochrome c oxidase activity (Figure 24). In line with these results, another recent study also did not find any differences in oxidative enzyme activity levels measuring succinate dehydrogenase in young subjects with type 1 diabetes and low habitual physical activity levels (Fritzsche *et al.*, 2008). In contrast, He *et al.* (He *et al.*, 2001) showed that skeletal muscle oxidative enzyme activity in obese and patients with type 2 diabetes are lower compared to lean healthy subjects. Considering that also the subjects from the group with type 2 diabetes were obese, it is not proven that the reduced oxidative enzyme activity results from diabetes itself or rather from obesity.

As we have shown, $M_{ox\ cap}$ of patients with type 1 diabetes is not impaired by means of mitochondrial enzymatic changes. Mitochondrial oxidative function stands for oxidative phosphorylation, e.g. the formation of ATP from ADP and P_i in association with the transfer of electrons from fuel molecules to coenzymes and finally to oxygen. Therefore, the delivery of oxygen from the ambient air to the skeletal muscle is another limiting factor of the oxidative function. It is believed that in healthy humans, high oxygen consumption primarily depends on oxygen delivery to the exercising muscles (Bassett & Howley, 2000; Saltin & Calbet, 2006). The capacity for oxygen delivery can be estimated by 4 main factors. First, the measurement of oxygen consumption serves as an indicator of whole-body oxygen consumption. Second, cardiac output is the volume of blood being pumped by the heart ventricle, and the main factor limiting maximal oxygen uptake (Bassett & Howley, 2000). Third, the abundance of skeletal muscle capillaries determines the capacity for oxygen flux from blood to the muscle fiber. Finally, the arterio-venous oxygen difference represents the extent to which oxygen is removed from the arterial

blood. Whereas it is believed that oxygen consumption and exercise performance is reduced in type 2 diabetes (Regensteiner *et al.*, 1998; Baldi *et al.*, 2003), it is not clear if it is also the case in type 1 diabetes (Veves *et al.*, 1997; Nadeau *et al.*, 2009). However, our data clearly show that oxygen consumption (Figure 25), the exercise performance assessed by peak power during the incremental exercise test, as well as the endurance capacity are similar in patients with type 1 diabetes compared to healthy controls. These data are underlined by the cardiovascular measurements of central (cardiac output) and peripheral (arterio-venous oxygen difference, skeletal muscle capillarization) factors (Figure 25), which figure to the oxidative capacity. These consistent findings confirm and emphasize, that the whole oxidative system is not altered in type 1 diabetes. To our knowledge, this is the first extensive study that has investigated the whole oxidative system, i.e. the cellular, energetic, and functional markers of oxidative capacity in patients with type 1 diabetes and healthy controls.

The body composition (Table 7) and the state of health (Table 8) of the subjects tested in this study were similar, expect of the existence of type 1 diabetes in the DIA group (no diabetic complications or cardiovascular diseases). This is of important note, since it is delicate to interpret a dependence of a specific condition to an adaptational effect when confounding variables cannot be minimized. Nevertheless, due to the fact that also visceral fat mass is central in type 1 diabetes (Wilkin, 2001), the subjects with diabetes in this study differ in both body mass and fat content when compared to the control group (Table 7). However, the average body mass index is just in the normal range (18.5-25 $kg \cdot m^{-2}$). This presents a difference to many studies conducted in patients with type 1 and type 2 diabetes, where the average subject was overweight or obese

with reported body mass index values well above 25 kg·m^{-2} (He *et al.*, 2001; Crowther *et al.*, 2003a; Mootha *et al.*, 2003b). Taken together, we could minimize the confounding variables and accomplish this study with 2 homogenous study groups.

Typically, insulin resistance is related to type 2 diabetes. However, it has been claimed that the etiology and conditions of type 1 and type 2 diabetes are blurring and overlapping (Wilkin, 2001; Donath & Halban, 2004). There is elevating evidence that a decreased β-cell function is the hallmark of both type 1 and type 2 diabetes (Donath & Halban, 2004) whereas insulin resistance is associated with visceral fat mass meaning that visceral weight gain is central in both types of diabetes (Wilkin, 2001). In line with these assumptions it has been shown that also patients with type 1 diabetes display decreased insulin sensitivity compared to healthy controls (DeFronzo *et al.*, 1982a; DeFronzo *et al.*, 1982b; Greenbaum, 2002; Dabelea *et al.*, 2003; Nadeau *et al.*, 2009). Therefore, based on our findings, we suggest that insulin resistance is not a consequence of a reduced oxidative function.

In summary, we present evidence that women with well-controlled type 1 diabetes exhibit similar skeletal muscle mitochondrial oxidative function, muscle capillarization, muscle fiber metabolic phenotype, and cardiorespiratory capacity as their age- and activity-matched controls, and therefore, supports the hypothesis that insulin resistance is not the result of a decreased mitochondrial function.

Chapter 7:
Conclusion and Outlook

The thesis aims at developing hardware and software to enable the reliable quantification of metabolite concentrations and metabolic parameters in human subjects at rest and during exercise. This goal is achieved by pursuing two different approaches. One approach focuses on the development of a method for the quantification of metabolite concentrations based on the ERETIC method. The second approach includes the design and implementation of an ergometer setup that enables the reliable standardization of exerted muscle force during dynamic MRS scans.

The quantification method ERETIC (Electric REference to access In vivo Concentrations, (Barantin, 1997)) has been successfully developed into a method that can now be applied for the quantification of metabolite concentrations *in vivo*. Several hurdles have been overcome to achieve this goal. The initial ERETIC setup was based on a sending antenna that was placed anywhere in the room. The amplitude of the calibration signal is then influenced by any objects in the vicinity of the antenna, such as the patient itself. To achieve a reliable scaling of the ERETIC signal amplitude with the coil load and the receiver gain, the signal had to be inductively coupled into the receive coil. In addition, an optic transmission of the signal was needed so that parasitic coupling with other cables or senders in the room could be avoided. In the end, a software interface was programmed so that the phase, frequency, amplitude and decay constant of the signal can be freely changed to adjust the signal to the free induction decay (FID) of the spins that are being measured. This way, spectra of metabolites containing different nuclei can be quantified and the spectra can subsequently be processed and quantified using standard software. Main advantages of this electric reference signal are the possibility to acquire the spectrum and the reference in a single scan (no additional

measurements are required), and its applicability to the measurement of spectra at any frequency (i.e. ^{13}C, ^{1}H, ^{31}P).

In principle, the advanced ERETIC setup may be used in combination with any coil, such as coils for different nuclei, multi-channel coil arrays, and surface coils. However, further hardware modifications are needed to enable a reliable quantification with surface coils and multi-channel coils due to their different B_1 homogeneity and reception sensitivity compared to single channel volume coils.

Promising future applications of the advanced ERETIC method include physiological and clinical studies in tissues where no internal reference metabolites are available for quantification, e.g. without the knowledge of the water content. Also, studies can be conducted for other nuclei, such as ^{13}C. The software can be readily adjusted to enable quantification of metabolite concentrations using other spectroscopy techniques than single voxel spectroscopy, such as chemical shift imaging (CSI). There, the phase of the ERETIC signal needs to be changed for each phase encoding step so that the reference signal appears in a single voxel of the spectroscopic grid only. Furthermore, one could think of similar adaptations that would enable the use of the ERETIC reference signal for the quantification of image data (Franconi *et al.*, 2002).

Dynamic spectroscopy measurements during exercise have been widely used in physiological and medical studies of muscle metabolism. In order to standardize these measurements, the used ergometers have to be able to quantify forces and a visual feedback of the momentary contraction for the subject is needed. The ergometer setup that has been developed and implemented during the course of this thesis takes these requirements into account and therefore enables the acquisition of well-standardized MRS scans

and the exploration of *basic muscle physiology in vivo*. For the development of the ergometer, special attention has been paid to the choice of the involved materials since they had to be MR-compatible. Moreover, a visual force feedback for the subjects was implemented. The setup was subsequently successfully applied in two physiological studies, which aimed at the examination of muscle metabolism during isometric muscle contractions in diabetes type 1 patients and subjects that were trained using an ischemic training paradigm.

In combination with biochemical methods and analysis of muscle biopsies, the presented ergometer setup is a promising way of obtaining information about the muscle metabolism. In the future, the ergometer setup could be extended to allow measurements during dynamic contractions of the muscle.

Danksagung

An dieser Stelle möchte ich allen danken, die mich während der der Dissertation unterstützt haben. Sie alle haben durch Ihren Rat, Ihre Hilfe am Scanner und im Labor, mit Hard- und Software, und durch ihre moralische Unterstützung und bei vielen gemeinsamen Freizeitaktivitäten zum Gelingen dieser Dissertation beigetragen.

Prof. ***Peter Bösiger***, der mir die spannende und vielseitige Arbeit auf dem Gebiet der MR- Spektroskopie ermöglicht hat, für das angenehme, kreative und inspirierende Arbeitsklima am IBT und für die vielen Freiheiten für eigene Ideen.

Anke Henning, für Ihr unermüdliches Engagement als Leiterin der Spektroskopiegruppe und für die vielen spannenden Diskussionen auf und neben dem Gebiet der Magnetresonanz.

Prof. ***Markus Rudin*** für das Korreferat und für die interdisziplinären Kontakte mit der Arbeitsgruppe am Hönggerberg.

Prof. ***Spyros Kollias*** für das Korreferat.

Prof. ***Nicola De Zanche und Matteo Pavan*** für die grosse Unterstützung beim Entwickeln der Hardware und beim Diskutieren der Messergebnisse.

MichaelWyss, für die vielen kurzweiligen Stunden beim Messen und in den Mittagspausen und für sein ansteckendes Interesse und Engagement beim Austüfteln neuer Möglichkeiten am Scanner.

Xing Chen, Alex Fuchs, Andreas Hock, Thomas Lange, Erin MacMillan, Ariane Fillmer, Thomas Kirchner, Dieter Meier, Milan Scheidegger, Marco Jauslin und Niklaus Zölch, mit denen die Arbeit in der Spektroskopiegruppe viel Spass macht, für die interessanten Gespräche und gemütlichen Treffen auch ausserhalb des Instituts.

Prof. ***Ulrike Dydak***, von der ich in diversen Kursen viel gelernt habe und die mir die Augen geöffnet hat für die faszinierende Welt der MR-Spektroskopie.

Prof. ***Roland Kreis*** für die interessanten Diskussionen rund um die Spektroskopie und die angenehme Zusammenarbeit.

Prof. ***Klaas Prüssmann*** für die Unterstützung und die spannenden Diskussionen rund ums Thema MR.

Roger Lüchinger und Urs Sturzenegger für die stetige Unterstützung bei allen möglichen Computer- und Scannerfragen und für die Geduld beim Lösen der auftauchenden Probleme.

David Brunner und Jurek Massner, für die vielen gemeinsamen Erlebnisse und Gespräche in Toronto, Hawaii, Berlin und in der Kaffeecke

Marianne Berg fürs Managen aller Papierangelegenheiten, für die super Organisation der Weihnachtsessen und Apéros und für die vielen schönen Konzerte.

Flurin Item und Marco Toigo für die interessanten Diskussionen über den Muskel- Metabolismus.

Gérard Crelier für seine grosse Unterstützung beim Programmieren der Spektroskopie-Software.

Stephen Wheeler, Dani Wegmann und Paul Lüthi für all Ihre Kunstwerke und kreativen Ideen.

Kai Lutz für seine Unterstützung beim Programmieren der fMRI –Software

Allen anderen IBT Kollegen für ihre Tips, die unterhaltsamen Kaffepausen und die vielen gemeinsamen Aktivitäten: Andrea Rutz, Andreas Steingötter, Bertram Wilm, Carolin Reischauer, Carsten Schirra, Christoph Barmet, Christof Baltes, Conny Schmidt, Jan Paska, Jelena Curcic, Johannes Schmidt, Kilian Weiss, Hendrik Mandelkow, Martin Bührer, Marco Piccirelli, Philipp Stämpfli, Reto Treier, Robert Manka, Robert Vorburger, Rudolf Fischer, Sebastian Kozerke, Thomas Järmann, Urs Gamper, Viton Vitanis.

Meinen ***Freunden*** für all die schönen Stunden und für die vielen gemeinsamen Gespräche und Jassabende, Wellnesswochenenden und Fotounternehmungen, insbesondere ***Daniel Rippstein, Tabea Kipfer, Céline Ramseier, Steffi Lehmann und Philipp Imoberdorf, Margarita Plesko und Samuel Murri, und allen Luzerner, Zürcher und Berner Fotofreunden***

Stefan 77 und Stefan 84*,* die stets für mich da waren und mich in allen Lebenslagen unterstützt und motiviert haben. Ein Riesengrosses Merci meinem Mann Stefan für seine Geduld, seine Aufmunterungen und seine Mithilfe bei all meinen Unterfangen!

Meinen Eltern, die mich schon früh für die Natur und die Naturwissenschaften begeistern konnten und ohne die diese Dissertation, das Studium und so vieles andere nicht möglich gewesen wären. Merci für Eure riesige Unterstützung!

Curriculum Vitae

I was born on Mai 9th 1981 as daughter of Hanna and Heinz Schweizer-Thomann and grew up in Bern. In 1997, I spent a year in the United States and obtained a High School Diploma at Immaculata Academy in Hamburg, NY. In 2001, I graduated from Gymnasium Kirchenfeld in Bern and made a study visit in the group of Prof. Hartmut Michel at the Max Planck Institute for Biophysics, Frankfurt (X-ray Cristallography). In fall 2001, I started my studies in Biochemistry at the ETH in Zürich. After working as an assistant of Prof. Dorothee Staiger at the Institute for Plant Biology and Prof. Ralph Müller at the Institute for Bioelectronics, I worked on a semester thesis at the institute of Bioelectronics and the analytical chemistry department (Semester Thesis on "Phantom Development for Micro- Computed Tomography"). In 2005, I graduated with a Diploma thesis on Diffusion Tensor Imaging in the group of Prof. Peter Bösiger at the Institute for Biomedical Engineering in collaboration with the goup of Prof. Detlef Günther at the Analytical Chemistry department. In October 2005, I joined the group of Peter Bösiger at the Institute for Biomedical Engineering, University and ETH Zürich, as a research and teaching assistant.

During my leisure time, I enjoy traveling, photography and hiking.

List of Publications

Brunner DO, Schweizer S & Pruessmann KP. (2007). Fast mapping of highly inhomogeneous RF fields. *Proc Intl Soc Mag Reson Med* **15**.

Chen X, Henning A, Heinzer-Schweizer S, Pavan M & Boesiger P. (2010a). Muscle group specific quantification of unsaturated fatty acids by localized DEPT-enhanced ^{13}C MRS and ERETIC. *Proc Intl Soc Mag Reson Med* **18**.

Chen X, Henning A, Pavan M, Heinzer-Schweizer S & Boesiger P. (2010b). ERETIC-based glycogen quantification using SNR-enhanced and localized ^{13}C MRS. *Proc Intl Soc Mag Reson Med* **18**.

Fuchs A, Heinzer-Schweizer S, Henning A & Boesiger P. (2009). Quantitative 2D in-vivo spectroscopy using the ERETIC method. *Proc Intl Soc Mag Reson Med* **17**.

Heinzer-Schweizer S, De Zanche N, Pavan M, Mens G, Henning A & Boesiger P. (2009a). In-vivo measurement of absolute metabolite concentrations using the ERETIC method. *Proc Intl Soc Mag Reson Med* **17**.

Heinzer-Schweizer S, Item F, Henning A, Wyss M, Denkinger J., Kreis R, Toigo M, Boutellier U & Boesiger P (2010). Changes in oxidative metabolism of skeletal muscle induced by loaded vibration exercise under vascular occlusion. *Proc Intl Soc Mag Reson Med* **18.**

Heinzer-Schweizer S, De Zanche N, Pavan M, Mens G, Sturzenegger U, Henning A & Boesiger P (2010). In-vivo assessment of tissue metabolite levels using 1H MRS and the Electric REference To access In vivo Concentrations (ERETIC) method. *NMR Biomed*., *in press*

Heinzer-Schweizer S, Item F, Henning A, Toigo M & Boesiger P. (2009b). Advanced Exercise Ergometer Setup for In Vivo MRS Studies of Skeletal Muscle Metabolism. *Proc Intl Soc Mag Reson Med* **17**.

Pavan M, Heinzer-Schweizer S, De Zanche N, Henning A, Boesiger P & Pruessmann KP. (2009). An RF-over-fiber system for reliable signal injection in ERETIC spectroscopy. *Proc Intl Soc Mag Reson Med* **17**.

Schweizer S, De Zanche N, Henning A & Boesiger P. (2007a). Implementation of a calibration method for absolute quantification of metabolites using in-vivo NMR spectroscopy. *SPS*.

Schweizer S, De Zanche N, Mens G, Henning A & Boesiger P. (2008). Advances in the ERETIC method for the quantification of in-vivo 1H and 31P spectra. *Proc Intl Soc Mag Reson Med* **16**.

Schweizer S, Hattendorf B, Schneider P, Aeschlimann B, Gauckler L, Muller R & Gunther D. (2007b). Preparation and characterization of calibration standards for bone density determination by micro-computed tomography. *Analyst* **132,** 1040-1045.

References

Akoka S, Barantin L & Trierweiler M. (1999). Concentration measurement by proton NMR using the ERETIC method. *Analytical Chemistry* **71,** 2554-2557.

Akoka S & Trierweiler M. (2002). Improvement of the ERETIC method by digital synthesis of the signal and addition of a broadband antenna inside the NMR probe. *Instrumentation Science & Technology* **30,** 21-29.

Allen DG & Orchard CH. (1987). Myocardial contractile function during ischemia and hypoxia. *Circ Res* **60,** 153-168.

Anagnosti E & Tedeschi H. (1970). The Mechanism of Low-Amplitude Orthophosphate-Induced Swelling in Isolated Rat Liver Mitochondria. *J Cell Biol* **47,** 520-525.

Andersen P & Saltin B. (1985). Maximal Perfusion of Skeletal-Muscle in Man. *Journal of Physiology-London* **366,** 233-249.

Arnold DL, Matthews PM & Radda GK. (1984). Metabolic recovery after exercise and the assessment of mitochondrial function in vivo in human skeletal muscle by means of 31P NMR. *Magn Reson Med* **1,** 307-315.

Austin SJ, Connelly A, Gadian DG, Benton JS & Brett EM. (1991). Localized H-1-Nmr Spectroscopy in Canavans Disease - a Report of 2 Cases. *Magnetic Resonance in Medicine* **19,** 439-445.

Baker EH, Basso G, Barker PB, Smith MA, Bonekamp D & Horska A. (2008). Regional apparent metabolite concentrations in young adult brain measured by H-1 MR spectroscopy at 3 tesla. *Journal of Magnetic Resonance Imaging* **27,** 489-499.

Balaban RS. (1990). Regulation of Oxidative-Phosphorylation in the Mammalian-Cell. *American Journal of Physiology* **258,** C377-C389.

Baldi JC, Aoina JL, Oxenham HC, Bagg W & Doughty RN. (2003). Reduced exercise arteriovenous O2 difference in Type 2 diabetes. *J Appl Physiol* **94,** 1033-1038.

Barantin L, Le Pape, A., Akoka, S. (1997). A New Method for Absolute Quantitation of MRS Metabolites. *Magnetic Resonance in Medicine* **38,** 197-182.

Barker PB, Soher BJ, Blackband SJ, Chatham JC, Mathews VP & Bryan RN. (1993). Quantitation of Proton Nmr-Spectra of the Human Brain Using Tissue Water as an Internal Concentration Reference. *Nmr in Biomedicine* **6,** 89-94.

Bassett DR, Jr. & Howley ET. (2000). Limiting factors for maximum oxygen uptake and determinants of endurance performance. *Med Sci Sports Exerc* **32,** 70-84.

Blei ML, Conley KE & Kushmerick MJ. (1993). Separate measures of ATP utilization and recovery in human skeletal muscle. *J Physiol* **465,** 203-222.

Bose S, French S, Evans FJ, Joubert F & Balaban RS. (2003). Metabolic network control of oxidative phosphorylation - Multiple roles of inorganic phosphate. *Journal of Biological Chemistry* **278,** 39155-39165.

Boushel R, Gnaiger E, Schjerling P, Skovbro M, Kraunsoe R & Dela F. (2007). Patients with type 2 diabetes have normal mitochondrial function in skeletal muscle. *Diabetologia* **50,** 790-796.

Brown GC. (1992). Control of respiration and ATP synthesis in mammalian mitochondria and cells. *Biochem J* **284 (Pt 1),** 1-13.

Brunner DO, Schweizer S & Pruessmann KP. (2007). Fast mapping of highly inhomogeneous RF fields. *Proc Intl Soc Mag Reson Med* **15**.

Buchli R & Boesiger P. (1993). Comparison of Methods for the Determination of Absolute Metabolite Concentrations in Human Muscles by P-31 Mrs. *Magnetic Resonance in Medicine* **30,** 552-558.

Buchli R, Duc CO, Martin E & Boesiger P. (1994). Assessment of Absolute Metabolite Concentrations in Human Tissue by P-31 Mrs in-Vivo .1. Cerebrum, Cerebellum, Cerebral Gray and White-Matter. *Magnetic Resonance in Medicine* **32,** 447-452.

Chance B, Im J, Nioka S & Kushmerick M. (2006). Skeletal muscle energetics with PNMR: personal views and historic perspectives. *Nmr in Biomedicine* **19,** 904-926.

Chance B, Leigh JS, Jr., Clark BJ, Maris J, Kent J, Nioka S & Smith D. (1985). Control of oxidative metabolism and oxygen delivery in human skeletal muscle: a steady-state analysis of the work/energy cost transfer function. *Proc Natl Acad Sci U S A* **82,** 8384-8388.

Chance B, Leigh JS, Jr., Kent J, McCully K, Nioka S, Clark BJ, Maris JM & Graham T. (1986). Multiple controls of oxidative metabolism in living tissues as studied by phosphorus magnetic resonance. *Proc Natl Acad Sci U S A* **83,** 9458-9462.

Conley KE, Jubrias SA & Esselman PC. (2000). Oxidative capacity and ageing in human muscle. *Journal of Physiology-London* **526,** 203-210.

Connett RJ. (1988). Analysis of Metabolic Control - New Insights Using Scaled Creatine-Kinase Model. *American Journal of Physiology* **254,** R949-R959.

Crowther GJ, Kemper WF, Carey MF & Conley KE. (2002). Control of glycolysis in contracting skeletal muscle. II. Turning it off. *Am J Physiol Endocrinol Metab* **282,** E74-79.

Crowther GJ, Milstein JM, Jubrias SA, Kushmerick MJ, Gronka RK & Conley KE. (2003a). Altered energetic properties in skeletal muscle of men with well-controlled insulin-dependent (type 1) diabetes. *Am J Physiol Endocrinol Metab* **284,** E655-662.

Crowther GJ, Milstein JM, Jubrias SA, Kushmerick MJ, Gronka RK & Conley KE. (2003b). Altered energetic properties in skeletal muscle of men with well-controlled insulin-dependent (type 1) diabetes. *American Journal of Physiology-Endocrinology and Metabolism* **284,** E655-E662.

Dabelea D, Kinney G, Snell-Bergeon JK, Hokanson JE, Eckel RH, Ehrlich J, Garg S, Hamman RF & Rewers M. (2003). Effect of type 1 diabetes on the gender difference in coronary artery calcification: a role for insulin resistance? The Coronary Artery Calcification in Type 1 Diabetes (CACTI) Study. *Diabetes* **52,** 2833-2839.

Danielsen ER, Michaelis T & Ross BD. (1995). 3 Methods of Calibration in Quantitative Proton Mr Spectroscopy. *Journal of Magnetic Resonance Series B* **106,** 287-291.

De Feyter HM, van den Broek NMA, Praet SFE, Nicolay K, van Loon LJC & Prompers JJ. (2008). Early or advanced stage type 2 diabetes is not accompanied by in vivo skeletal muscle mitochondrial dysfunction. *European Journal of Endocrinology* **158,** 643-653.

De Graaf RA. (2007). In vivo NMR Spectroscopy - Principles and Techniques. *John Wiley & Sons Ltd* **Second edition**.

DeFronzo RA, Hendler R & Simonson D. (1982a). Insulin resistance is a prominent feature of insulin-dependent diabetes. *Diabetes* **31,** 795-801.

DeFronzo RA, Simonson D & Ferrannini E. (1982b). Hepatic and peripheral insulin resistance: a common feature of type 2 (non-insulin-dependent) and type 1 (insulin-dependent) diabetes mellitus. *Diabetologia* **23,** 313-319.

Donath MY & Halban PA. (2004). Decreased beta-cell mass in diabetes: significance, mechanisms and therapeutic implications. *Diabetologia* **47,** 581-589.

Dubowitz V & M. B. (1985). *Muscle Biopsy*. Bailliere Tindall, Eastbourne.

Duc CO, Weber OM, Trabesinger AH, Meier D & Boesiger P. (1998). Quantitative H-1 MRS of the human brain in vivo based on the simulation phantom calibration strategy. *Magnetic Resonance in Medicine* **39,** 491-496.

Edden RAE & Barker PB. (2007). Spatial effects in the detection of gamma-aminobutyric acid: Improved sensitivity at high fields using inner volume saturation. *Magnetic Resonance in Medicine* **58,** 1276-1282.

Edden RAE, Schar M, Hillis AE & Barker PB. (2006). Optimized detection of lactate at high fields using inner volume saturation. *Magnetic Resonance in Medicine* **56,** 912-917.

Ernst T, Kreis R & Ross BD. (1993). Absolute Quantitation of Water and Metabolites in the Human Brain .1. Compartments and Water. *Journal of Magnetic Resonance Series B* **102,** 1-8.

Fontana P, Boutellier U & Toigo M. (2009). Reliability of Measurements with InnocorTM during Exercise. *Int J Sports Med.*

Frahm J, Bruhn H, Gyngell ML, Merboldt KD, Hanicke W & Sauter R. (1989). Localized Proton Nmr-Spectroscopy in Different Regions of the Human-Brain Invivo - Relaxation-Times and Concentrations of Cerebral Metabolites. *Magnetic Resonance in Medicine* **11,** 47-63.

Franconi F, Chapon C, Lemaire L, Lehmann V, Barantin L & Akoka S. (2002). Quantitative MR renography using a calibrated internal signal (ERETIC). *Magnetic Resonance Imaging* **20,** 587-592.

Fritzsche K, Bluher M, Schering S, Buchwalow IB, Kern M, Linke A, Oberbach A, Adams V & Punkt K. (2008). Metabolic profile and nitric oxide synthase expression of skeletal muscle fibers are altered in patients with type 1 diabetes. *Exp Clin Endocrinol Diabetes* **116,** 606-613.

Funk CI, Clark A & Connett RJ. (1990). A Simple-Model of Aerobic Metabolism - Applications to Work Transitions in Muscle. *American Journal of Physiology* **258,** C995-C1005.

Garlid KD. (1980). On the mechanism of regulation of the mitochondrial K+/H+ exchanger. *J Biol Chem* **255,** 11273-11279.

Garwood M & DelaBarre L. (2001). The return of the frequency sweep: Designing adiabatic pulses for contemporary NMR. *Journal of Magnetic Resonance* **153,** 155-177.

Greenbaum CJ. (2002). Insulin resistance in type 1 diabetes. *Diabetes Metab Res Rev* **18,** 192-200.

Gruetter R. (1993). Automatic, localized in vivo adjustment of all first- and second-order shim coils. *Magn Reson Med* **29,** 804-811.

Gunter TE, Restrepo D & Gunter KK. (1988). Conversion of esterified fura-2 and indo-1 to Ca2+-sensitive forms by mitochondria. *Am J Physiol* **255,** C304-310.

Gupta RK & Moore RD. (1980). P-31 Nmr-Studies of Intracellular Free Mg-2+ in Intact Frog Skeletal-Muscle. *Journal of Biological Chemistry* **255,** 3987-3993.

Guth L & Samaha FJ. (1970). Procedure for the histochemical demonstration of actomyosin ATPase. *Exp Neurol* **28,** 365-367.

Halestrap AP. (1994). Regulation of mitochondrial metabolism through changes in matrix volume. *Biochem Soc Trans* **22,** 522-529.

Hall N & Deluca M. (1984). The Effect of Inorganic-Phosphate on Creatine-Kinase in Respiring Rat-Heart Mitochondria. *Archives of Biochemistry and Biophysics* **229,** 477-482.

Hammarsten J, Bylund-Fellenius AC, Holm J, Schersten T & Krotkiewski M. (1980). Capillary supply and muscle fibre types in patients with intermittent claudication: relationships between morphology and metabolism. *Eur J Clin Invest* **10,** 301-305.

Harkema SJ & Meyer RA. (1997). Effect of acidosis on control of respiration in skeletal muscle. *Am J Physiol* **272,** C491-500.

He J, Watkins S & Kelley DE. (2001). Skeletal muscle lipid content and oxidative enzyme activity in relation to muscle fiber type in type 2 diabetes and obesity. *Diabetes* **50,** 817-823.

Heinzer-Schweizer S, De Zanche N, Pavan M, Mens G, Sturzenegger U, Henning A & Boesiger P. In-vivo assessment of tissue metabolite levels using 1H MRS and the Electric REference To access In vivo Concentrations (ERETIC) method. *NMR Biomed.*

Heinzer-Schweizer S, Item F, Henning A, Toigo M & Boesiger P. (2009). Advanced Exercise Ergometer Setup for In Vivo MRS Studies of Skeletal Muscle Metabolism. *Proc Intl Soc Mag Reson Med* **17**.

Helms G. (2001). Volume correction for edema in single-volume proton MR spectroscopy of contrast-enhancing multiple sclerosis lesions. *Magnetic Resonance in Medicine* **46,** 256-263.

Hennig J, Pfister H, Ernst T & Ott D. (1992). Direct Absolute Quantification of Metabolites in the Human Brain with Invivo Localized Proton Spectroscopy. *Nmr in Biomedicine* **5,** 193-199.

Henning A, Schar M, Schulte RF, Wilm B, Pruessmann KP & Boesiger P. (2008). SELOVS: Brain MRSI localization based on highly selective T-1- and B-1-insensitive outer-volume suppression at 3T. *Magnetic Resonance in Medicine* **59,** 40-51.

Holloszy JO. (2009). Skeletal muscle "mitochondrial deficiency" does not mediate insulin resistance. *Am J Clin Nutr* **89,** 463S-466S.

Hoult DI. (2000). The principle of reciprocity in signal strength calculations - A mathematical guide. *Concepts in Magnetic Resonance* **12,** 173-187.

Hoult DI & Richards RE. (1976). Signal-to-Noise Ratio of Nuclear Magnetic-Resonance Experiment. *Journal of Magnetic Resonance* **24,** 71-85.

Iotti S, Lodi R, Frassineti C, Zaniol P & Barbiroli B. (1993). In vivo assessment of mitochondrial functionality in human gastrocnemius muscle by 31P MRS. The role of pH in the evaluation of phosphocreatine and inorganic phosphate recoveries from exercise. *NMR Biomed* **6,** 248-253.

Izzard S & Tedeschi H. (1973). Characterization of orthophosphate-induced active cation transport in isolated liver mitochondria. *Arch Biochem Biophys* **154,** 527-539.

Johansen L & Quistorff B. (2003). 31P-MRS characterization of sprint and endurance trained athletes. *Int J Sports Med* **24,** 183-189.

Jung DW, Apel L & Brierley GP. (1990). Matrix free Mg2+ changes with metabolic state in isolated heart mitochondria. *Biochemistry* **29,** 4121-4128.

Kaiser LG, Schuff N, Cashdollar N & Weiner MW. (2005). Age-related glutamate and glutamine concentration changes in normal human brain: H-1 MR spectroscopy study at 4T. *Neurobiology of Aging* **26,** 665-672.

Kelley DE. (2002). Skeletal muscle triglycerides: an aspect of regional adiposity and insulin resistance. *Ann N Y Acad Sci* **967,** 135-145.

Kemp GJ, Meyerspeer M & Moser E. (2007). Absolute quantification of phosphorus metabolite concentrations in human muscle in vivo by P-31 MRS: a quantitative review. *Nmr in Biomedicine* **20,** 555-565.

Kemp GJ & Radda GK. (1994). Quantitative interpretation of bioenergetic data from 31P and 1H magnetic resonance spectroscopic studies of skeletal muscle: an analytical review. *Magn Reson Q* **10,** 43-63.

Kemp GJ, Taylor DJ & Radda GK. (1993). Control of Phosphocratine Resynthesis during Recovery from Exercise in Human Skeletal-Muscle. *Nmr in Biomedicine* **6,** 66-72.

Khoja SM. (1986). Phosphofructokinase from the epithelial cells of rat small intestine. Comparison of regulatory properties with those of skeletal

muscle, liver and brain phosphofructokinase. *Comp Biochem Physiol B* **85,** 337-341.

Kim J, Wang ZM, Heymsfield SB, Baumgartner RN & Gallagher D. (2002). Total-body skeletal muscle mass: estimation by a new dual-energy X-ray absorptiometry method. *American Journal of Clinical Nutrition* **76,** 378-383.

Klabunde RE & Mayer SE. (1979). Effects of ischemia on tissue metabolites in red (slow) and white (fast) skeletal muscle of the chicken. *Circ Res* **45,** 366-373.

Knoepfli-Lenzin C, Sennhauser C, Toigo M, Boutellier U, Bangsbo J, Krustrup P, Junge A & Dvorak J. Effects of a 12-week intervention period with football and running for habitually active men with mild hypertension. *Scand J Med Sci Sports*.

Koretsky AP, Brosnan MJ, Chen LH, Chen JD & Vandyke T. (1990). Nmr Detection of Creatine-Kinase Expressed in Liver of Transgenic Mice - Determination of Free Adp Levels. *Proceedings of the National Academy of Sciences of the United States of America* **87,** 3112-3116.

Kreis R. (1997). Quantitative localized H-1 MR spectroscopy for clinical use. *Progress in Nuclear Magnetic Resonance Spectroscopy* **31,** 155-195.

Kreis R. (2004). Issues of spectral quality in clinical 1H-magnetic resonance spectroscopy and a gallery of artifacts. *NMR Biomed* **17,** 361-381.

Kreis R, Ernst T & Ross BD. (1993). Absolute Quantitation of Water and Metabolites in the Human Brain .2. Metabolite Concentrations. *Journal of Magnetic Resonance Series B* **102,** 9-19.

Kreis R, Slotboom J, Pietz J, Jung B & Boesch C. (2001). Quantitation of localized P-31 magnetic resonance spectra based on the reciprocity principle. *Journal of Magnetic Resonance* **149,** 245-250.

Kushmerick MJ, Moerland TS & Wiseman RW. (1992). Mammalian skeletal muscle fibers distinguished by contents of phosphocreatine, ATP, and Pi. *Proc Natl Acad Sci U S A* **89,** 7521-7525.

Lange T, Dydak U, Roberts TPL, Rowley HA, Bieljac M & Boesiger P. (2006). Pitfalls in lactate measurements at 3T. *American Journal of Neuroradiology* **27,** 895-901.

Laule C, Vavasour IM, Moore GRW, Oger J, Li DKB, Paty DW & MacKay AL. (2004). Water content and myelin water fraction in multiple sclerosis - A T-2 relaxation study. *Journal of Neurology* **251,** 284-293.

Lee D, Shankland, E.G., Mathis, M.,Marro, K.I., Amara,C.E., Hayes, C.E., Kushmerick, M.J. (2007). New synthetic reference signal injection Method for absolute quantification of metabolite concentration. *Proc Intl Soc Mag Reson Med* **15**.

Lowell BB & Shulman GI. (2005). Mitochondrial dysfunction and type 2 diabetes. *Science* **307,** 384-387.

Mackay A, Whittall K, Adler J, Li D, Paty D & Graeb D. (1994). In-Vivo Visualization of Myelin Water in Brain by Magnetic-Resonance. *Magnetic Resonance in Medicine* **31,** 673-677.

Marro KI, Lee D, Shankland EG, Mathis CM, Hayes CE, Amara CE & Kushmerick MJ. (2008). Synthetic signal injection using inductive coupling. *Journal of Magnetic Resonance* **194,** 67-75.

Marshall I, Wardlaw J, Cannon J, Slattery J & Sellar RJ. (1996). Reproducibility of metabolite peak areas in 1H MRS of brain. *Magn Reson Imaging* **14,** 281-292.

Matthews DR, Hosker JP, Rudenski AS, Naylor BA, Treacher DF & Turner RC. (1985). Homeostasis model assessment: insulin resistance and beta-cell function from fasting plasma glucose and insulin concentrations in man. *Diabetologia* **28,** 412-419.

McCall GE, Byrnes WC, Dickinson AL & Fleck SJ. (1998). Sample size required for the accurate determination of fiber area and capillarity of human skeletal muscle. *Can J Appl Physiol* **23,** 594-599.

McCully KK, Boden BP, Tuchler M, Fountain MR & Chance B. (1989). Wrist flexor muscles of elite rowers measured with magnetic resonance spectroscopy. *J Appl Physiol* **67,** 926-932.

McGuigan MR, Bronks R, Newton RU, Sharman MJ, Graham JC, Cody DV & Kraemer WJ. (2001). Muscle fiber characteristics in patients with peripheral arterial disease. *Med Sci Sports Exerc* **33,** 2016-2021.

Menon RS & Allen PS. (1991). Application of Continuous Relaxation-Time Distributions to the Fitting of Data from Model Systems and Excised Tissue. *Magnetic Resonance in Medicine* **20,** 214-227.

Michaelis T, Merboldt KD, Bruhn H, Hanicke W & Frahm J. (1993). Absolute Concentrations of Metabolites in the Adult Human Brain Invivo - Quantification of Localized Proton Mr Spectra. *Radiology* **187,** 219-227.

Michel N & Akoka S. (2004). The application of the ERETIC method to 2D-NMR. *Journal of Magnetic Resonance* **168,** 118-123.

Mlynarik V, Gruber S & Moser E. (2001). Proton T-1 and T-2 relaxation times of human brain metabolites at 3 Tesla. *Nmr in Biomedicine* **14,** 325-331.

Mootha VK, Lindgren CM, Eriksson KF, Subramanian A, Sihag S, Lehar J, Puigserver P, Carlsson E, Ridderstrale M, Laurila E, Houstis N, Daly MJ, Patterson N, Mesirov JP, Golub TR, Tamayo P, Spiegelman B, Lander ES, Hirschhorn JN, Altshuler D & Groop LC. (2003a). PGC-1 alpha-responsive genes involved in oxidative phosphorylation are coordinately downregulated in human diabetes. *Nature Genetics* **34,** 267-273.

Mootha VK, Lindgren CM, Eriksson KF, Subramanian A, Sihag S, Lehar J, Puigserver P, Carlsson E, Ridderstrale M, Laurila E, Houstis N, Daly MJ, Patterson N, Mesirov JP, Golub TR, Tamayo P, Spiegelman B, Lander ES, Hirschhorn JN, Altshuler D & Groop LC. (2003b). PGC-1alpha-responsive genes involved in oxidative phosphorylation are coordinately downregulated in human diabetes. *Nat Genet* **34,** 267-273.

Morino K, Petersen KF & Shulman GI. (2006). Molecular mechanisms of insulin resistance in humans and their potential links with mitochondrial dysfunction. *Diabetes* **55 Suppl 2,** S9-S15.

Moyher SE, Vigneron DB & Nelson SJ. (1995). Surface Coil Mr-Imaging of the Human Brain with an Analytic Reception Profile Correction. *Jmri-Journal of Magnetic Resonance Imaging* **5,** 139-144.

Mukherjee A, Wong TM, Buja LM & Willerson JT. (1980). Oxidative phosphorylation in isolated canine myocardial mitochondria. Effects of in vitro volume dilution, lactate, phosphate, and calcium addition, and lactic acidosis. *Adv Myocardiol* **2,** 339-347.

Muntener M. (1979). Variable pH dependence of the myosin-ATPase in different muscles of the rat. *Histochemistry* **62,** 299-304.

Murphy-Boesch J, Jiang H, Stoyanova R & Brown TR. (1998). Quantification of phosphorus metabolites from chemical shift imaging spectra with corrections for point spread effects and B-1 inhomogeneity. *Magnetic Resonance in Medicine* **39,** 429-438.

Nadeau KJ, Regensteiner JG, Bauer TA, Brown MS, Dorosz JL, Hull A, Zeitler P, Draznin B & Reusch JE. (2009). Insulin Resistance in Adolescents with Type 1 Diabetes and Its Relationship to Cardiovascular Function. *J Clin Endocrinol Metab*.

Narayana PA, Fotedar LK, Jackson EF, Bohan TP, Butler IJ & Wolinsky JS. (1989). Regional Invivo Proton Magnetic-Resonance Spectroscopy of Brain. *Journal of Magnetic Resonance* **83,** 44-52.

Naressi A, Couturier C, Devos JM, Janssen M, Mangeat C, de Beer R & Graveron-Demilly D. (2001). Java-based graphical user interface for the MRUI quantitation package. *Magma* **12,** 141-152.

Nevill ME, Boobis LH, Brooks S & Williams C. (1989). Effect of training on muscle metabolism during treadmill sprinting. *J Appl Physiol* **67,** 2376-2382.

Pathare N, Walter GA, Stevens JE, Yang ZH, Okerke E, Gibbs JD, Esterhai JL, Scarborough MT, Gibbs CP, Sweeney HL & Vandenborne K. (2005). Changes in inorganic phosphate and force production in human skeletal muscle after cast immobilization. *J Appl Physiol* **98,** 307-314.

Perman WH, Bernstein MA & Sandstrom JC. (1989). A method for correctly setting the rf flip angle. *Magn Reson Med* **9,** 16-24.

Petroff OA, Prichard JW, Ogino T & Shulman RG. (1988). Proton magnetic resonance spectroscopic studies of agonal carbohydrate metabolism in rabbit brain. *Neurology* **38,** 1569-1574.

Porter MM, Koolage CW & Lexell J. (2002). Biopsy sampling requirements for the estimation of muscle capillarization. *Muscle Nerve* **26,** 546-548.

Pouwels PJW & Frahm J. (1998). Regional metabolite concentrations in human brain as determined by quantitative localized proton MRS. *Magnetic Resonance in Medicine* **39,** 53-60.

Provencher SW. (1993). Estimation of metabolite concentrations from localized in vivo proton NMR spectra. *Magn Reson Med* **30,** 672-679.

Quistorff B, Nielsen S, Thomsen C, Jensen KE & Henriksen O. (1990). A simple calf muscle ergometer for use in a standard whole-body MR scanner. *Magn Reson Med* **13,** 444-449.

Rayment I, Rypniewski WR, Schmidtbase K, Smith R, Tomchick DR, Benning MM, Winkelmann DA, Wesenberg G & Holden HM. (1993). 3-Dimensional Structure of Myosin Subfragment-1 - a Molecular Motor. *Science* **261,** 50-58.

Regensteiner JG, Bauer TA, Reusch JE, Brandenburg SL, Sippel JM, Vogelsong AM, Smith S, Wolfel EE, Eckel RH & Hiatt WR. (1998). Abnormal oxygen uptake kinetic responses in women with type II diabetes mellitus. *J Appl Physiol* **85,** 310-317.

Rittweger J, Schiessl H & Felsenberg D. (2001). Oxygen uptake during whole-body vibration exercise: comparison with squatting as a slow voluntary movement. *Eur J Appl Physiol* **86,** 169-173.

Roth K & Weiner MW. (1991). Determination of Cytosolic Adp and Amp Concentrations and the Free-Energy of Atp Hydrolysis in Human Muscle and Brain-Tissues with P-31 Nmr-Spectroscopy. *Magnetic Resonance in Medicine* **22,** 505-511.

Rush JW & Spriet LL. (2001). Skeletal muscle glycogen phosphorylase a kinetics: effects of adenine nucleotides and caffeine. *J Appl Physiol* **91,** 2071-2078.

Sahlin K. (1978). Intracellular Ph and Energy-Metabolism in Skeletal-Muscle of Man, with Special Reference to Exercise. *Acta Physiologica Scandinavica***,** 7-56.

Sahlin K, Soderlund K, Tonkonogi M & Hirakoba K. (1997). Phosphocreatine content in single fibers of human muscle after sustained submaximal exercise. *Am J Physiol* **273,** C172-178.

Saltin B & Calbet JA. (2006). Point: in health and in a normoxic environment, VO2 max is limited primarily by cardiac output and locomotor muscle blood flow. *J Appl Physiol* **100,** 744-745.

Shen J, Rycyna RE & Rothman DL. (1997). Improvements on an in vivo automatic shimming method [FASTERMAP]. *Magn Reson Med* **38,** 834-839.

Slotboom J, Boesch C & Kreis R. (1998). Versatile frequency domain fitting using time domain models and prior knowledge. *Magnetic Resonance in Medicine* **39,** 899-911.

Spurway N & Wackerhage H. (2006). *Genetics and Molecular Biology of Muscle Adaptation*. Churchill Livingstone.

Stollberger R & Wach P. (1996). Imaging of the active B-1 field in vivo. *Magnetic Resonance in Medicine* **35,** 246-251.

Takahashi H, Kuno SY, Katsuta S, Shimojo H, Masuda K, Yoshioka H, Anno I & Itai Y. (1996). Relationships between fiber composition and NMR measurements in human skeletal muscle. *Nmr in Biomedicine* **9,** 8-12.

Taylor DJ, Bore PJ, Styles P, Gadian DG & Radda GK. (1983). Bioenergetics of intact human muscle. A 31P nuclear magnetic resonance study. *Mol Biol Med* **1,** 77-94.

Taylor DJ, Styles P, Matthews PM, Arnold DA, Gadian DG, Bore P & Radda GK. (1986). Energetics of human muscle: exercise-induced ATP depletion. *Magn Reson Med* **3,** 44-54.

Thulborn KR & Ackerman JJH. (1983). Absolute Molar Concentrations by Nmr in Inhomogeneous B1 - a Scheme for Analysis of Invivo Metabolites. *Journal of Magnetic Resonance* **55,** 357-371.

Tofts P. (2003). Quantitative MRI of the brain -measuring changes caused by disease. *John Wiley & Sons Ltd***,** page 308.

Toigo M & Boutellier U. (2006). New fundamental resistance exercise determinants of molecular and cellular muscle adaptations. *European Journal of Applied Physiology* **97,** 643-663.

Toigo M, Item F, Denkinger J, Fontana P, Weber M & Boutellier U. (2010). Synthetic exercise concurrently increases endurance and strength in young women. *J Appl Physiol* **submitted**.

Unwin N, Shaw J, Zimmet P & Alberti KG. (2002). Impaired glucose tolerance and impaired fasting glycaemia: the current status on definition and intervention. *Diabet Med* **19,** 708-723.

van den Broek NM, De Feyter HM, de Graaf L, Nicolay K & Prompers JJ. (2007). Intersubject differences in the effect of acidosis on phosphocreatine recovery kinetics in muscle after exercise are due to differences in proton efflux rates. *Am J Physiol Cell Physiol* **293,** C228-237.

van Deursen J, Ruitenbeek W, Heerschap A, Jap P, ter Laak H & Wieringa B. (1994). Creatine kinase (CK) in skeletal muscle energy metabolism: a study of mouse mutants with graded reduction in muscle CK expression. *Proc Natl Acad Sci U S A* **91,** 9091-9095.

Veech RL, Lawson JW, Cornell NW & Krebs HA. (1979). Cytosolic phosphorylation potential. *J Biol Chem* **254,** 6538-6547.

Veksler V & Ventura-Clapier R. (1994). Ischaemic metabolic factors-high inorganic phosphate and acidosis--modulate mitochondrial creatine

kinase functional activity in skinned cardiac fibres. *J Mol Cell Cardiol* **26,** 335-339.

Venkatesan R, Lin W, Gurleyik K, He YY, Paczynski RP, Powers WJ & Hsu CY. (2000). Absolute measurements of water content using magnetic resonance imaging: Preliminary findings in an in vivo focal ischemic rat model. *Magnetic Resonance in Medicine* **43,** 146-150.

Veves A, Saouaf R, Donaghue VM, Mullooly CA, Kistler JA, Giurini JM, Horton ES & Fielding RA. (1997). Aerobic exercise capacity remains normal despite impaired endothelial function in the micro- and macrocirculation of physically active IDDM patients. *Diabetes* **46,** 1846-1852.

Vial C, Font B, Goldschmidt D & Gautheron DC. (1979). Dissociation and Reassociation of Creatine-Kinase with Heart-Mitochondria - Ph and Phosphate Dependence. *Biochemical and Biophysical Research Communications* **88,** 1352-1359.

Wallimann T. (1996). 31P-NMR-measured creatine kinase reaction flux in muscle: a caveat! *J Muscle Res Cell Motil* **17,** 177-181.

Walsh B, Tiivel T, Tonkonogi M & Sahlin K. (2002). Increased concentrations of P(i) and lactic acid reduce creatine-stimulated respiration in muscle fibers. *J Appl Physiol* **92,** 2273-2276.

Wang JH, Qiu ML, Yang QX, Smith MB & Constable RT. (2005). Measurement and correction of transmitter and receiver induced nonuniformities in vivo. *Magnetic Resonance in Medicine* **53,** 408-417.

Warntjes JB, Dahlqvist O & Lundberg P. (2007). Novel method for rapid, simultaneous T1, T*2, and proton density quantification. *Magn Reson Med* **57,** 528-537.

Wilkin TJ. (2001). The accelerator hypothesis: weight gain as the missing link between Type I and Type II diabetes. *Diabetologia* **44,** 914-922.

Wilson RC & Jones PW. (1991a). Differentiation between the intensity of breathlessness and the distress it evokes in normal subjects during exercise. *Clin Sci (Lond)* **80,** 65-70.

Wilson RC & Jones PW. (1991b). Long-Term Reproducibility of Borg Scale Estimates of Breathlessness during Exercise. *Clinical Science* **80,** 309-312.

Wu F, Zhang EY, Zhang JY, Bache RJ & Beard DA. (2008). Phosphate metabolite concentrations and ATP hydrolysis potential in normal and ischaemic hearts. *Journal of Physiology-London* **586,** 4193-4208.

Wyszynski DF, Waterworth DM, Barter PJ, Cohen J, Kesaniemi YA, Mahley RW, McPherson R, Waeber G, Bersot TP, Sharma SS, Nolan V, Middleton LT, Sundseth SS, Farrer LA, Mooser V & Grundy SM. (2005). Relation between atherogenic dyslipidemia and the Adult Treatment Program-III definition of metabolic syndrome (Genetic Epidemiology of Metabolic Syndrome Project). *Am J Cardiol* **95,** 194-198.